POLITECNICO DI TORINO

Corso di Laurea Magistrale in Ingegneria Civile

Master Thesis

A B.I.M methodology approach to design, optimization and augmented reality integration in a Cable-Stayed bridge

Supervisors:

Prof. Giuseppe Carlo Marano

Dr.Ing. Andrea Alberto

Prof. Anna Osello

Candidate:

Amirhossein Aboutalebi

April 2024

Table of Contents

LIST OF FIGURES

LIST OF TABLES

1. Abstract

This thesis explores the application of Building Information Modeling (B.I.M) methodology in the design, optimization, and augmented reality (AR) integration of a Cable-Stayed bridge. The study focuses on achieving structural efficiency, optimal design choices, and technological innovation through the implementation of BIM principles. Key considerations include material selection, such as the utilization of HEB sections for the steel deck, and the optimization process, which employs genetic algorithms to reduce the overall weight of the bridge while maintaining structural integrity.

In the design and modeling stages, standard software tools such as SAP2000 and Tekla are utilized to ensure accuracy and precision. MATLAB is employed for the optimization process, enabling the exploration of various design configuration and material choices.

Augmented reality is utilized to visualize various phases of the construction process and facilitate maintenance activities. Unity software serves as the primary platform for AR implementation, allowing for dynamic visualization and user interaction. The incorporation of toggles, sliders, and buttons enables the sequential display of construction phases, rescaling and rotation of the bridge model, and highlighting critical components for maintenance purposes.

Overall, this thesis presents a comprehensive approach to cable-stayed bridge design, optimization, and AR integration, demonstrating the potential of BIM methodology to enhance efficiency, sustainability, and innovation in bridge engineering.

2. Introduction

The aim of this particular section within the broader project is to address the issue of traffic congestion in urban areas, specifically targeting the historic center of Caraglio, along with the hamlets of San Defendente di Cervasca and San Rocco di Bernezzo. In recent years, the responsible office has been actively planning and implementing strategies to establish a swift road connection, involving the challenge of crossing a river with a width of 100 meters.

This leads us to the focal point of our investigation. As part of the proposed solution, a significant opportunity arises—the construction of a bridge becomes the centerpiece of our study. This thesis is focused on the design of a cable-stayed bridge for this new route, giving specific attention to optimizing the steel deck and cables. Additionally, we explore the incorporation of augmented reality into the construction process. Through the seamless integration of these elements, our goal extends beyond addressing immediate traffic challenges. We aspire to make a substantial contribution to the progression of contemporary bridge design and construction methodologies.

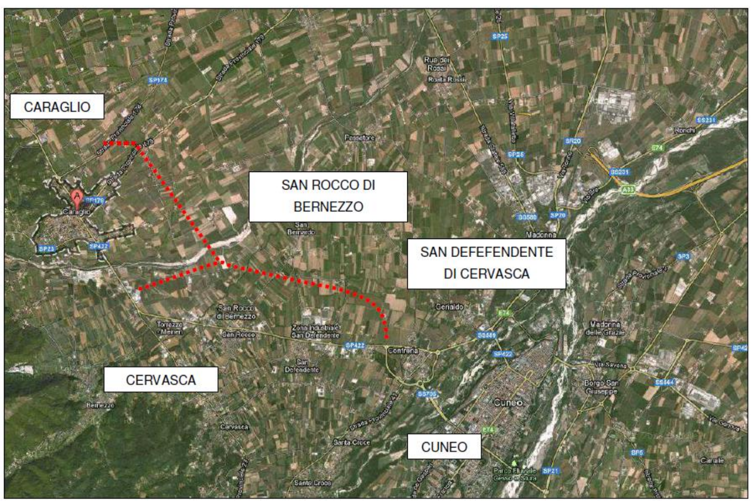

Figure 1. Territorial framework of the intervention area

Furthermore, this study aims to not only alleviate traffic congestion but also to enhance the aesthetic appeal of the urban landscape. By integrating innovative design principles and sustainable construction practices, our initiative seeks to create a bridge that not only serves as a functional infrastructure but also stands as an architectural landmark, enriching the cultural heritage of the region. Additionally, through the utilization of augmented reality technologies, we engage the community in the construction process.

2.1. Deck

The bridge deck features six longitudinal main beams, complemented by diaphragms and bracings, both upper and lower horizontal, as well as vertical, creating a reticular section. The truss components are meticulously interconnected using bolted fully joint and welding techniques, ensuring structural integrity and stability.

Spanning across five sections longitudinally, the bridge extends over a total length of 250 meters. The first and fifth spans measure 37.5 meters each, while the central portion comprises two spans of 82.5 meters each, flanked by one 10-meter span.

To enhance structural robustness, a system of precast slabs (predalles) with a total thickness of 300 mm is strategically positioned on top of the beams. These slabs are interconnected and reinforced by a concrete slab, efficiently distributing load forces. Shear connectors meticulously placed and welded onto the upper flanges of the primary beams secure the entire configuration.

Furthermore, the incorporation of innovative cable designs complements the deck structure, enhancing overall stability and load-bearing capacity.

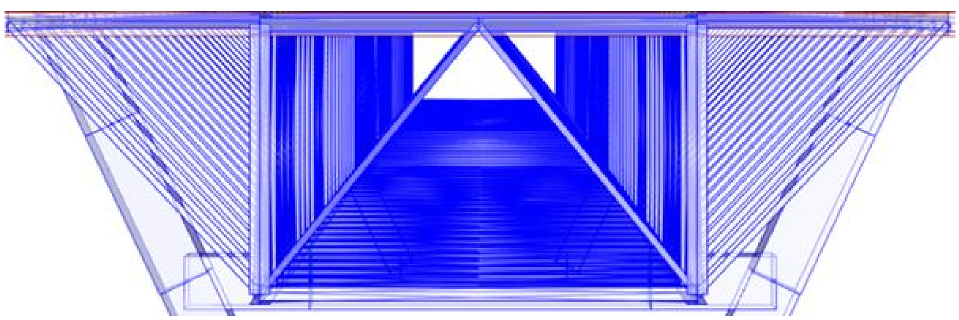

Figure 2. Deck

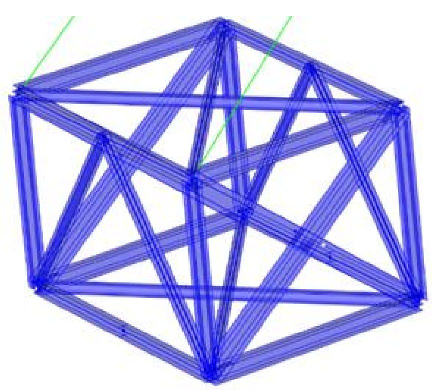

Figure 3. Deck portion

2.2. Calculation Criteria

The safety criteria for calculating actions and material properties align with the Ministerial law (D.M. 17.01.2018) and the 'Technical construction standards' (NTC2018) and its accompanying explanatory circular. In accordance with NTC2018's chapter 2.4, the nominal project life (V_N) signifies the expected durability, contingent on necessary maintenance, to uphold specific performance levels. Furthermore, the class of use and its coefficient (C_U) must be precisely defined. In the case of a strategic structure such as a bridge, we have:

- V_N= 150 years
- Class of use= IV
- C_U= 2

2.3. Execution Class

The EN 1090-2 introduced the concept of Execution Class as an aid to designers when specifying the Execution requirements for steel structures. To choose the EXC, the type of material, reliability of construction and potential failure has to be taking into account.

The consequence class (CC) is intended to categorize the structural reliability of buildings and their impact of the population, environment, and human and social life. Similarly, the service class (SC) and production category (PC) are crucial for considering the structural behavior of the intended construction.

Consequences classes		CC1		CC2		CC2	
Service category		SC1	SC2	SC1	SC2	SC1	SC2
Production categories	PC1	EXC1	EXC2	EXC2	EXC3	EXC3[a]	EXC3[a]
	PC2	EXC2	EXC2	EXC2	EXC3	EXC3[a]	EXC4
[a] EXC4 should be applied to special structures or structures with extreme consequences of a structural failure as required by national provisions							

Table 1. Execution Class

2.4. Material Used

2.4.1. Steel Work

The type of steel employed in fabricating the main deck is S355.

- The yielding strength $f_{ayk} = 355 \frac{N}{mm^2}$
- The failure strength $f_{auk} = 510 \frac{N}{mm^2}$

SLU condition $f_{ayd} = \frac{355}{1.05} = 338.1 \frac{N}{mm^2}$

2.4.2. Reinforcement Steel

The weight density $\gamma_s = 7850 \frac{kg}{m^3}$

- The yielding strength $f_{ayk} = 450 \frac{N}{mm^2}$
- The failure strength $f_{auk} = 540 \frac{N}{mm^2}$

SLU condition $f_{syd} = \frac{450}{1.15} = 331.3 \frac{N}{mm^2}$

SLE condition $f_{ayd} = \frac{450}{1.25} = 360 \frac{N}{mm^2}$

2.4.3. Concrete

The weight is assumed: $\gamma_{cls} = 2500 \frac{kg}{m^3}$

2.4.4. Strands

The strands are composed of multiple individual steel wires twisted together to form a cable.

Concrete Design Properties according to EN1992-1-1 (γ_c = 1.50, f_{yk} = 355 MPa)

Symbol	**Description**	**C25/30**	**C30/37**
f_{ck} (MPa)	Characteristic cylinder compressive strength	25	30
$f_{ck,cube}$ (MPa)	Characteristic cube compressive strength	30	37
f_{cm} (MPa)	Mean cylinder compressive strength	33	38
f_{ctm} (MPa)	Mean tensile strength	2.56	2.90
E_{cm} (MPa)	Elastic modulus	31476	32837
f_{cd} (MPa) (for α_{cc}=1.00)	Design compressive strength (for α_{cc}=1.00)	16.67	20.00
f_{cd} (MPa) (for α_{cc}=0.85)	Design compressive strength (for α_{cc}=0.85)	14.17	17.00
f_{ctd} (MPa) (for α_{ct}=1.00)	Design tensile strength (for α_{ct}=1.00)	1.20	1.35
ρ_{min} (%)	Minimum longitudinal tension reinforcement ratio	0.188	0.212
$\rho_{w,min}$ (%)	Minimum shear reinforcement ratio	0.113	0.123

Table 2. Concrete Design Properties

2.5. Geometrical Properties

Initially, the design comprised four main beams using IPE sections, along with diaphragms and horizontal bracings. However, it was later revised to incorporate reticular sections with HEB profiles. The updated design features six longitudinal beams, with four of them utilizing HEB 300 profiles. The updated design features six longitudinal beams, with four of them utilizing HEB 300 profiles and the remaining two employing HEB 200 profiles. Additionally, the design includes diaphragms, horizontal bracings at the top and bottom, and vertical bracings in the longitudinal direction. Below are the detailed geometric characteristics of each profile.

2.5.1. Main Beams

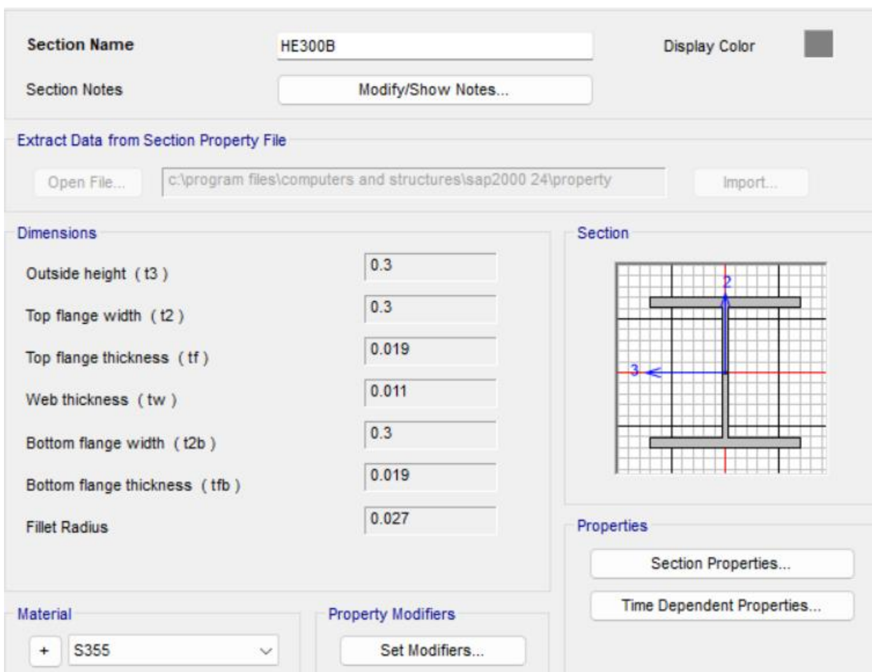

Figure 4. HEB 300 dimensions

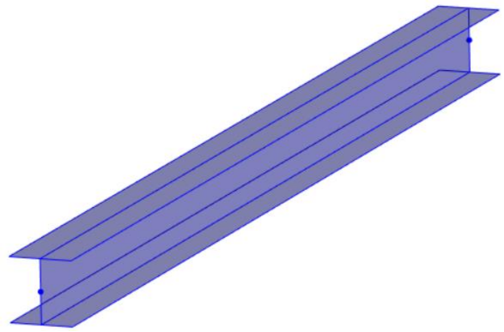

Figure 5. HEB 300 shape

Properties

Cross-section (axial) area	0.0149	Section modulus about 3 axis (top)	1.678E-03
Moment of Inertia about 3 axis	2.517E-04	Section modulus about 3 axis (bottom)	1.678E-03
Moment of Inertia about 2 axis	8.563E-05	Section modulus about 2 axis (left)	5.709E-04
Product of Inertia about 2-3	0.	Section modulus about 2 axis (right)	5.709E-04
Torsional constant	1.890E-06	Warping Constant (Cw)	1.688E-06
Shear area in 2 direction	3.300E-03	Plastic modulus about 3 axis	1.869E-03
Shear area in 3 direction	9.500E-03	Plastic modulus about 2 axis	8.700E-04
CG offset in 3 direction	0.	Radius of Gyration about 3 axis	0.13
CG offset in 2 direction	0.	Radius of Gyration about 2 axis	0.0758
Shear Center Offset (x3)*	0.		
Shear Center Offset (x2)*	0.	* Value is not used in analysis	

Figure 6. HEB 300 Properties

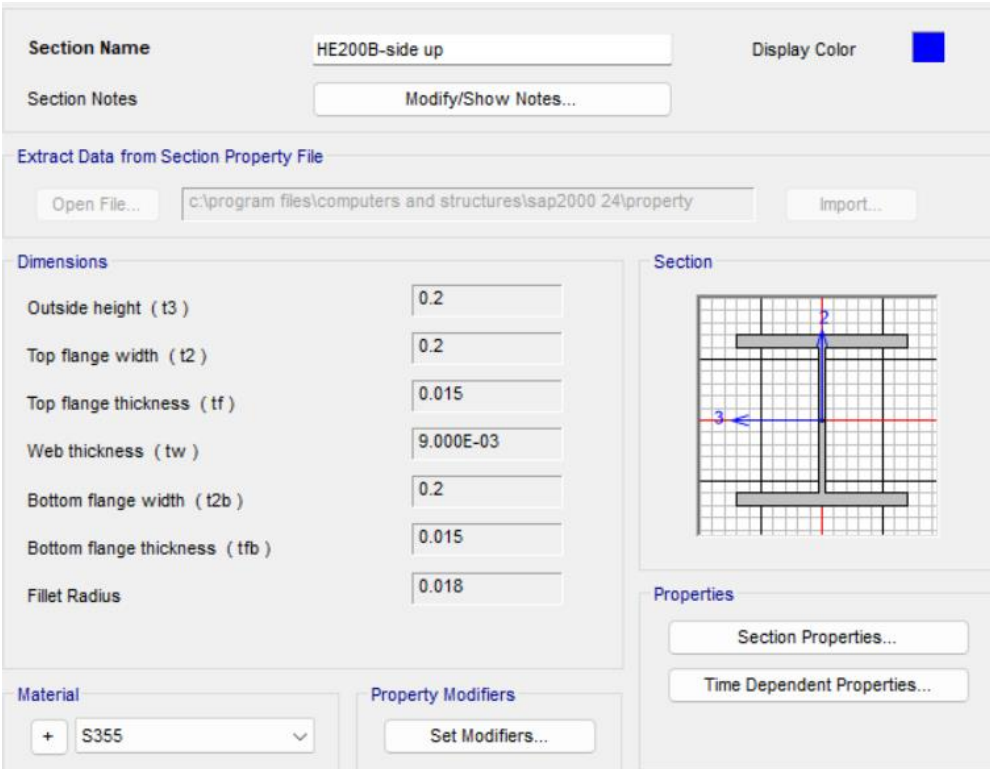

Figure 7. HEB200 dimensions

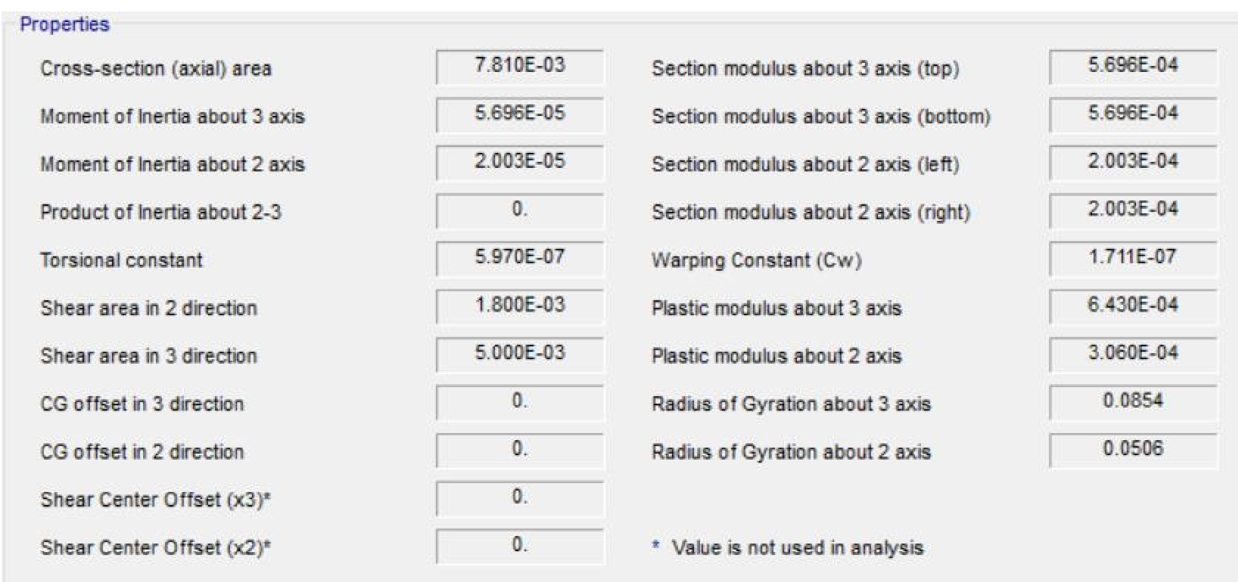

Figure 8. HEB 200 properties

2.5.2. Diaphragm

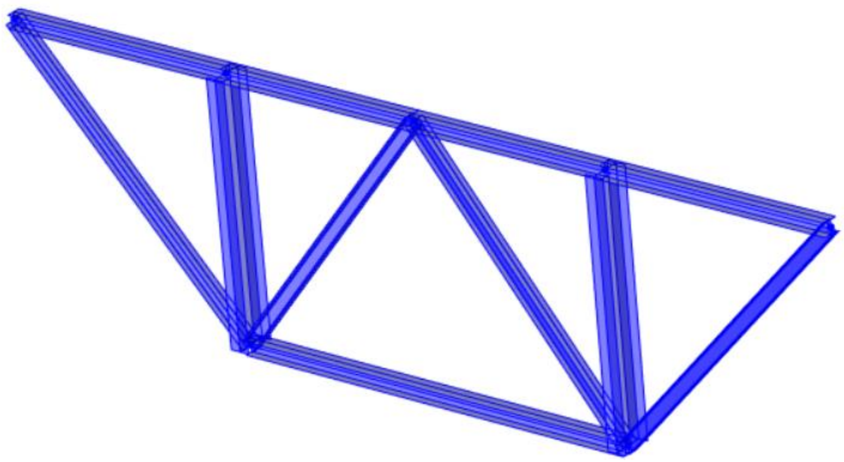

Figure 9. Diaphragm

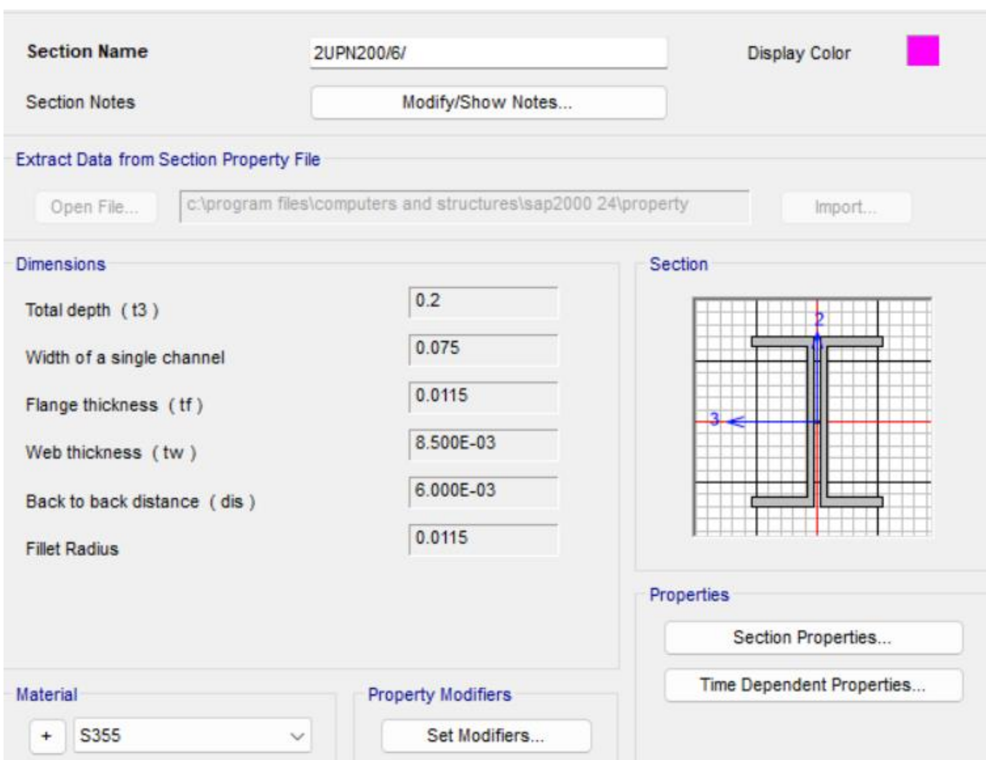

Figure 10. Two UPN 200 dimensions

Properties			
Cross-section (axial) area	6.437E-03	Section modulus about 3 axis (top)	3.821E-04
Moment of Inertia about 3 axis	3.821E-05	Section modulus about 3 axis (bottom)	3.821E-04
Moment of Inertia about 2 axis	6.392E-06	Section modulus about 2 axis (left)	8.195E-05
Product of Inertia about 2-3	0.	Section modulus about 2 axis (right)	8.195E-05
Torsional constant	2.246E-07	Warping Constant (Cw)	2.110E-08
Shear area in 2 direction	3.400E-03	Plastic modulus about 3 axis	4.583E-04
Shear area in 3 direction	2.875E-03	Plastic modulus about 2 axis	1.485E-04
CG offset in 3 direction	0.	Radius of Gyration about 3 axis	0.077
CG offset in 2 direction	0.	Radius of Gyration about 2 axis	0.0315
Shear Center Offset (x3)*	0.		
Shear Center Offset (x2)*	0.	* Value is not used in analysis	

Figure 11. Two UPN 200 properties

2.5.3. Bracing

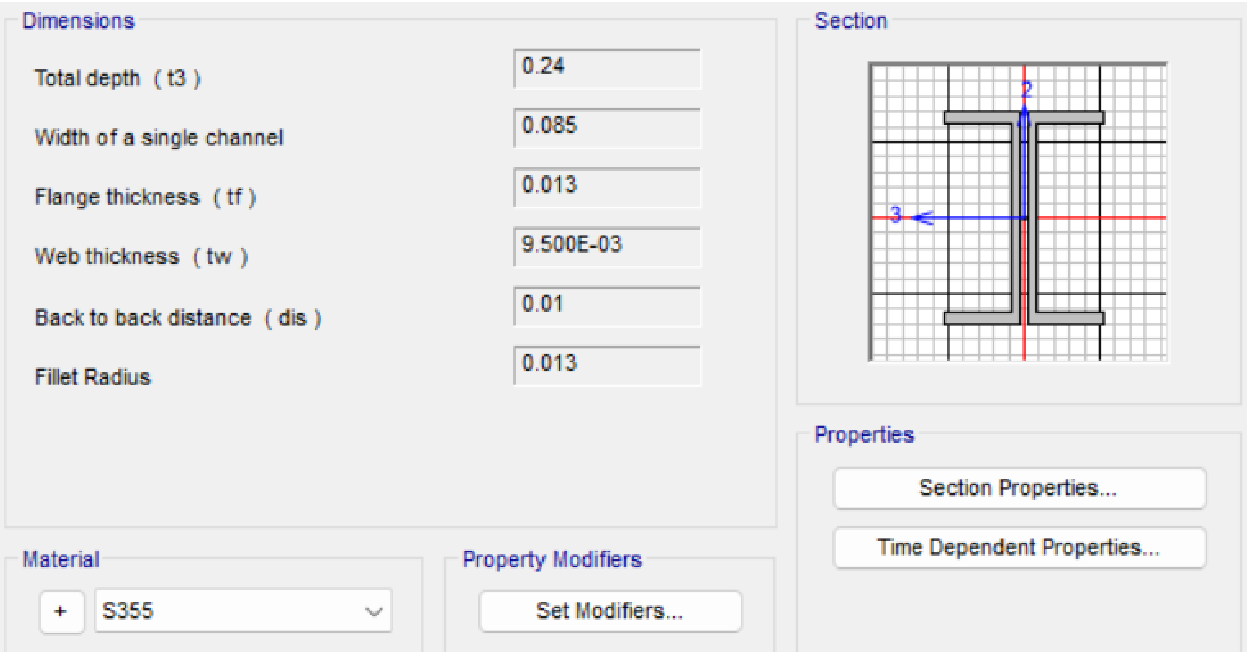

Figure 12. Two UPN 240 dimensions

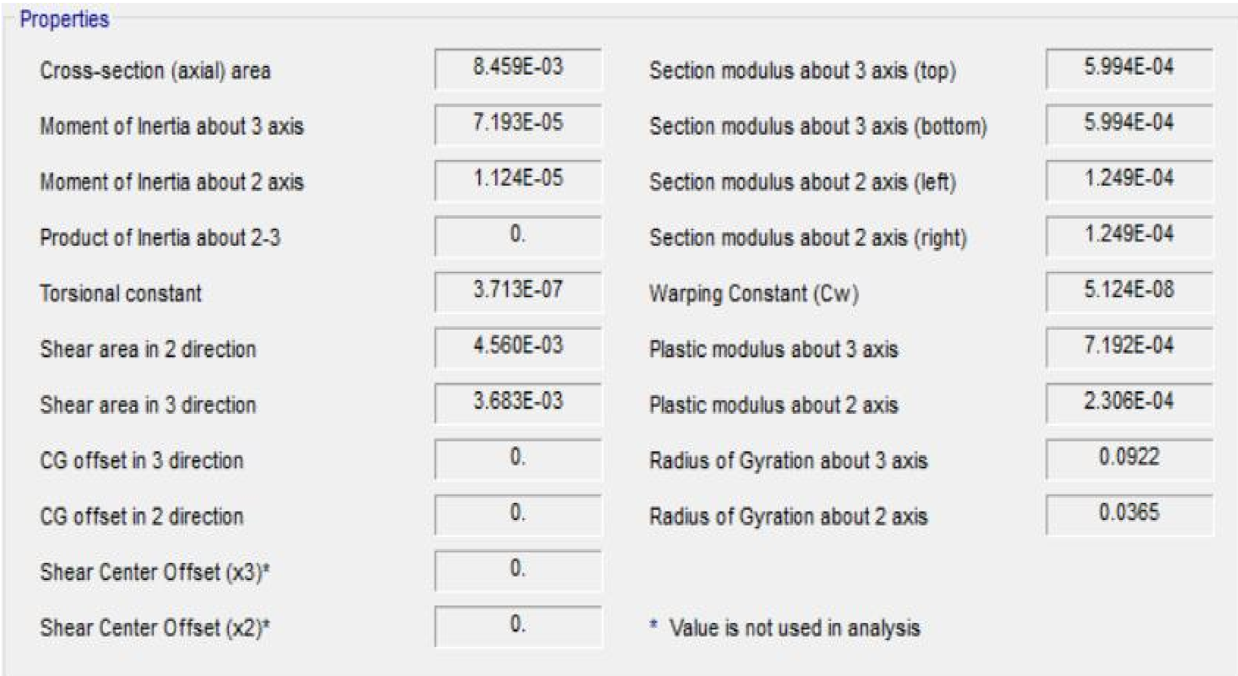

Properties

Cross-section (axial) area	8.459E-03	Section modulus about 3 axis (top)	5.994E-04
Moment of Inertia about 3 axis	7.193E-05	Section modulus about 3 axis (bottom)	5.994E-04
Moment of Inertia about 2 axis	1.124E-05	Section modulus about 2 axis (left)	1.249E-04
Product of Inertia about 2-3	0.	Section modulus about 2 axis (right)	1.249E-04
Torsional constant	3.713E-07	Warping Constant (Cw)	5.124E-08
Shear area in 2 direction	4.560E-03	Plastic modulus about 3 axis	7.192E-04
Shear area in 3 direction	3.683E-03	Plastic modulus about 2 axis	2.306E-04
CG offset in 3 direction	0.	Radius of Gyration about 3 axis	0.0922
CG offset in 2 direction	0.	Radius of Gyration about 2 axis	0.0365
Shear Center Offset (x3)*	0.		
Shear Center Offset (x2)*	0.	* Value is not used in analysis	

Figure 13. Two UPN 240 Properties

2.5.4. Cables

For the cables, a structured approach was implemented, where the minimum diameter was situated at the center of the bridge. Accordingly, the maximum diameter was set at 220 mm at the edges, gradually decreasing to 200 mm and then to 170 mm towards the center. This arrangement aimed to optimize structural integrity and load distribution, with larger diameters at the edges providing additional support while minimizing weight towards the center.

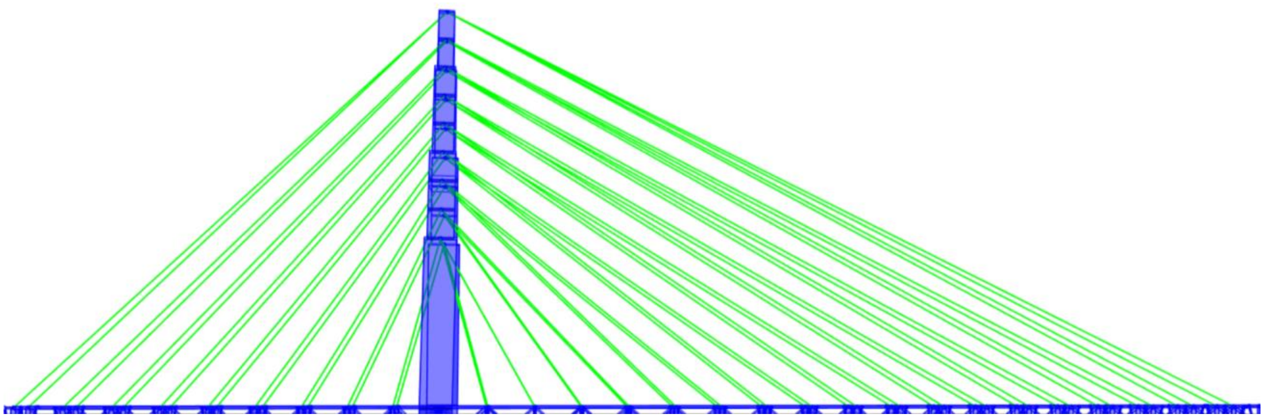

Figure 14. longitudinal view of Cables

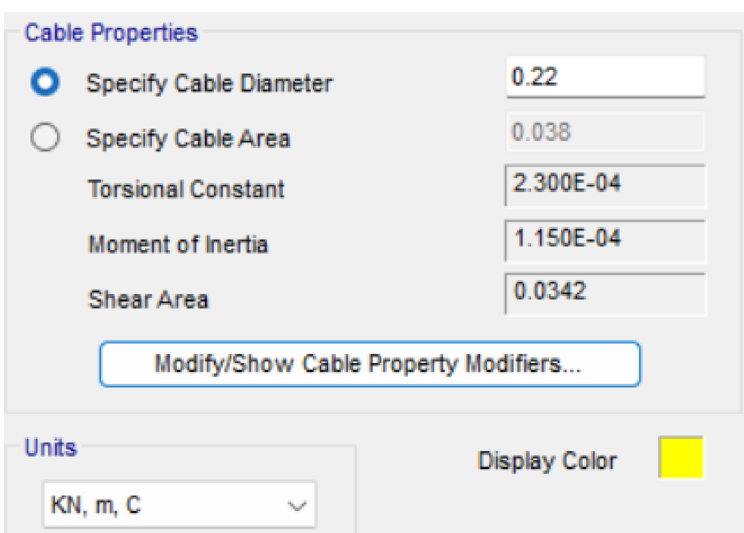

Figure 15. Cable diameter, 220mm

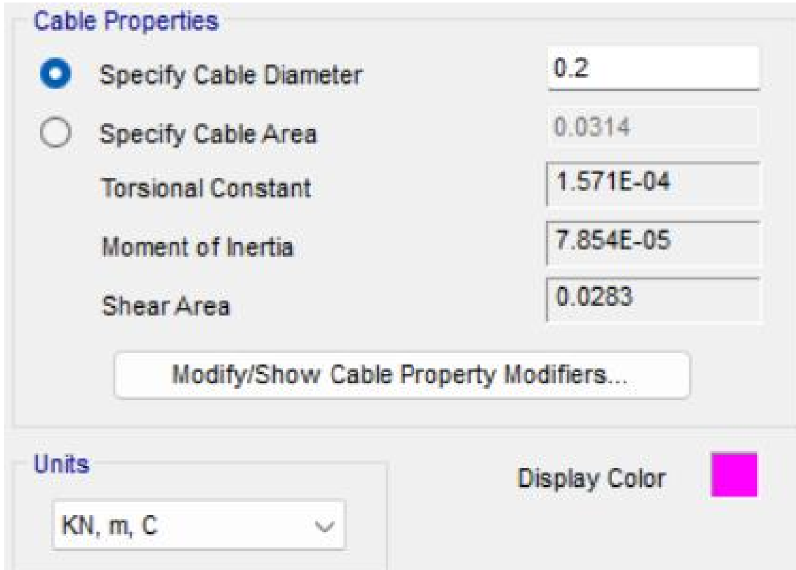

Figure 16. Cable diameter, 200mm

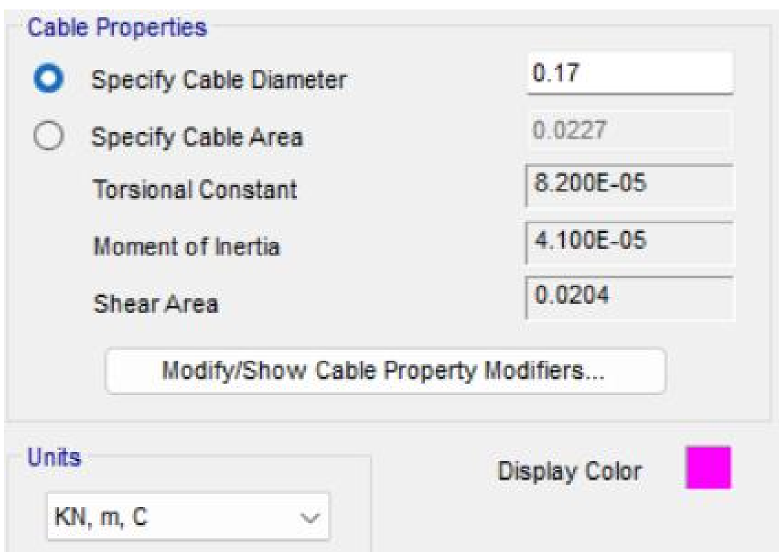

Figure 17. Cable diameter, 170mm

3. Load Analysis:

In this section, our aim is to provide a comprehensive description of the applied loads and all corresponding loading conditions in accordance with both Eurocode and Italian technical standards.

3.1. Dead Load

The initial phase involved determining the moment of inertia for the presumed sections. This was crucial in identifying potential sections for our structure by evaluating the load ratio between the moment of inertia and the applied loads (G1, G2, and Traffic load).

Subsequently, by extracting the bending moment data from the FEM software (SAP2000), we established the ratio and constrained the verified ratios to a maximum of approximately 60 percent. This constraint was essential to account for additional factors such as seismic, wind, and snow actions on the sections.

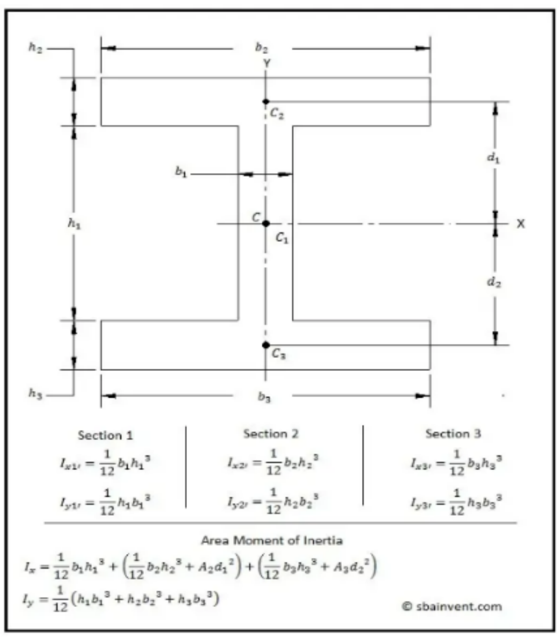

Figure 18. MOMENT OF INERTIA

Cross section of the deck:

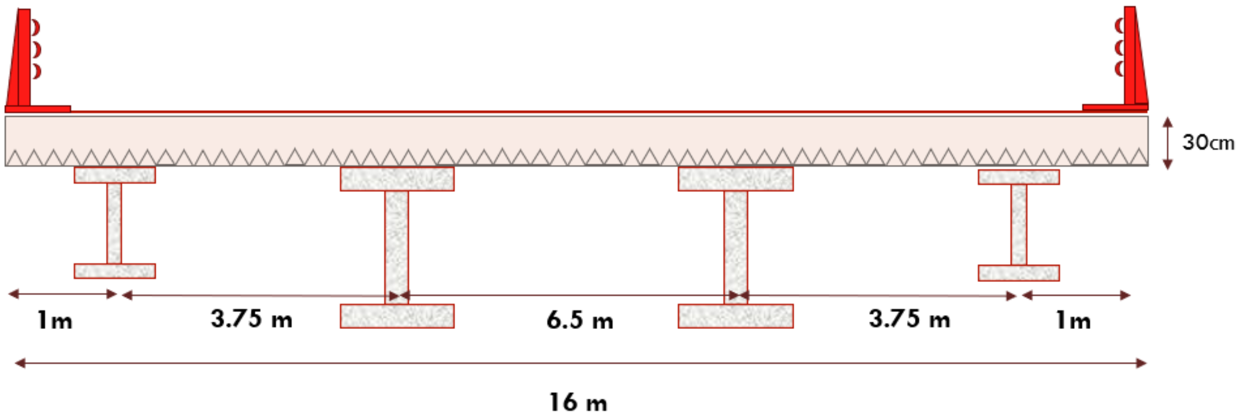

Figure 19. Cross section of Deck

3.2. Permanent Loads :

Looking at the schematic deck section, we can identify the potential permanent loading factors present.

- Pavement = 3 $\frac{KN}{m^2}$
- Kerb = 3.75 $\frac{KN}{m^2}$
- VRS = 1.5 $\frac{KN}{m^2}$
- Predalles = 5 $\frac{KN}{m^2}$

3.3. Accidental Loads :

3.3.1. Traffic Load :

The applied loads on road bridges are generated by a variety of vehicle types and pedestrian activity. Road traffic, cars and trucks, induces both vertical and horizontal, static and dynamic forces.

The composition of vehicle traffic, including the maximum weights and axle loads can vary between bridges. To address these variations, it is essential to employ load models to the specific location of a bridge.

Traffic Load Models	Characteristic values	Frequent values	Quasi-permanent values
Road bridges			
LM1 (4.3.2)	1000 year return period (or probability of exceedance of 5% in 50 years) for traffic on the main roads in Europe (α factors equal to 1, see 4.3.2).	1 week return period for traffic on the main roads in Europe (α factors equal to 1, see 4.3.2).	Calibration in accordance with definition given in EN 1990.
LM2 (4.3.3)	1000 year return period (or probability of exceedance of 5% in 50 years) for traffic on the main roads in Europe (β factor equal to 1, see 4.3.3).	1 week return period for traffic on the main roads in Europe (β factor equal to 1, see 4.3.3).	Not relevant
LM3 (4.3.4)	Set of nominal values. Basic values defined in annex A are derived from a synthesis based on various national regulations.	Not relevant	Not relevant
LM4 (4.3.5)	Nominal value deemed to represent the effects of a crowd. Defined with reference to existing national standards.	Not relevant	Not relevant
Footbridges			
Uniformly distributed load (5.3.2.1)	Nominal value deemed to represent the effects of a crowd. Defined with reference to existing national standards.	Equivalent static force calibrated on the basis of 2 pedestrians/m^2 (in the absence of particular dynamic behaviour). It can be considered, for footbridges in urban areas, as a load of 1 week return period.	Calibration in accordance with definition given in EN 1990.
Concentrated load (5.3.2.2)	Nominal value. Defined with reference to existing national standards.	Not relevant	Not relevant
Service vehicle (5.3.2.3)	Nominal value. As specified or given in 5.6.3.	Not relevant	Not relevant

Table 1. Bases for the cali bration of the main Load Models (fatigue excluded)

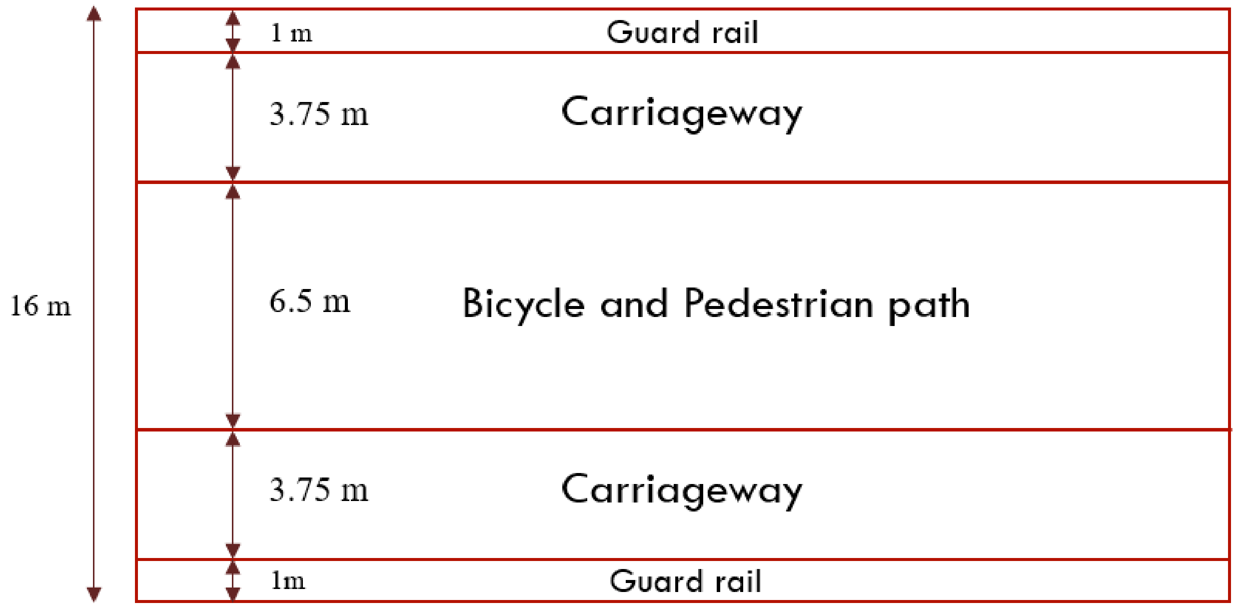

Figure 20. Lanes

The Load models considered in this bridge are LM1 and LM2 for the motorway path.

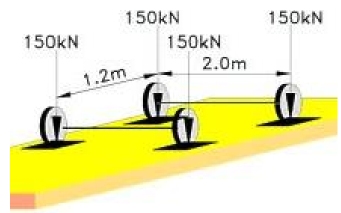

Figure 21. Axle load, LM1

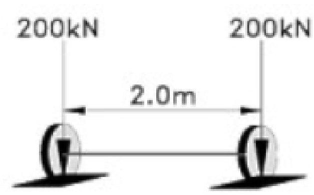

Figure 22. Single axle load, LM2

3.3.2. Divisions of the carriageway into notional lanes :

The measurement of carriageway width, denoted as *w,* is defined as the distance between kerbs or the inner boundaries of vehicle restraint systems. It should exclude the space between fixed vehicle restraint systems or kerbs of a central reservation, as well as the widths of these vehicle restraint system.

Carriageway width w	Number of notional lanes	Width of a notional lane w_l	Width of the remaining area
$w < 5{,}4$ m	$n_l = 1$	3 m	w - 3 m
$5{,}4 \text{ m} \leq w < 6$ m	$n_l = 2$	$\frac{w}{2}$	0
$6 \text{ m} \leq w$	$n_l = Int\left(\frac{w}{3}\right)$	3 m	$w - 3 \times n_l$
NOTE For example, for a carriageway width equal to 11m, $n_l = Int\left(\frac{w}{3}\right) = 3$, and the width of the remaining area is 11 - 3×3 = 2m.			

Table 2. Number and width of notional lanes

3.3.3. LOAD MODEL 1:

Load model 1 represents a set of concentrated loads with 150 kN for each wheel with a total of 4 and uniform distributed load with 9 kN/m^2 applied on the structure.

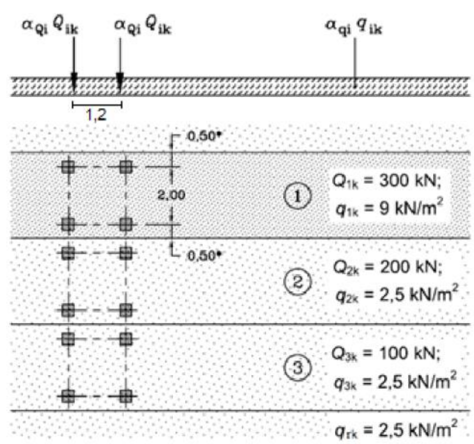

Figure 23. Load Model 1

3.3.4. LOAD MODEL 2 :

Load Model 2 consists of a single axle load $\beta_Q Q_{ak}$ with Q_{ak} equal to 400 kN, dynamic amplification included, which should be applied at any location on the carriageway. The contact surface of each wheel should be taken into account as a rectangle of sides 0.35 m and 0.6 m. The contact areas of Load Model 2 are normally relevant for orthotropic decks and are used for local verification.

The lane giving the most unfavorable effect is numbered Lane Number 1.

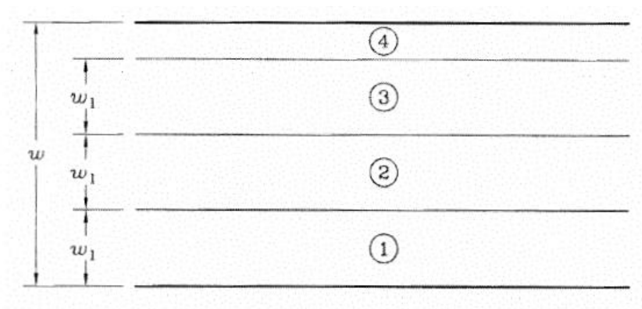

Key
w Carriageway width
w_l Notional lane width
1 Notional Lane Nr. 1
2 Notional Lane Nr. 2
3 Notional Lane Nr. 3
4 Remaining area

Figure 24. Lane numbering in general

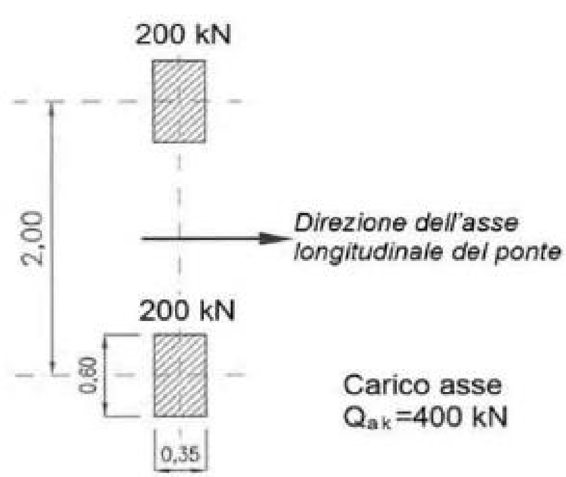

Figure 25. Load Model 2

Load model 1 disribution :

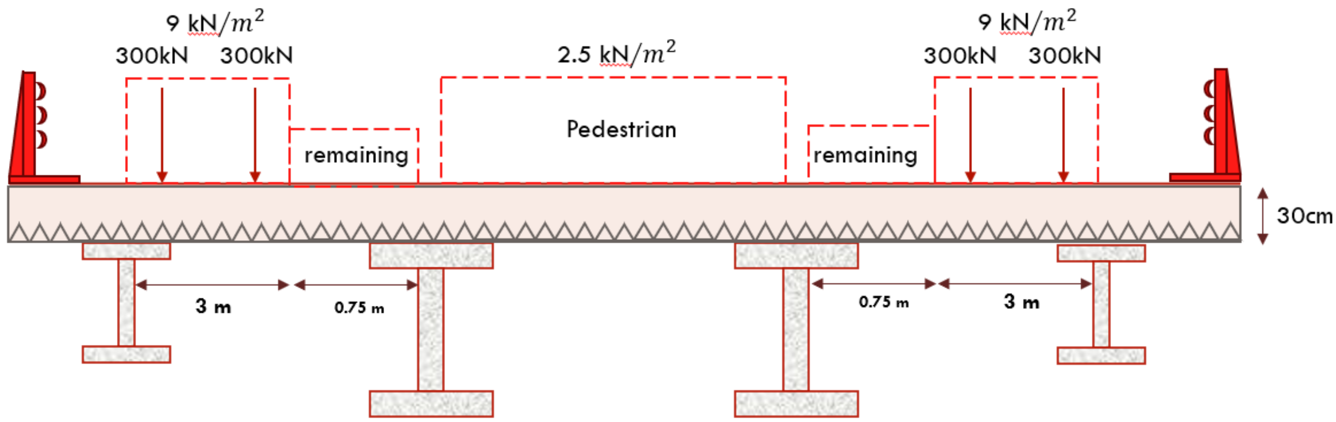

Figure 26. Deck LM1

Load model 2 disribution :

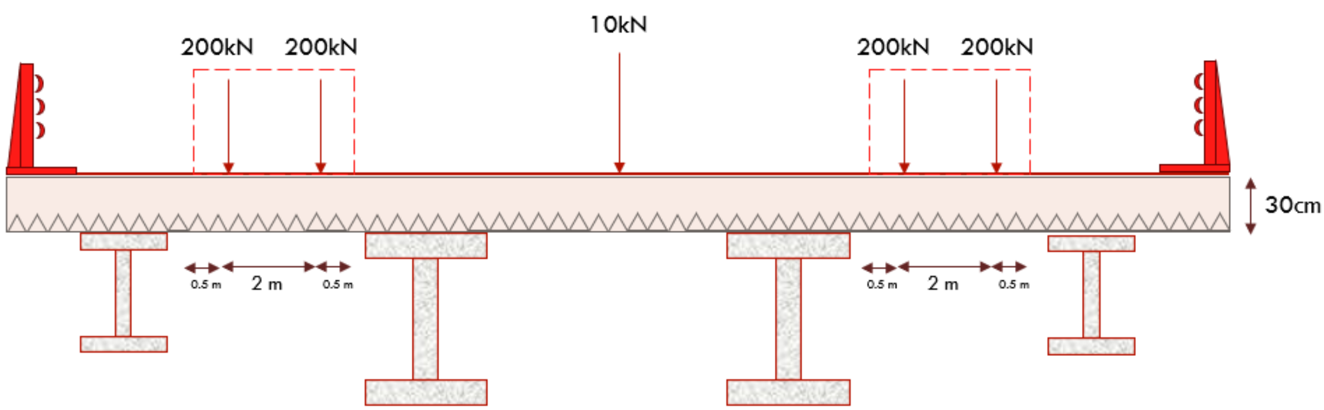

Figure 27. Deck LM2

Note: Load distribution along the bridge was defined first by applying the Tandem system and UDL of the Traffic load in the transversal direction, then using the reactions obtained in transversal direction, in longitudinal direction to define the bending moment, shear and deformation of the main beams

		CARRIAGEWAY						FOOTWAYS AND CYCLE TRACKS
Load type		**Vertical forces**				**Horizontal forces**		**Vertical forces only**
Reference		4.3.2	4.3.3	4.3.4	4.3.5	4.4.1	4.4.2	5.3.2-(1)
Load system		LM1 (TS and UDL systems)	LM2 (Single axle)	LM3 (Special vehicles)	LM4 (Crowd loading)	Braking and acceleration forces [a]	Centrifugal and transverse forces [a]	Uniformly Distributed load
Groups of Loads	gr1a	Characteristic values						Combination value [b]
	gr1b		Characteristic value					
	gr2	Frequent values				Characteristic value	Characteristic value	
	gr3 [d]							Characteristic value [c]
	gr4				Characteristic value			Characteristic value
	gr5	See annex A		Characteristic value				
	Dominant component action (designated as component associated with the group)							

[a] May be defined in the National Annex (for the cases mentioned).
[b] May be defined in the National Annex. The recommended value is 3 kN/m^2.
[c] See 5.3.2.1-(2). One footway only should be considered to be loaded if the effect is more unfavourable than the effect of two loaded footways.
[d] This group is irrelevant if gr4 is considered.

Figure 28. Assessment of groups of traffic loads

3.3.5. Dispersal of Concentrated Loads :

For local verifications, the various concentrated loads related to Load Models 1 and 2 should be regarded as uniformly distributed across their complete contact area.

The spread-to-depth ratio for the dispersal through the pavement and concrete slabs should be considered as 1:1 horizontally to vertically, extending down to the level of the slab centroid.

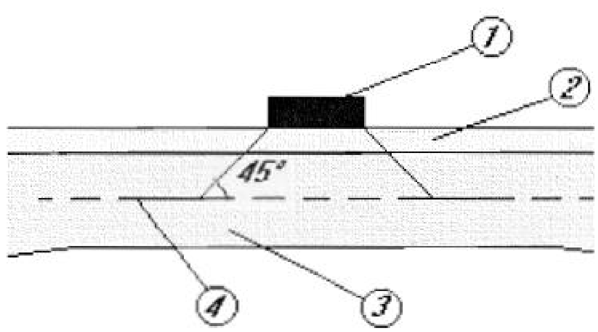

Figure 29. Dispersal of Concentrated Loads through pavement and a concrete slab

2.3.2. Effective Width :

The assessment of the effective width of the concrete slab at the top of the main beam is required to be conducted as follows:

$$b_{eff} = b_0 + b_{e1} + b_2$$

Where,

b_0 is the distance between shear connectors.

$b_{ei} = (\frac{L_e}{8}; b_i - \frac{b_0}{2})$, is the effective width encompasses both the left and right sides of the composite cross-section.

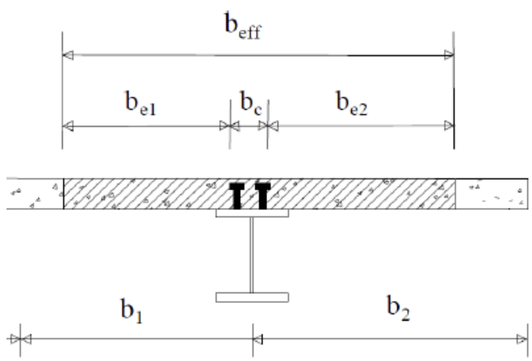

Figure 30. effective width-1

Distribution of load:

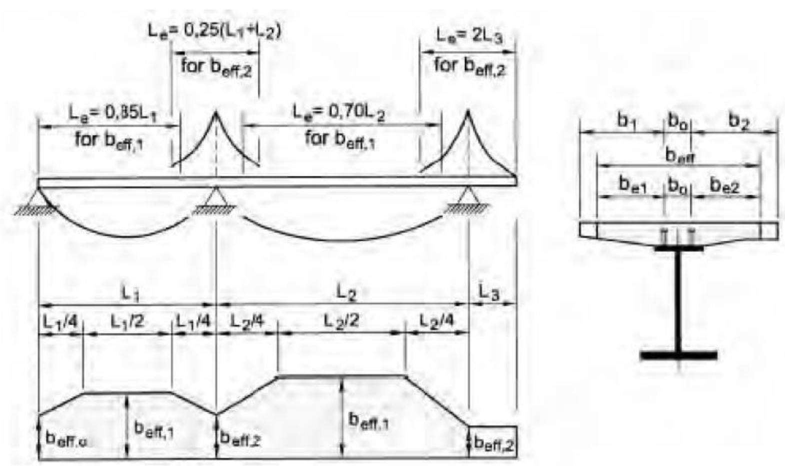

Figure 31.effective width-2

Figure 32. Load Distribution

The distributed length:

distribute	1160 mm

Beff:	1415.715 mm

2.3.3. Horizontal forces, Braking and acceleration forces :

A Braking force Q_{lk} is to be considered as a longitudinal force acting at the surfacing level of the carriageway. Its characteristic value is limited to 900 kN for the total width of the bridge.

$$180\ kN \leq q_3 = 0.6(2Q_{1k}) + 0.1 * q_{1k} * w_1 * L \leq 900kN$$

Where,

- w, notional lane width
- L, bridge length
- q_{lk}, UDL corresponded

$q_3 = 915\ kN$

The braking force obtained is not between the range of 180 and 900, Hence the maximum value is considered as 900 kN.

2.4. Variable Loads :

2.4.1. Wind Effects :

Wind effects are computed in compliance with chapter 3 of NTC2018, following the guidelines outlined in Eurocode EN 1991-1-4. This force is comparable to a static horizontal force, aligned perpendicular to the bridge axis and projected in the vertical plane of the relevant surfaces.

In the case of a loaded bridge, the exposed area expands with the presence of moving vehicles, forming a resemblance to a continuous rectangular barrier situated 3 meters above the road surface.

2.4.1.1. Reference base velocity

Zona	Descrizione	$v_{b,0}$ [m/s]	a_0 [m]	k_s
1	Valle d'Aosta, Piemonte, Lombardia, Trentino Alto Adige, Veneto, Friuli Venezia Giulia (con l'eccezione della provincia di Trieste)	25	1000	0,40
2	Emilia Romagna	25	750	0,45
3	Toscana, Marche, Umbria, Lazio, Abruzzo, Molise, Puglia, Campania, Basilicata, Calabria (esclusa la provincia di Reggio Calabria)	27	500	0,37
4	Sicilia e provincia di Reggio Calabria	28	500	0,36
5	Sardegna (zona a oriente della retta congiungente Capo Teulada con l'Isola di Maddalena)	28	750	0,40
6	Sardegna (zona a occidente della retta congiungente Capo Teulada con l'Isola di Maddalena)	28	500	0,36
7	Liguria	28	1000	0,54
8	Provincia di Trieste	30	1500	0,50
9	Isole (con l'eccezione di Sicilia e Sardegna) e mare aperto	31	500	0,32

Figure 33. Description of Italian Zone

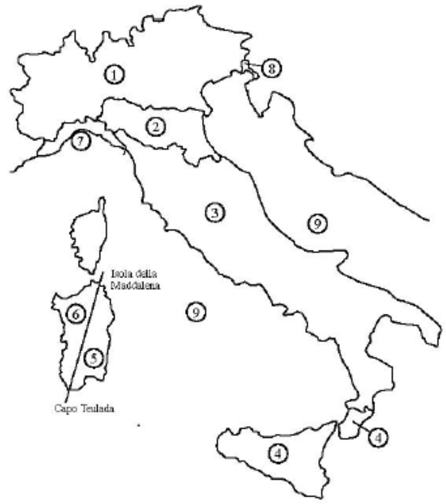

Figure 34. Geographical Subdivision

According to standards:

$v_b = v_{b0} * c_a$

$c_a = 1$ for $a_s \leq a_0$

$c_a = 1 + k_s\left(\frac{a_s}{a_0} - 1\right)$ for $a_0 < a_s < 1500m$

Based on location of the bridge, we obtain:

$$v_b = 28 * 1 = 28\ \frac{m}{s}$$

a_s (altitudine sul livello del mare della costruzione):	542	[m]
Distanza dalla costa	70	[km]
T_R (Tempo di ritorno):	150	[anni]
Categoria di esposizione	IV	

2.4.1.2. *Reference base velocity*

As outlined in the Italian technical standard, the exposure coefficient is directly influenced by the elevation of the specific point above ground level and the topography of the surrounding terrain. The calculation includes parameters that are associated with tabular values specified in NTC18. By taking into account variables such as exposure class, ground roughness, and distance from the sea, this coefficient can be easily determined.

Categoria di esposizione del sito	K_r	z_0 [m]	z_{min} [m]
I	0,17	0,01	2
II	0,19	0,05	4
III	0,20	0,10	5
IV	0,22	0,30	8
V	0,23	0,70	12

Figure 35. Exposure coefficients

The coefficient is determined as:

$$c_e(z) = k_r^2 c_t \ln(\frac{z}{z_0})[7 + c_t \ln(\frac{z}{z_0})] \qquad \text{for } z \geq z_{min}$$

$$c_e(z) = c_e(z_{\min}) \qquad \text{for } z < z_{min}$$

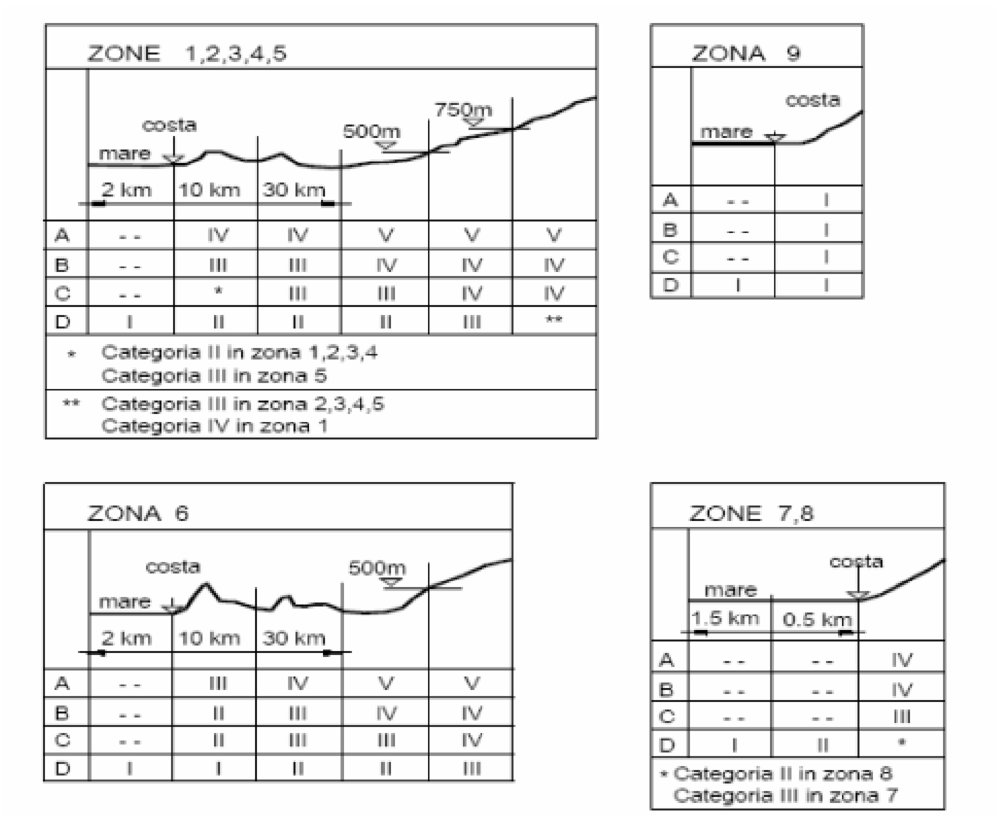

Table 3. Class of Exposure

At 10 meters of the pier height:

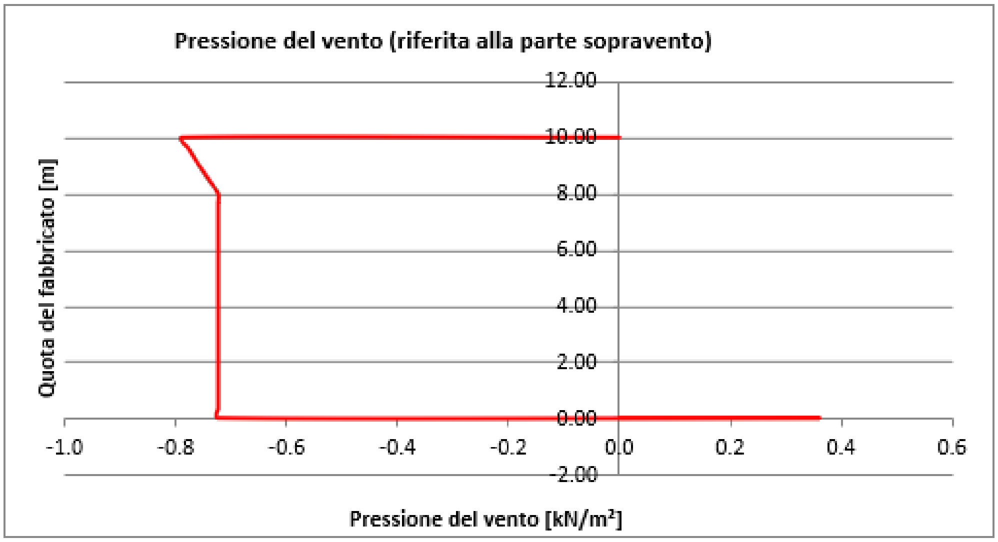

Figure 36. Wind pressure at 10m

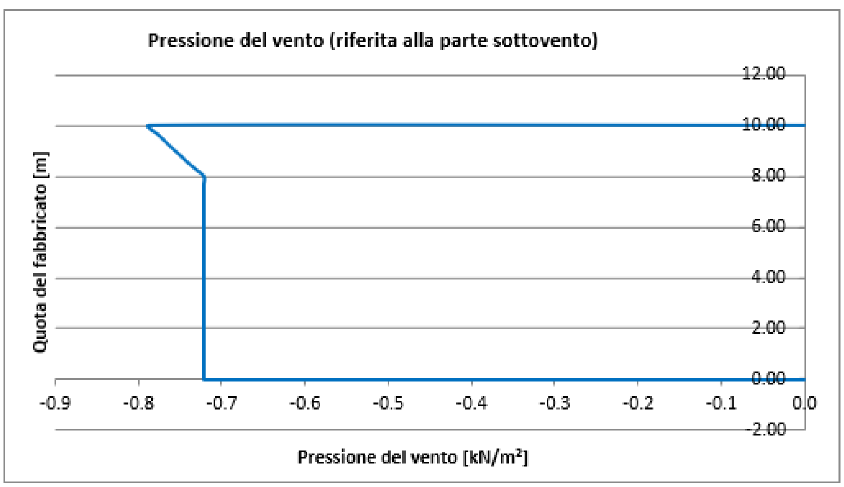

PRESSIONI DEL VENTO IN DIREZIONE TANGENZIALE [§3.3.5]

Tipo di superficie:	Scabra

Pressione tangenziale del vento qtan **19.67** **[N/m²]**

Figure 37 . Tangential wind pressure at 10m

At 40 meters of the pier height:

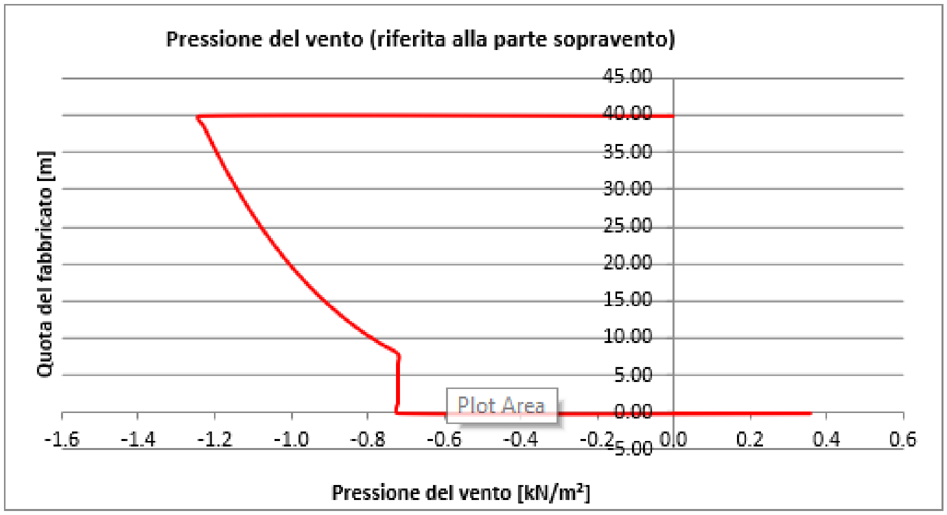

Figure 38. . Wind pressure at 40m

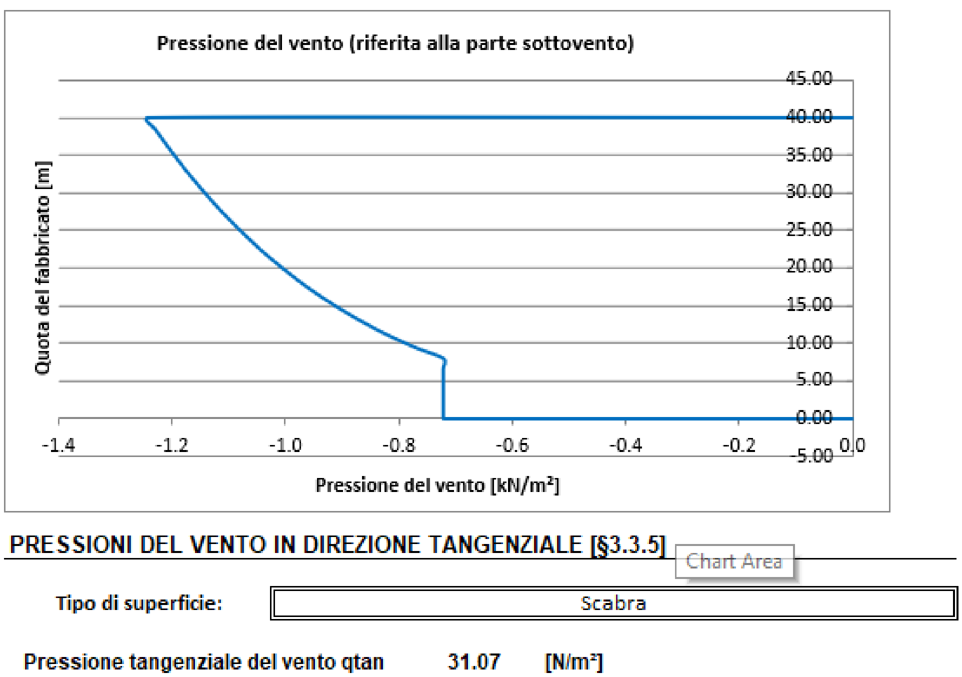

Figure 39. Tangential wind pressure at 40m

2.4.2. Snow Load :

In the construction of the bridge, due consideration has been given to the impact of snow load on the structure’s integrity. However, it’s important to note that once the bridge is completed and open to traffic, the effect of snow load is often not factored in during regular use. While vehicles traverse the bridge, the weight of the snow and its potential impact on the structure are typically overlooked. Nevertheless, during the design and construction phases, engineers ensure that the bridge is robust enough to withstand anticipated snow loads, safeguarding its stability and safety over its operational lifespan.

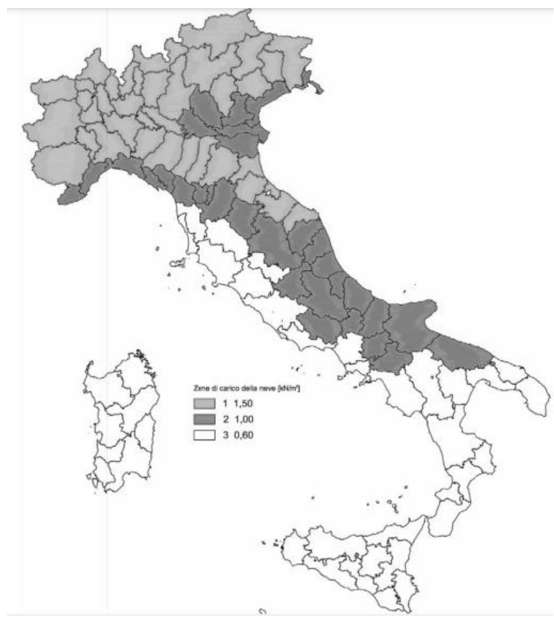

q_{sk} valore caratteristico della neve al suolo 2.16 [kN/m²]

2.5. Seismic Load :

2.5.1. Seismic force evaluation :

The design of seismic actions is derived based on the fundamental seismic hazard characteristics of the construction site. This constitutes a crucial informational element for determining seismic action. The hazard is determined by the highest anticipated horizontal acceleration (a_g) in open field conditions on a rigid reference site with a flat topographic surface. Furthermore, with respect to the probability of surpassing a peak ground acceleration within the period V_R, it involves the ordinates of the acceleration elastic response spectrum associated with Se (T).

2.5.1.1. Function Classification :

The constructions are divided into different classes in terms of seismic actions.

2.5.1.2. Limit State :

Limit states, both in terms of serviceability and ultimate conditions, are determined by evaluating the overall performance of the entire construction, considering both structural and non-structural elements.

………

2.5.1.3. Design Parameters :

The determination of the elastic response spectrum is defined from the following parameters:

- a_g represents the maximum acceleration experienced by ground during earthquake.
- F_0 frequency response at maximum spectrum acceleration under horizontal acceleration.
- T^*_C effective period considering damping-determination of the start period of the constant velocity under horizontal acceleration.

The spectral shapes anticipated by NTCs are identified by:

- V_R service life of the structure
- P_{VR} the probability of surpassing the service life

Expressing the seismic hazard is conveniently done by employing the return period (TR) as a parameter denoted in years. Maintaining the service life V_R constant, the connection between TR and P_{VR}, can be easily described through the following expression:

$$T_R = -\frac{V_R}{\ln(1 - P_{VR})}$$

To determine the design seismic action in accordance with Italian technical regulations, a simplified approach was applied. This method employes the elastic response spectrum for the horizontal components, based on the recognition of reference subsoil categories, topographical conditions, and probability of exceedance.

Categoria sottosuolo	S_S	C_C
A	1,00	1,00
B	$1{,}00 \le 1{,}40 - 0{,}40 \cdot F_o \cdot \frac{a_g}{g} \le 1{,}20$	$1{,}10 \cdot (T_C^*)^{-0{,}20}$
C	$1{,}00 \le 1{,}70 - 0{,}60 \cdot F_o \cdot \frac{a_g}{g} \le 1{,}50$	$1{,}05 \cdot (T_C^*)^{-0{,}33}$
D	$0{,}90 \le 2{,}40 - 1{,}50 \cdot F_o \cdot \frac{a_g}{g} \le 1{,}80$	$1{,}25 \cdot (T_C^*)^{-0{,}50}$
E	$1{,}00 \le 2{,}00 - 1{,}10 \cdot F_o \cdot \frac{a_g}{g} \le 1{,}60$	$1{,}15 \cdot (T_C^*)^{-0{,}40}$

Table 4. S_S and C_C expressions

The following expressions outline the elastic acceleration response spectrum (S_e) for the following horizontal component of seismic motion.

$0 \leq T < T_B$ $\qquad S_e(T) = a_g * S * \eta * F_0 * \left[\frac{T}{T_B} + \frac{1}{\eta * F_0}\left(1 - \frac{T}{T_B}\right)\right]$

$T_B \leq T < T_C$ $\qquad S_e(T) = a_g * S * \eta * F_0$

$T_C \leq T < T_D$ $\qquad S_e(T) = a_g * S * \eta * F_0 * \left[\frac{T_C}{T}\right]$

$T_D \leq T$ $\qquad S_e(T) = a_g * S * \eta * F_0 * \left[\frac{T_C * T_D}{T^2}\right]$

Where,

- S, it is the coefficient that considers the subsoil category and topographical, as detailed in the following report:
  $S = S_S * S_T$
- η, is the factor that modifies the elastic spectrum for conventional viscous damping coefficients ζ other than 5%, as determined by the following relationship:

$$\eta = \sqrt{\frac{10}{(5 + \zeta)}} \geq 0.55$$

  where ζ (expressed as a percentage) it is assessed based on material, structural type, and foundation soil.
- F_0, this factor quantifies the maximum spectral amplification on a rigid horizontal reference site and maintains a minimum value of 2.2.
- T_0, this is the period corresponding to the initiation of the constant-speed of the spectrum, calculated as follows:

$$T_C = C_C * T_C^*$$

- T_B, the period associated with initiation of the constant accelerating section of the spectrum is calculated based on the provided ratio:

$$T_C = \frac{T_C}{3}$$

- $T_{D,}$ this represents the period at the start of the constant-shift section of the spectrum, expressed in seconds according to the given relationship:

$$T_C = 4 * \frac{a_g}{g} + 1.6$$

Categoria topografica	Ubicazione dell'opera o dell'intervento	S_T
T1	-	1,0
T2	In corrispondenza della sommità del pendio	1,2
T3	In corrispondenza della cresta di un rilievo con pendenza media minore o uguale a 30°	1,2
T4	In corrispondenza della cresta di un rilievo con pendenza media maggiore di 30°	1,4

Table 5. Maximum values of the S_T topographic amplification coefficient

The site is located in a seismic zone with a low-risk classification. Considering this location, the subsoil category is designated as B, and the topographic category is specified as T1.

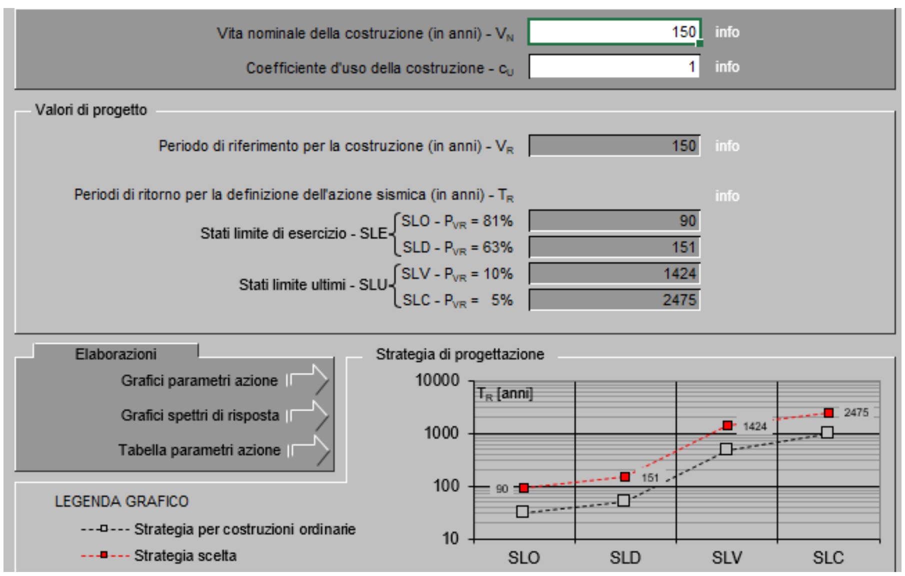

Figure 40. Service life determination

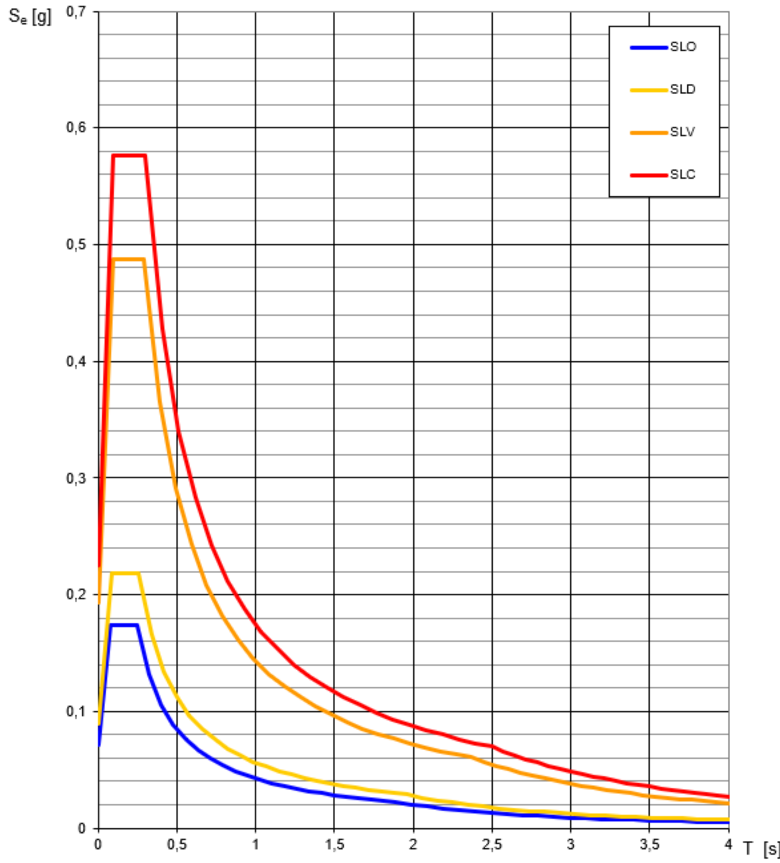

Figure 41. Limit state curve

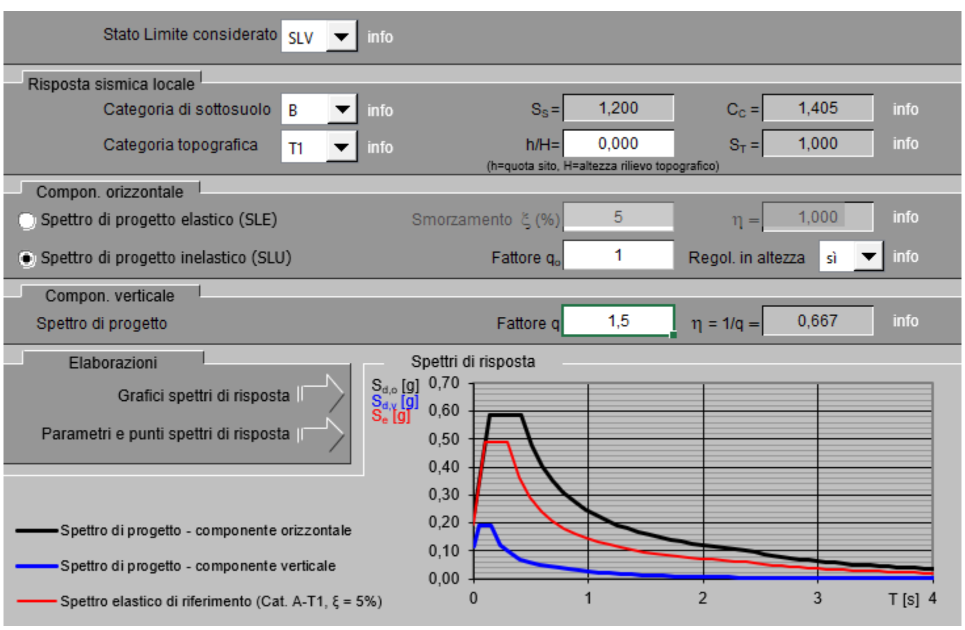

Figure 42. Limit state parameters

Limit State	Probability of exceedence	T_R $[years]$	a_g $[g]$	F_0 $[-]$	T_C^* $[s]$
SLO	81%	90	0,072	2,419	0,246
SLD	63%	151	0,090	2,433	0,257
SLV	10%	1424	0,193	2,531	0,294
SLC	5%	2475	0,225	2,559	0,303

Table 6. Limit state parameters and values

The 4 limit states consideration is based on the subsoil category and topographic condition, B and T1 respectively, the dependent and independent parameters with the graph of each one is as follow:

SLV:

a_g	0,193 g
F_o	2,531
T_C^*	0,294 s
S_S	1,200
C_C	1,405
S_T	1,000
q	1,000

Table 7. Independent parameters SLV

S	1,200
η	1,000
T_B	0,138 s
T_C	0,413 s
T_D	2,371 s

Table 8. Dependent parameters SLV

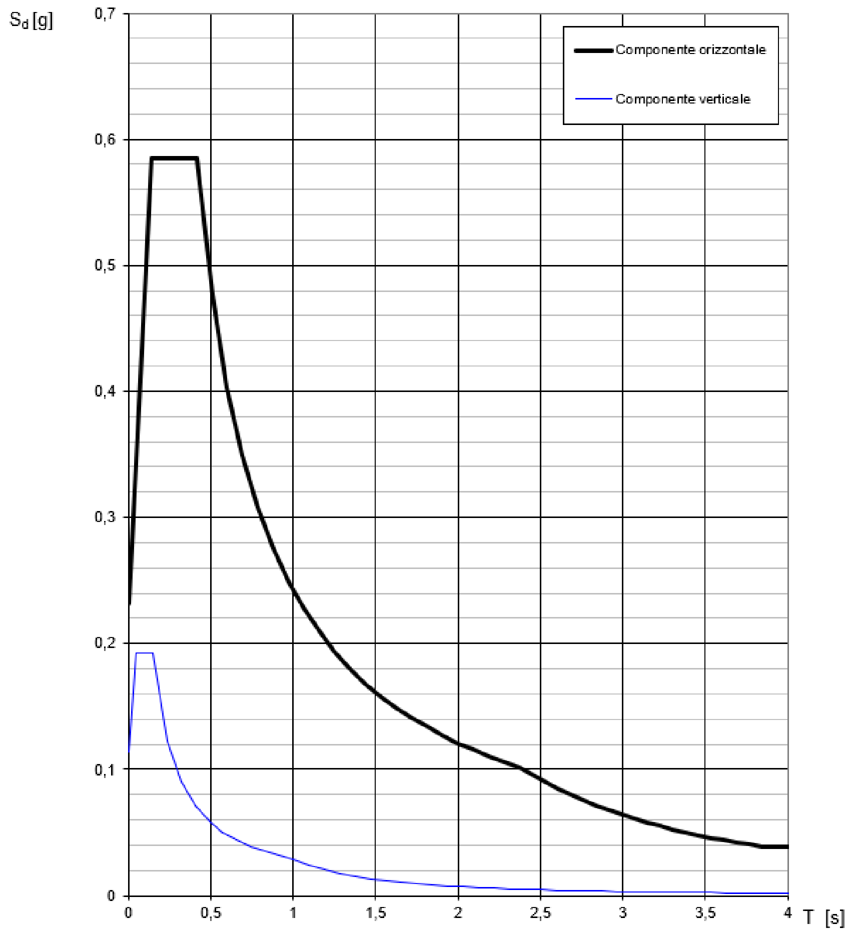

Figure 43. Response Spectra for SLV

SLO:

a_g	0,072 g
F_o	2,419
T_C^*	0,246 s
S_S	1,200
C_C	1,457
S_T	1,000
q	1,000

Table 9. Independent parameters SLO

S	1,200
η	1,000
T_B	0,119 s
T_C	0,358 s
T_D	1,887 s

Table 10. Dependent parameters SLO

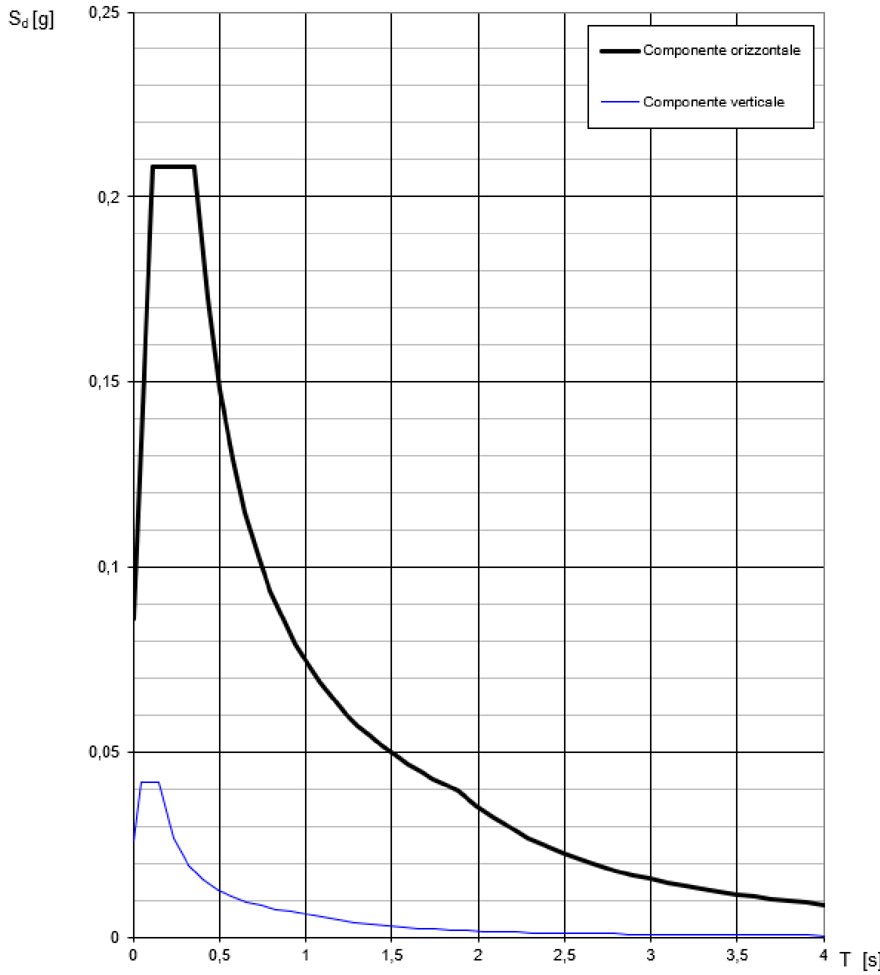

Figure 44. Response Spectra for SLO

SLD:

a_g	0,090 g
F_o	2,433
T_C^*	0,257 s
S_S	1,200
C_C	1,444
S_T	1,000
q	1,000

Table 11. Independent parameters SLD

S	1,200
η	1,000
T_B	0,124 s
T_C	0,371 s
T_D	1,960 s

Table 12. Dependent parameters SLD

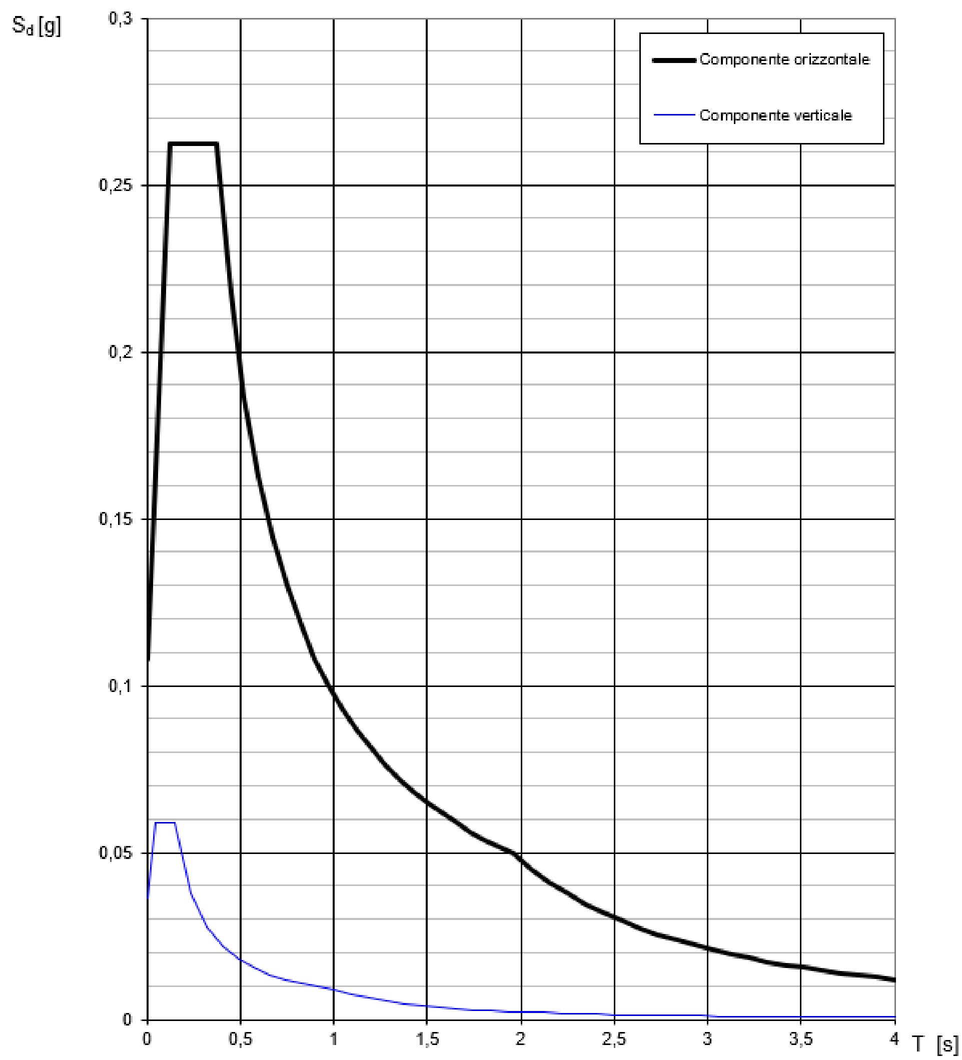

Figure 45. Response Spectra for SLD

SLC:

a_g	0,225 g
F_o	2,559
T_C^*	0,303 s
S_S	1,170
C_C	1,397
S_T	1,000
q	1,000

Table 13. Independent parameters SLC

S	1,170
η	1,000
T_B	0,141 s
T_C	0,423 s
T_D	2,500 s

Table 14. Dependent parameters SLC

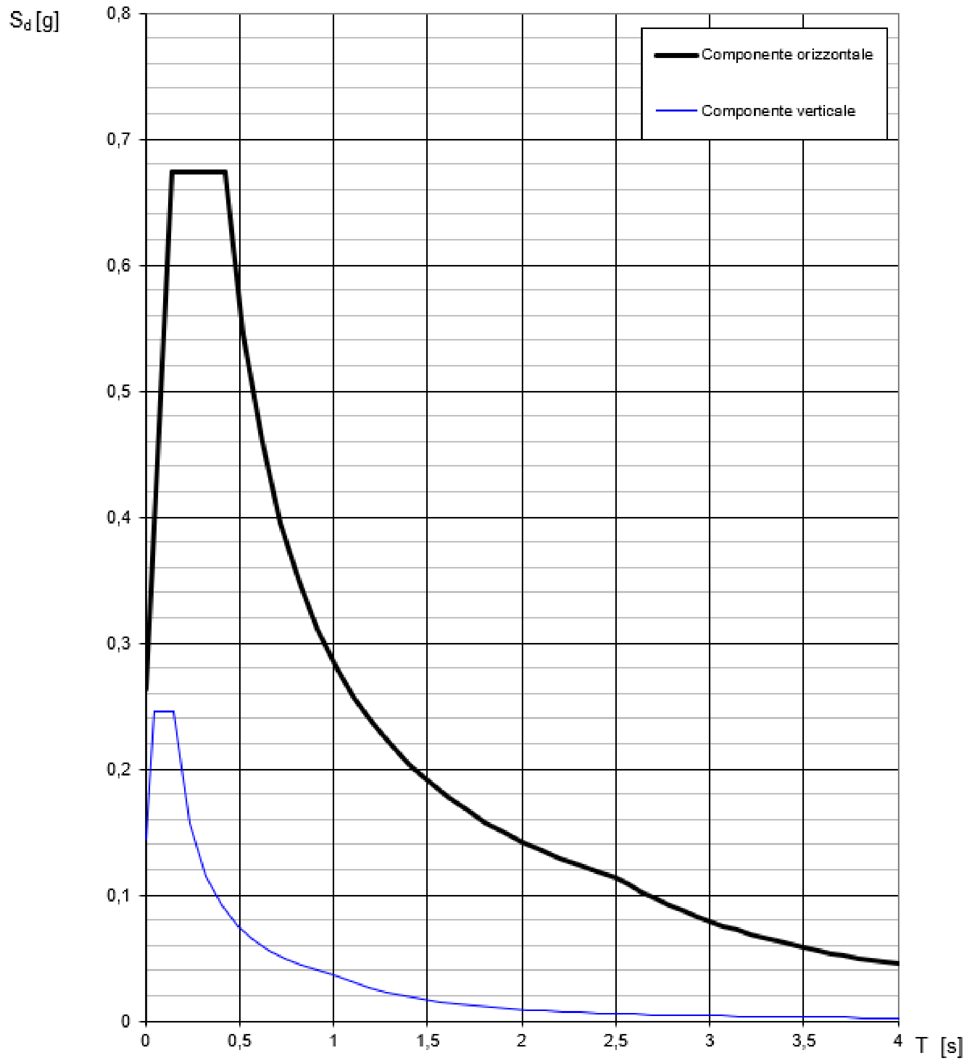

Figure 46. Response Spectra for SLC

2.6. Temperature Effect :

Daily and seasonal temperature fluctuations, coupled with sun radiation and convection, lead to variations in the temperature distribution within specific structural elements. The intensity of thermal effects is typically influenced by factors including the climatic conditions of the site, exposure, the total mass of the structure, and the possible existence of insulating non-structural elements.

Figure 47. Zones

Bridge location is in zone I:

$$T_{min} = -15 - 4 \cdot a_s / 1000$$

$$T_{max} = 42 - 6 \cdot a_s / 1000$$

Tmin:	Tmax:
-17,168	38,748

2.6.1 Uniform Thermal Variation :

The uniform temperature components is of course, determined by the minimum and maximum temperatures that the bridge experiences. As per the guideline outline in the European standard EN 1991-1-5, which outlines the temperature variation for a composite deck of type 2, the maximum and minimum values can be specified as:

$$T_{e,min} = T_{min} + 4 = -17.168 + 4 = -13.168 \quad ℃$$

$$T_{e,max} = T_{max} + 4 = 38.748 + 4 = 42.748 \quad ℃$$

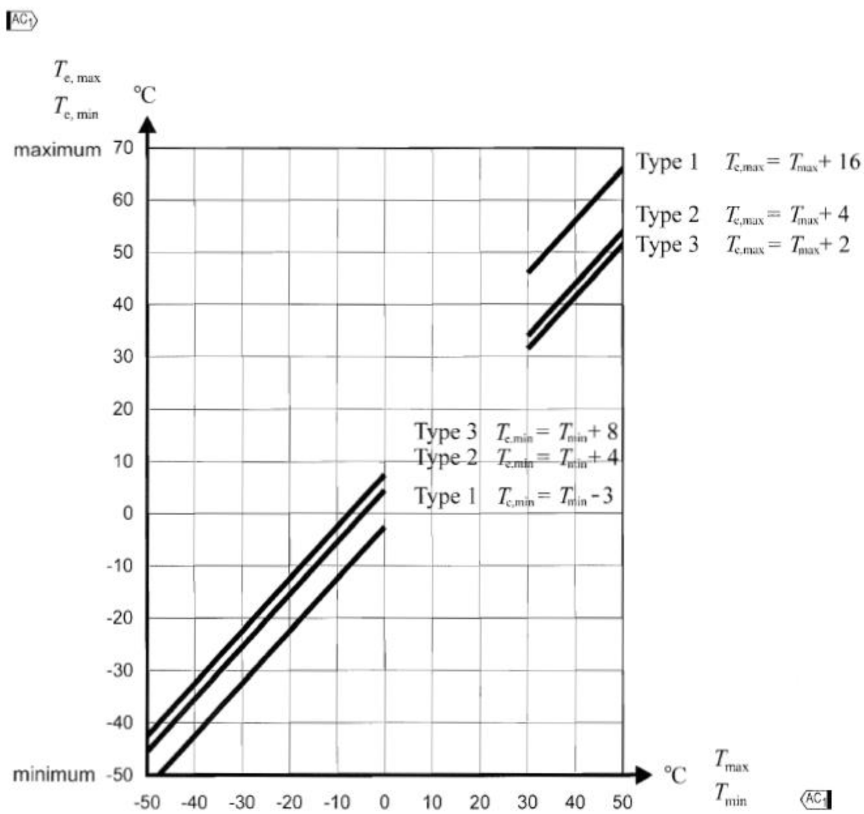

Figure 48. Temperature

2.6. Shrinkage Effect :

Shrinkage and creep are time-dependent properties of concrete that are typically factored into the verification of serviceability limit states (SLS). When accounted for, they should be assessed within the quasi-permanent combination of the design scenario being considered.

When considering shrinkage effects in structural design, it's important to distinguish between determinate and indeterminate systems. Determinate systems are those where the external reactions and internal forces can be completely determined using equilibrium equations alone.

In the determinate system, shrinkage-induced deformations can directly affect member lengths and may lead to localized stresses or distortions. Since determinates systems lack redundancy, any changes in member dimensions due to shrinkage can have a direct impact on the overall structural response.

Procedure:

In the composite structures, the concrete slab's shrinkage-induced shortening is partially restrained by the steel beam. If the steel beam had zero stiffness, the concrete would freely shorten, resulting in zero tensile stress ($\sigma_{ct} = 0$).

Conversely, if the steel beam had infinite stiffness, shrinkage would be entirely prevented, leading to concrete experiencing a tensile stress ($\sigma_{ct} = E_c^* \varepsilon_{sh}$), where $E_c^* = \frac{E_a}{n_L}$ is a fictitious Young's modulus considering creep effects.

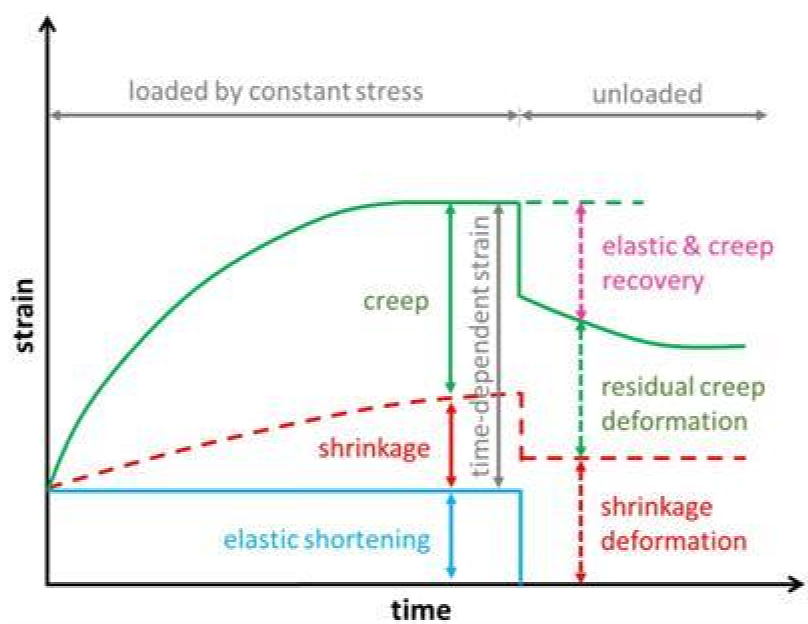

Figure 49. Strain-time

Concrete and steel stresses may be evaluated using the following approximate procedure:

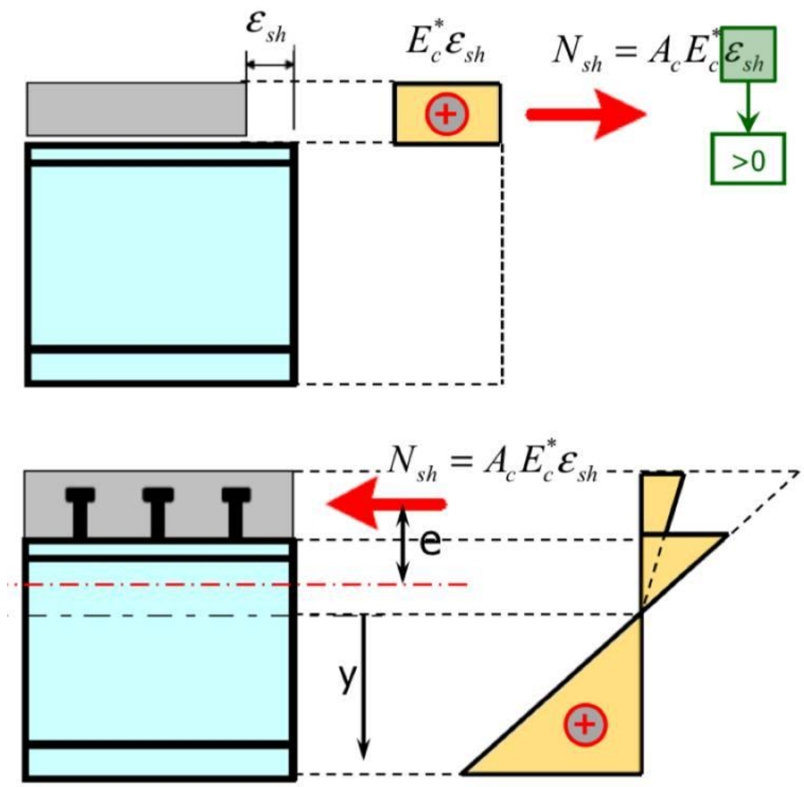

Figure 50. Shrinkage procedure-a

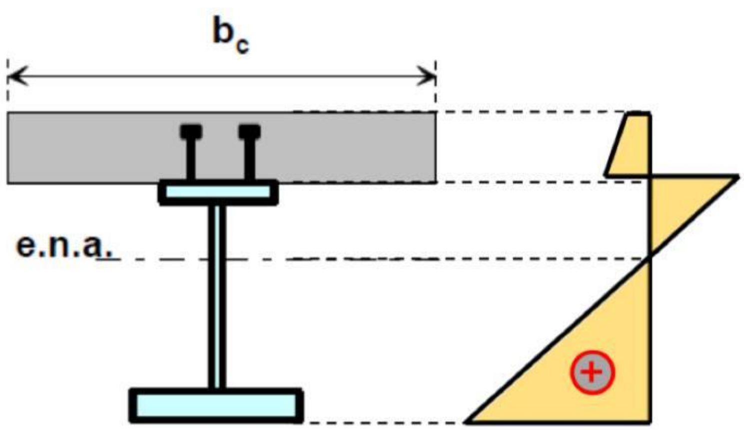

Figure 51. Shrinkage procedure-b

In statically indeterminate system, the state of stress can be evaluated as in determinate system, whereas the reverse of the force N_{sh} on the composite structures gives secondary effects.

Note: Shrinkage should be considered only in uncracked areas.

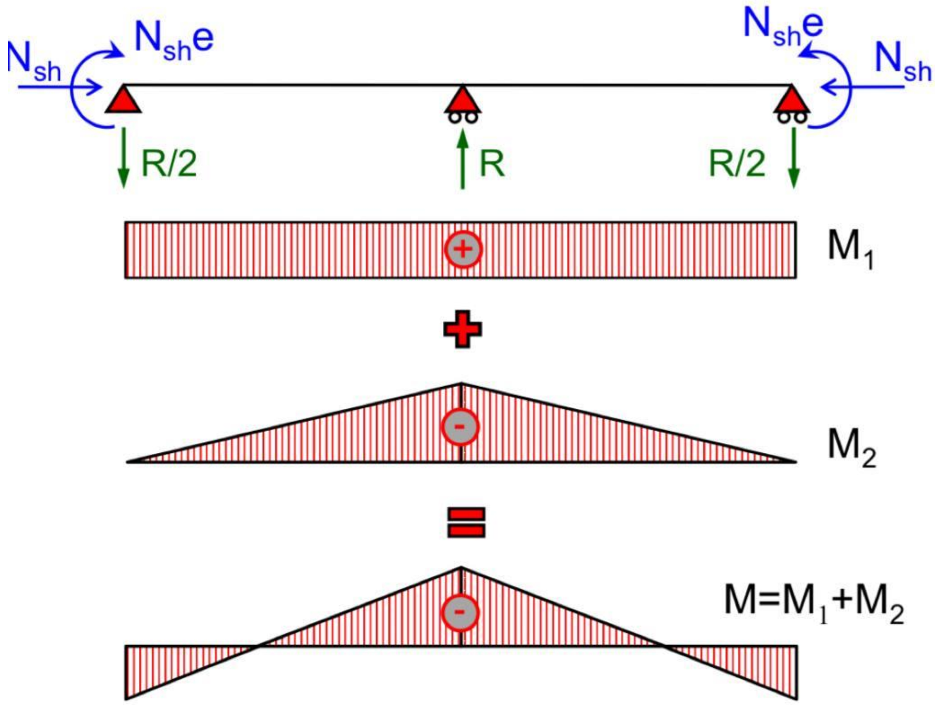

Figure 52. Indeterminate system

Where,

$N_{sh} = \varepsilon_{sh} * E * A_c$

M_1 : Statically determinate

M_2 : due to statically indeterminate from the extra reaction in the middle (reaction is not zero)

4. Load Combination Criterion :

The load combinations criterion refers to the rules and guidelines used in structural engineering to determine how different types of loads should be combined to assess the overall response and safety of a structure. These combinations consider factors including load types (such as dead load, live load, wind load, snow load, etc.)

Load combinations play a vital role in assessing how structures perform under various loading scenarios, ensuring they can withstand the most challenging conditions they might face over their operational lifespan. These combinations are usually derived from engineering standards and regional building codes.

There are two main categories of limit states :

1) Ultimate limit state (ULS) : It ensures the safety and stability of a structure when subjected to serve loading scenarios like earthquakes, high winds, or other extreme events. These states primarily assess the structure's capacity to resist collapse or failure.

2) Service limit state (SLS) : It address the structural performance during regular operational conditions. These states encompass considerations like deflection, vibration, cracking, and other types of deformation that could impact the structure's functionality, appearance, or user comfort.

Load combination	Principal load	Factored load combination
1	Dead	$1.4D + 1.0T$
2	Dead + live	$1.25D + 1.5L + (0.4W \text{ or } 0.5S) + 1.5H + 1.0T$
3	Dead + snow	$1.25D + 1.5S + (0.5L \text{ or } 0.4W) + 1.5H + 1.0T$
4	Dead + wind	$1.25D + 1.35W + (0.5L \text{ or } 0.5S) + 1.5H + 1.0T$
5	Dead counteracting L, S, or W	$0.9D + (1.5H \text{ or } 1.5L \text{ or } 1.5S \text{ or } 1.35W)$

Note: In load combinations 2 and 5, a live load factor of 1.25 may be used for liquids in tanks. In load combinations 3 and 4, a companion load factor of 0.5 shall be 1.0 for storage occupancies, and the factored companion live load shall not be less than the sustained live load, L_S.

Table 15. Load Combination

To assess crack distance or maximum spacing between bars conveniently and indirectly, NTC 18 provides two crucial tables for quickly verifying reinforcements. These tables are depicted below:

Steel stress[2] [MPa]	Maximum bar size [mm] w_k= 0,4 mm	w_k= 0,3 mm	w_k= 0,2 mm
160	40	32	25
200	32	25	16
240	20	16	12
280	16	12	8
320	12	10	6
360	10	8	5
400	8	6	4
450	6	5	-

Notes: 1. The values in the table are based on the following assumptions:
AC1 c = 25mm; $f_{ct,eff}$ = 2,9MPa; h_{cr} = 0,5h; (h-d) = 0,1h; k_1 = 0,8; k_2 = 0,5; k_c = 0,4; k = 1,0; k_t = 0,4 and k_4= 1,0 AC1
2. Under the relevant combinations of actions

Table 16. Maximum bar size NTC18

Steel stress[2] [MPa]	Maximum bar spacing [mm] w_k=0,4 mm	w_k=0,3 mm	w_k=0,2 mm
160	300	300	200
200	300	250	150
240	250	200	100
280	200	150	50
320	150	100	-
360	100	50	-

Table 17. Maximum bar spacing NTC18

4.1. Safety Control :

Safety control is paramount in the field of engineering and construction, as it ensures structures meet the standards and regulations. It involves various approaches and protocols geared towards recognizing, evaluating, and lessening risks linked to structural planning. Through the effective safety protocols, engineers can reduce the probability of structural malfunctions.

In the assessment of construction safety, scientifically probabilistic criteria must be adopted and proven. This entails utilizing standardized partial safety coefficients for limit states based on use, a method known as the first level method.

Within the semi-probabilistic method for limit states, structural safety is verified by comparing the resistance and effects of actions. This involves representing the resistance of materials and actions through characteristic value, R_{kj} , E_{kj} , respectively, defined as the lower fractile of resistances and the fractile of actions that minimize risk. Typically, a fractile of 5% is assumed.

Ultimately, safety control encompasses a range of measures aimed at protecting against various hazards, including natural disasters and human error. By integrating risk assessment, and ongoing monitoring and maintenance practices, safety control ensures the reliability, durability, and sustainability of infrastructure.

$$R_d \geq E_d$$

Where,

R_d, is the design resistance

E_d, is the project value of the effect of the actions

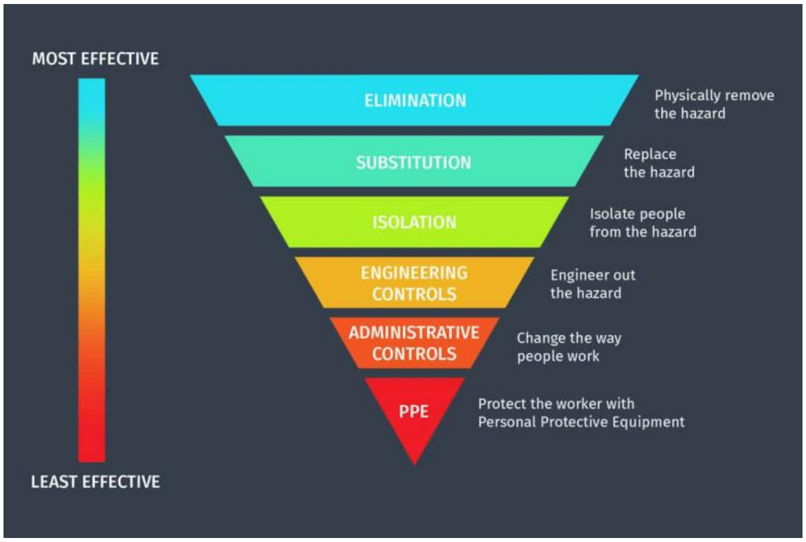

Figure 53. Safety Control

4.2. Load Combination :

Chapter five of the NTC18 addresses general criteria and technical guidelines for designing and constructing road bridges and railways. Specifically, for road bridges, alongside defining key geometric features, it outlines various potential actions and assigns load patterns corresponding to traffic-induced factors. The load patterns for both road and rail bridges, utilized for static and fatigue assessments, typically align with UNI EN 1991-2 schemes. Additionally, the term *bridges* encompasses structures known by specific names such as viaducts, underpasses, overpasses, and elevated roads, depending on their intended use. In this regulation context, the roadway width of a bridge refers to the distance measured orthogonally to the road axis.

Actions considered during road bridge design encompass permanent actions, imposed distortions and deformations, traffic-induced variable actions, thermal fluctuations, hydrodynamic forces, wind and snow loads, railings' effect, passive resistance from restraints, vehicular impact on safety barriers, seismic forces and accidental occurrences. Load combinations for verification are determined to ensure safety. For calculating characteristic values of traffic-induced actions, combinations of specific factor outlined in the table below are generally employed.

	Loads on carriageway					Loads on footways
	Vertical			Horizontal		Vertical
Group of actions	Main action LM1-2-3-4-6	Special vehicles	Crowd	Braking Accel.	Centrifugal	Uniform
1	Characteristic value					2.5 kN/m²
2a	Frequent value			Characteristic value		
2b	Frequent value				Characteristic value	
3 (*)						5.0 kN/m²
4 (**)			5.0 kN/m²			5.0 kN/m²
5(***)	To be defined in design	Characteristic value				
(*) Only for footbridges						
(**) Only for urban bridges						
(***) Only if special vehicles are taken into account						

Table 18. Characteristics action value due traffic loads

		Coefficiente	EQU[(1)]	A1	A2
Azioni permanenti g_1 e g_3	favorevoli sfavorevoli	γ_{G1} e γ_{G3}	0,90 1,10	1,00 1,35	1,00 1,00
Azioni permanenti non strutturali [(2)] g_2	favorevoli sfavorevoli	γ_{G2}	0,00 1,50	0,00 1,50	0,00 1,30
Azioni variabili da traffico	favorevoli sfavorevoli	γ_Q	0,00 1,35	0,00 1,35	0,00 1,15
Azioni variabili	favorevoli sfavorevoli	γ_{Qi}	0,00 1,50	0,00 1,50	0,00 1,30
Distorsioni e presollecita-zioni di progetto	favorevoli sfavorevoli	$\gamma_{\varepsilon 1}$	0,90 1,00[(3)]	1,00 1,00[(4)]	1,00 1,00
Ritiro e viscosità, Cedimenti vincolari	favorevoli sfavorevoli	$\gamma_{\varepsilon 2}$, $\gamma_{\varepsilon 3}$, $\gamma_{\varepsilon 4}$	0,00 1,20	0,00 1,20	0,00 1,00

Table 19. Partial safety coefficients for ULS load combinations

Where,

γ_{G1}, partial coefficient for dead load.

γ_{G2}, partial coefficient for not structural loads.

γ_Q, partial coefficient for traffic loads.

Azioni	Gruppo di azioni (Tab. 5.1.IV)	Coefficiente ψ_0 di combinazione	Coefficiente ψ_1 (valori frequenti)	Coefficiente ψ_2 (valori quasi permanenti)
Azioni da traffico (Tab. 5.1.IV)	Schema 1 (carichi tandem)	0,75	0,75	0,0
	Schemi 1, 5 e 6 (carichi distribuiti	0,40	0,40	0,0
	Schemi 3 e 4 (carichi concentrati)	0,40	0,40	0,0
	Schema 2	0,0	0,75	0,0
	2	0,0	0,0	0,0
	3	0,0	0,0	0,0
	4 (folla)	--	0,75	0,0
	5	0,0	0,0	0,0
Vento	a ponte scarico SLU e SLE	0,6	0,2	0,0
	in esecuzione	0,8	0,0	0,0
	a ponte carico SLU e SLE	0,6	0,0	0,0
Neve	SLU e SLE	0,0	0,0	0,0
	in esecuzione	0,8	0,6	0,5
Temperatura	SLU e SLE	0,6	0,6	0,5

Table 20. Coefficients Ψ for variable actions for road and pedestrian bridges

4.3. ULS and SLS Load Combination :

The following combinations of actions are defined for the purpose of checking the limit states :

1) Fundamental combination, generally used for ultimate limit states (ULS)

$$\gamma_{G1} * \mathrm{G}_1 + \gamma_{G2} * \mathrm{G}_2 + \gamma_{Q1} * \mathrm{Q}_{k1} + \gamma_{Qw} * \Psi_{02} * \mathrm{Q}_{k2} + \gamma_{Q3} * \Psi_{03} * \mathrm{Q}_{k3} + \cdots$$

2) Characteristics combination (rare), generally used for irreversible limit state (SLS)

$$\mathrm{G}_1 + \mathrm{G}_2 + \mathrm{Q}_{k1} + \Psi_{02} * \mathrm{Q}_{k2} + \Psi_{03} * \mathrm{Q}_{k3} + \cdots$$

3) Frequent combination, generally used for reversible operating limit state (SLS)

$$\mathrm{G}_1 + \mathrm{G}_2 + \Psi_{11} * \mathrm{Q}_{k1} + \Psi_{22} * \mathrm{Q}_{k2} + \Psi_{23} * \mathrm{Q}_{k3} + \cdots$$

4) Quasi-permanent combination, generally used for long-term effects (SLS)

$$\mathrm{G}_1 + \mathrm{G}_2 + \Psi_{21} * \mathrm{Q}_{k1} + \Psi_{22} * \mathrm{Q}_{k2} + \Psi_{23} * \mathrm{Q}_{k3} + \cdots$$

5) Exceptional combination, used for the final limit states related to exceptional actions A.

$$\mathrm{G}_1 + \mathrm{G}_2 + \mathrm{A}_D + \Psi_{21} * \mathrm{Q}_{k1} + \Psi_{22} * \mathrm{Q}_{k2} + \Psi_{23} * \mathrm{Q}_{k3} + \cdots$$

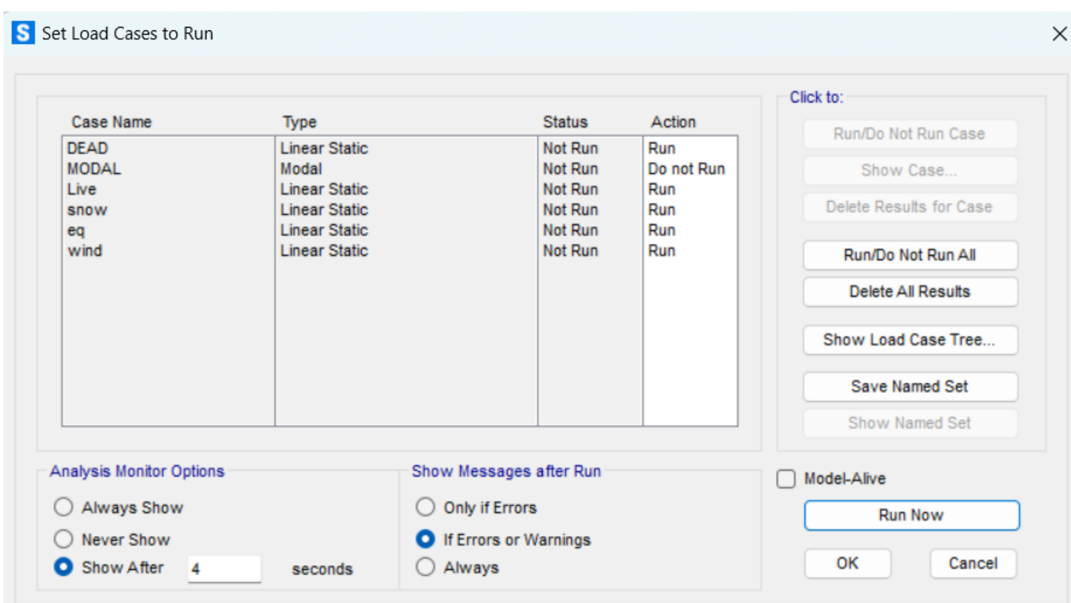

Table 21. SAP2000 Load cases

4.4. Seismic Load Combination :

The preferred method for evaluating the impact pf seismic forces on both dissipative and non-dissipative systems is through modal analysis using response spectrum or dynamic linear analysis. This linear dynamic analysis involves several steps:

- Identifying the vibration modes of the structure through modal analysis.
- Calculating the effects of seismic forces for each detected vibration mode based on the design response spectrum.
- Combining these effects to assess overall seismic performance.

All modes with significant portion of mass involvement should be accounted for. Typically, this entails considering modes with a mass contribution exceeding 5% and ensuring that the cumulative mass participation of selected modes exceeds 85%.

The final checks for operating limit state, suggested by the technical regulations:

$$G_1 + G_2 + E + \sum \Psi_{2j} * Q_{kj}$$

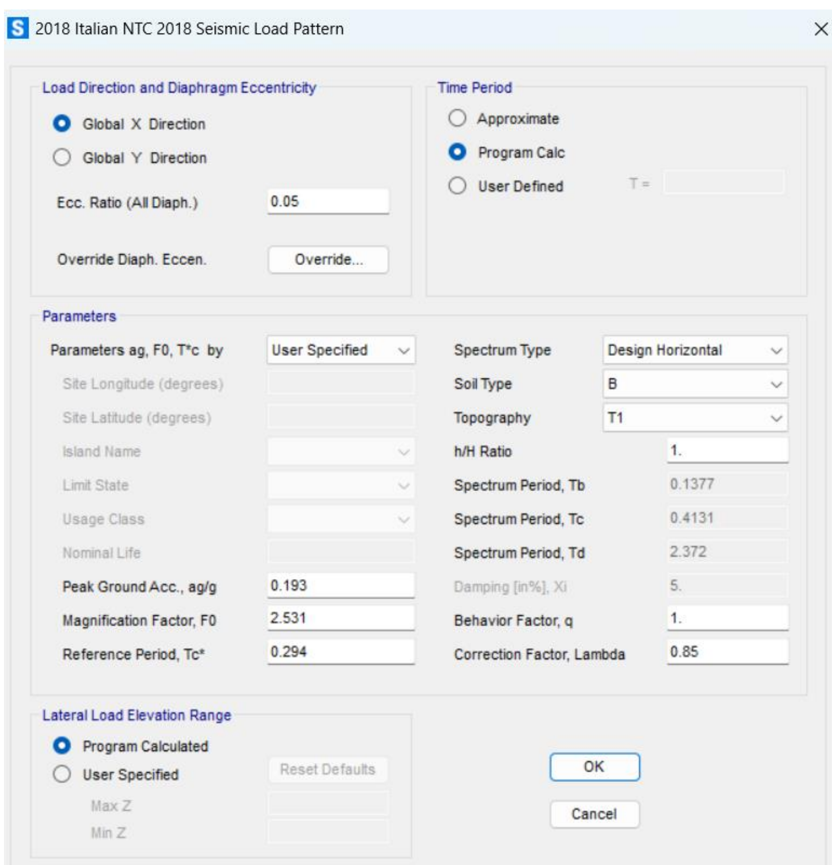

Table 22. Seismic load combination

5. Stress Analysis:

After all the calculations and regulations in the first part, the bridge has been modeled in the Sap2000 in order to verify and define the result of steel decks, concrete piers and the cables.

First Scenario:

In the initial design configuration, utilizing IPE profiles, there were four primary longitudinal beams, complemented by four horizontal transverse beams and four transverse breaces as shown below:

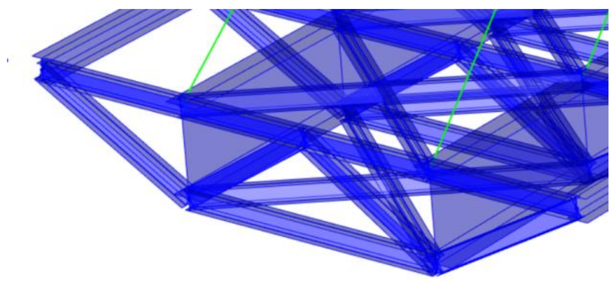

Figure 54. 1st scenario-3d view

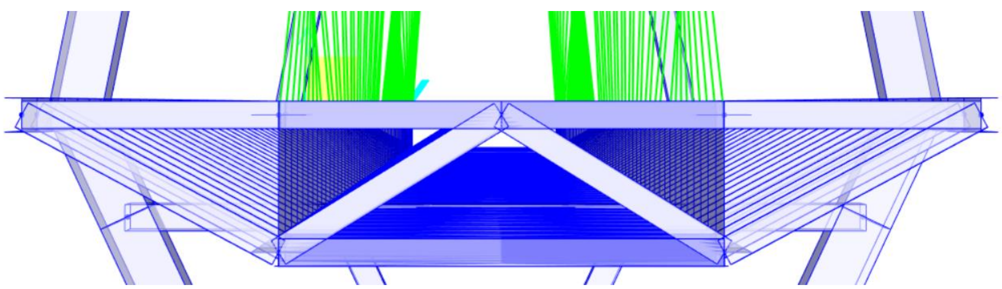

Figure 55. 1st scenario-cross section

Second Scenario:

In the second phase of the design proceess, we made a significant shift by adopting a reticular section for the bridge structure. This involved a change in the cross-section profile, and for this purpose, we chose to utilize HEB profiles. This alteratuon in the design aimed to enhance structural performance, taking advantage of the specific characteristics offered by HEB profiles in compariosn to the previous IPE profiles.

The section became as follow:

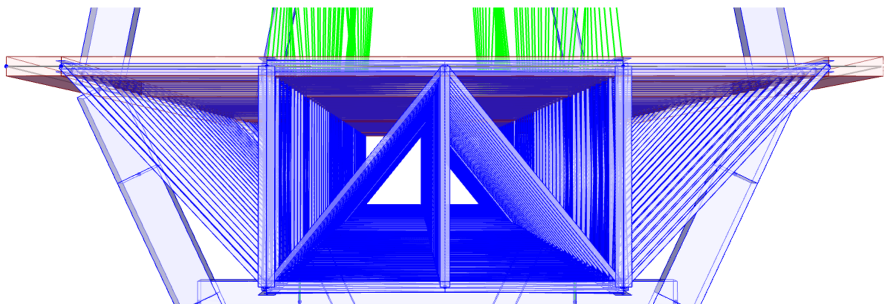

Figure 56. 2nd scenario- cross section

The final cross-sectional configuration adopted excluded the central vertical beam, eliminating the need for it. This modification not only reduced weight substantially but also simplified the overal cross-section.

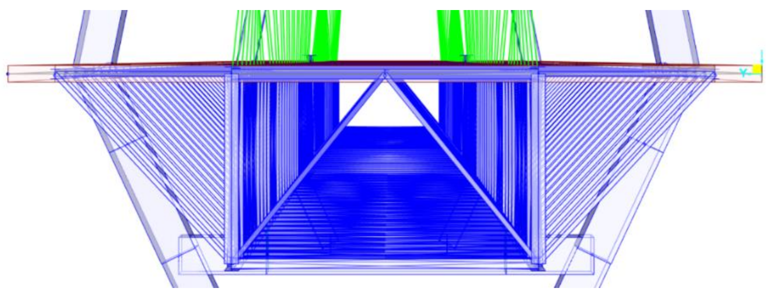

Figure 57. 2nd scenario-final cross section

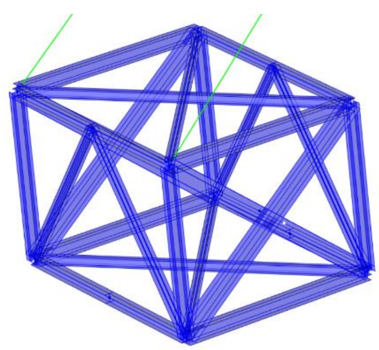

Figure 58. 2nd scenario-final 3d.view

5.1. Graphical Results :

These graphs present the outcomes derived from the finite element analysis conducted utilizing SAP2000. These visualizations encompass crucial parameters such as displacement and stresses. Additionally, considering the primary objective of this thesis, which is to optimize the steel deck elements represented by HEB profiles, the graphs also exhibit preliminary sections along with identified areas of concern or failure. These aspects will be further addressed and rectified in subsequent iterations of the optimization process.

5.1.1. Displacement:

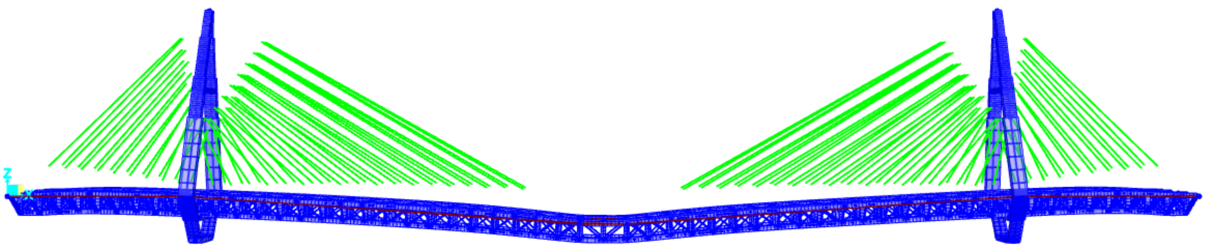

The vertical displacement at the center of the bridge is 24 cm.

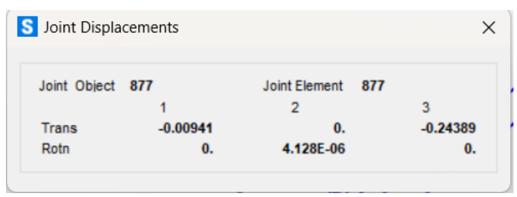

Figure 59. Maximum displacement

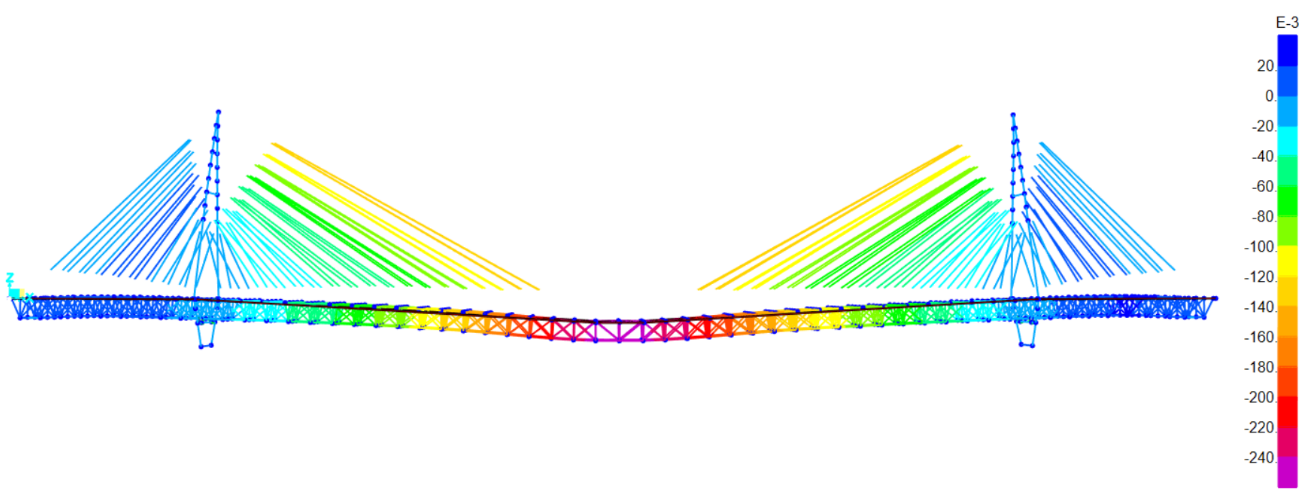

Figure 60. Whole bridge-Displacement

5.2. Different Load Combination Phases :

1) Dead Load only

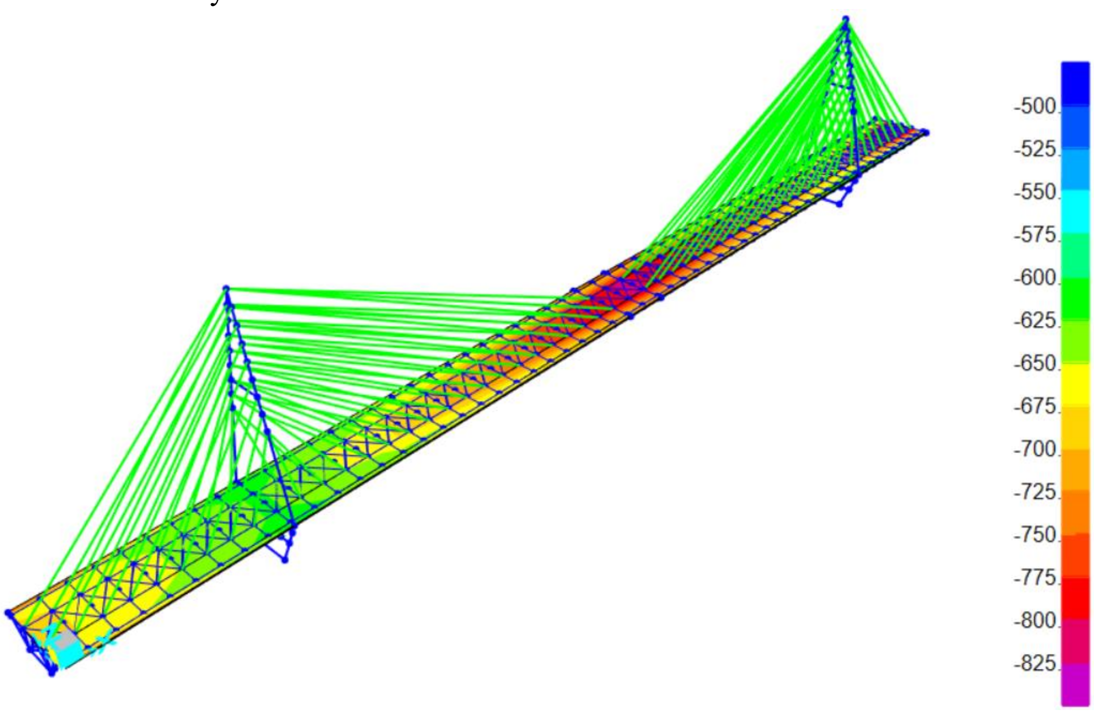

Figure 61. Shell Stress-Dead Load only

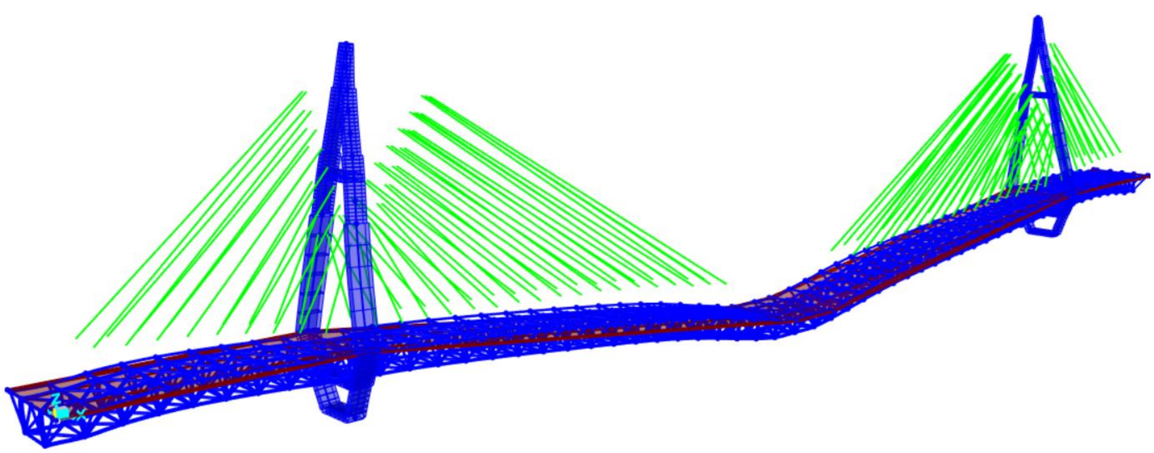

Figure 62. Deformation due to Dead Load only

2) Wind Load only :

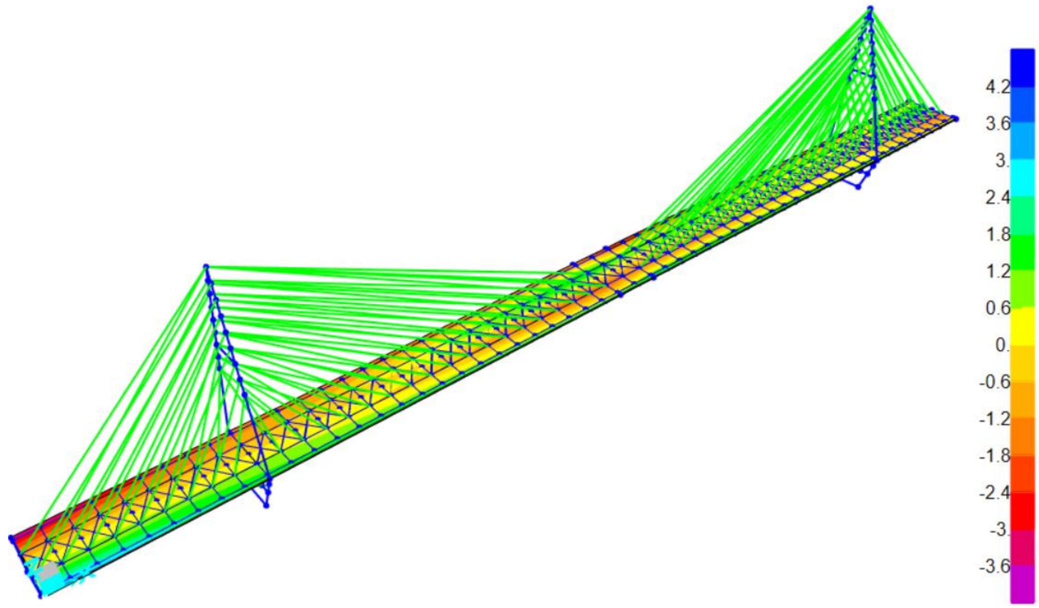

Figure 63. Shell stress-Wind load only

3) Earthquake only :

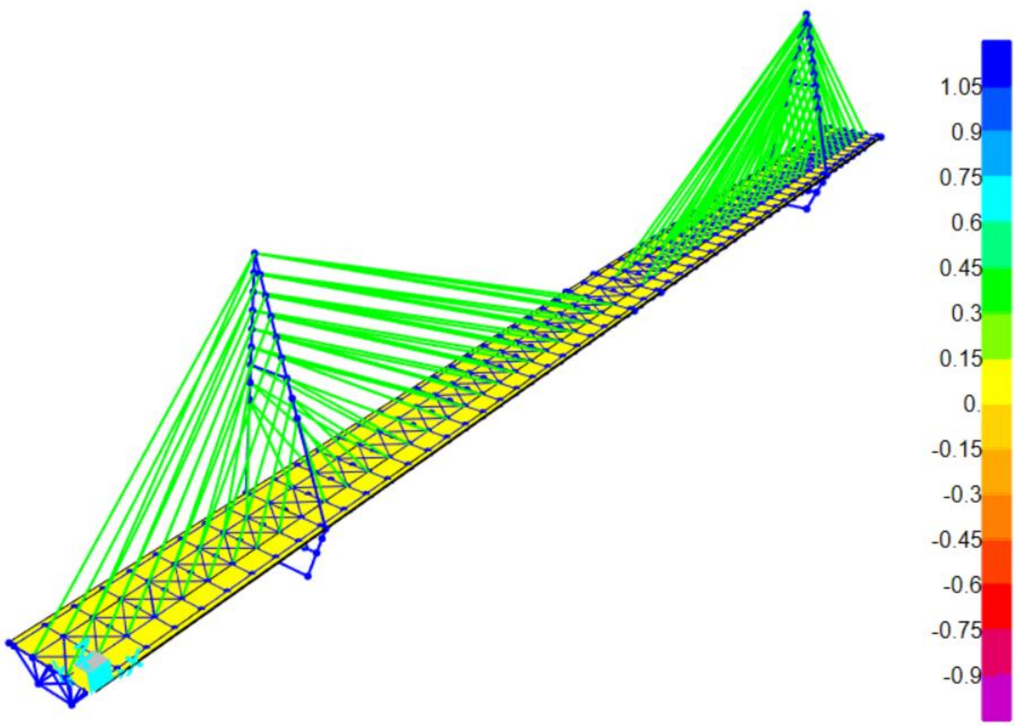

Figure 64. Shell stress-Earthquake only

4) Quasi-permanent combination :

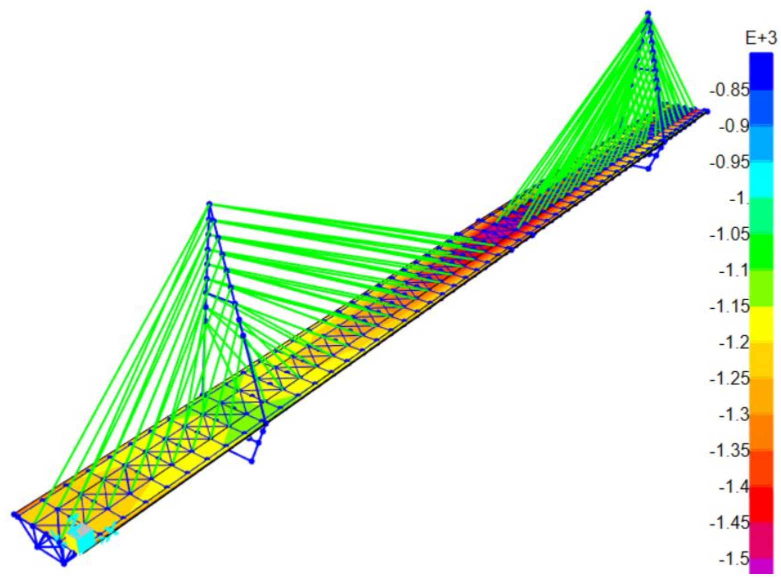

Figure 65. Shell stress / Quasi-permanent combination

5) Dead-Live-Wind Load :

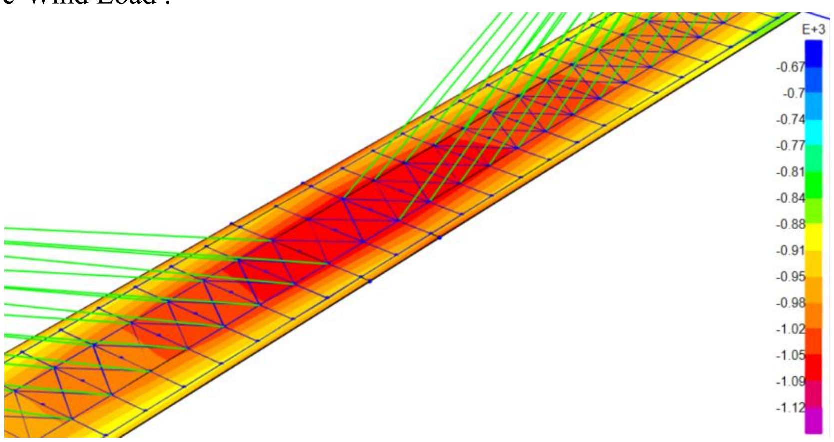

Figure 66. Shell stress of the Center part. Dead-Live-Wind Load

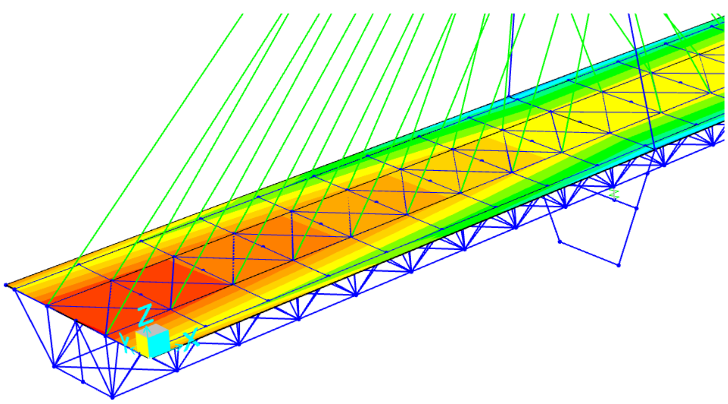

Figure 67. Shell stress of the Edge part. Dead-Live-Wind Load

5.3. Steel Verification :

The primary function of the main beams is to support the reinforced concrete slab, connected to them via shear connectors. Subsequently, we will present verifications pertaining to the most critical sections, particularly the central part of the bridge.

The analysis for the main beams will involve two approaches : initially, considering membrane resistance, and subsequently, ensuring there is no buckling or instability during various loading phases.

As outlined in the Italian technical regulations, structural element cross-sections are classified based on their rotational capacity denoted as $C_\theta = \frac{\theta_r}{\theta_y} - 1$, where θ_r and θ_y represent rotations corresponding to ultimate deformation and yield strength, respectively. The classification of structural steel element cross-sections is based on their ability to deform within the plastic field, resulting in the identification of four distinct classes of sections ranked by their rotational capacity.

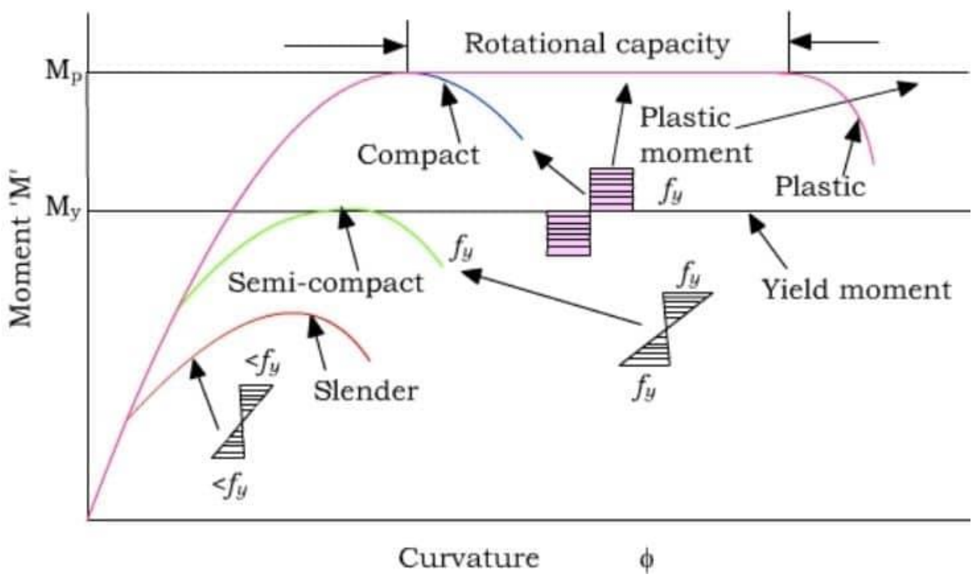

Figure 68. Cross Section Classification

Verification in the elastic field :

$$\sigma_{x,Ed}^2 + \sigma_{z,Ed}^2 - \sigma_{x,Ed}\sigma_{z,Ed} + 3\tau_{Ed}^2 \leq \left(\frac{f_{yk}}{\gamma_{M0}}\right)^2$$

Normal tensile stress at the acting point in the direction parallel to the axis of the element

Normal tensile stress at the acting point in the direction perpendicular to the axis of the member

Tangential tensile stress in the plane of the element

Internal compression parts			

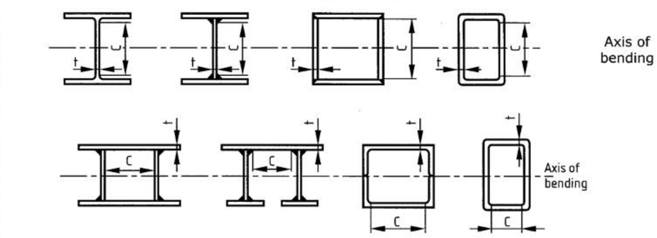

Class	Part subject to bending	Part subject to compression	Part subject to bending and compression
Stress distribution in parts (compression positive)	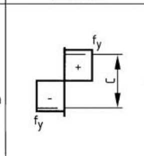	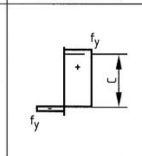	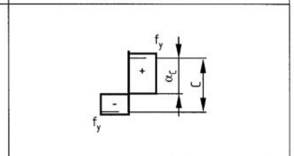
1	$c / t \le 72\varepsilon$	$c / t \le 33\varepsilon$	when $\alpha > 0,5 : c / t \le \frac{396\varepsilon}{13\alpha - 1}$ when $\alpha \le 0,5 : c / t \le \frac{36\varepsilon}{\alpha}$
2	$c / t \le 83\varepsilon$	$c / t \le 38\varepsilon$	when $\alpha > 0,5 : c / t \le \frac{456\varepsilon}{13\alpha - 1}$ when $\alpha \le 0,5 : c / t \le \frac{41,5\varepsilon}{\alpha}$
Stress distribution in parts (compression positive)	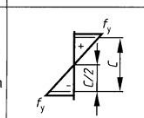	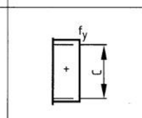	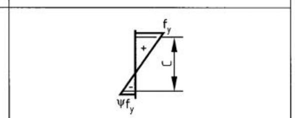
3	$c / t \le 124\varepsilon$	$c / t \le 42\varepsilon$	when $\psi > -1 : c / t \le \frac{42\varepsilon}{0,67 + 0,33\psi}$ when $\psi \le -1 : c / t \le 62\varepsilon (1 - \psi) \sqrt{(-\psi)}$

$\varepsilon = \sqrt{235 / f_y}$	f_y	235	275	355	420	460
	ε	1,00	0,92	0,81	0,75	0,71

*) $\psi \le -1$ applies where either the compression stress $\sigma < f_y$ or the tensile strain $\varepsilon_y > f_y / E$.

Table 23. Maximum width-to-thickness ratios for compression parts

Outstand flanges			

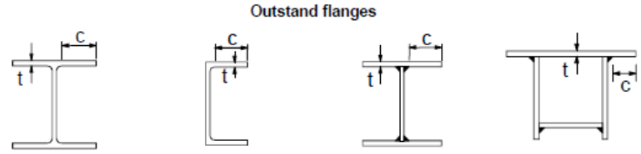

Rolled sections — Welded sections

Class	Part subject to compression	Part subject to bending and compression: Tip in compression	Part subject to bending and compression: Tip in tension
Stress distribution in parts (compression positive)	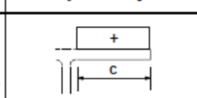	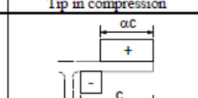	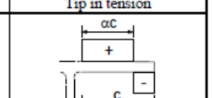
1	$c / t \le 9\varepsilon$	$c / t \le \frac{9\varepsilon}{\alpha}$	$c / t \le \frac{9\varepsilon}{\alpha\sqrt{\alpha}}$
2	$c / t \le 10\varepsilon$	$c / t \le \frac{10\varepsilon}{\alpha}$	$c / t \le \frac{10\varepsilon}{\alpha\sqrt{\alpha}}$
Stress distribution in parts (compression positive)	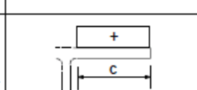	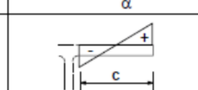	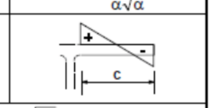
3	$c / t \le 14\varepsilon$	$c / t \le 21\varepsilon\sqrt{k_\sigma}$ For k_σ see EN 1993-1-5	

$\varepsilon = \sqrt{235 / f_y}$	f_y	235	275	355	420	460
	ε	1,00	0,92	0,81	0,75	0,71

Table 24. outstand flange

Before embarking on the verification process, it's essential to account for the partial factors outlined in the table below:

Resistance of the Class 1-2-3-4	γ_{M0}=1.05
Resistance to buckling of members	γ_{M1}=1.05
Resistance to buckling of members of road and railway bridges	γ_{M1}=1.1
Resistance, towards fracture, of the tensioned sections (weakened by the holes)	γ_{M2}=1.25

Table 25. Safety coefficients for the resistance of the members and the stability

5.3.1. Membrane Resistance :

<u>Normal stress Verification :</u>

$N_{ed} < N_{pl,Rd}$

Where, $N_{pl,Rd} = \frac{A * f_{yk}}{\gamma_{M0}}$

<u>Compression Verification :</u>

$N_{ed} < N_{c,Rd}$

Where, $N_{pl,Rd} = \frac{A * f_{yk}}{\gamma_{M0}}$

<u>Bending moment Verification :</u>

$M_{ed} < M_{c,Rd}$

$$M_{c,Rd} = \frac{W_{min} * f_{yk}}{\gamma_{M0}}$$

The calculation of W_{min} involves removing the inactive parts of the section caused by local instability.

Shear Verification :

$V_{ed} < V_{c,Rd}$

With a plastic calculation (in the absence of torsion) it is defined :

$$V_{pl,Rd} = A_V \frac{\frac{f_y}{\sqrt{3}}}{\gamma_{M0}}$$

Where, A_V is the shear resistant area (based on the profile)

In the case of torsion, the resisting shear force shall be :

$$V_{pl,T,Rd} = V_{pl,Rd} \sqrt{1 - \frac{\tau_{t,Ed}}{\frac{1.25 * f_y}{\sqrt{3} * \gamma_{M0}}}}$$

Where, $\tau_{t,Ed}$ is the tangential shear stress due to St.Venant torsion

5.3.2. Membrane Stability :

Compression Verification :

$N_{ed} < N_{b,Rd}$

Where, $N_{pl,Rd} = \frac{\chi * A * f_{yk}}{\gamma_{M1}}$

The reduction factor χ depends on non-dimensional slenderness and imperfection parameter, which can be calculated as follows:

$$\chi = \frac{1}{\phi + \sqrt{\phi^2 + \bar{\lambda}^2}}$$

$$\phi = \frac{1}{2}[1 + \alpha(\bar{\lambda} - 0.2) + \bar{\lambda}^2]$$

α is imperfection factor associated with buckling curves (function of the axis around which instability occurs)

Buckling curve	**a_0**	**a**	**b**	**c**	**d**
Imperfection factor	0.13	0.21	0.34	0.49	0.76

Table 26. imperfection factors for buckling curves

Cross section		Limits		Buckling about axis	Buckling curve: S235 S275 S355 S420	Buckling curve: S460
Rolled sections	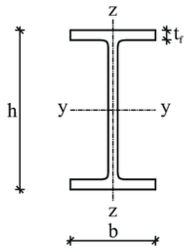	$h/b > 1.2$	$t_f \leq 40$ mm	y-y z-z	a b	a_0 a_0
			40 mm $< t_f \leq 100$ mm	y-y z-z	b c	a a
		$h/b \leq 1.2$	$t_f \leq 100$ mm	y-y z-z	b c	a a
			$t_f > 100$ mm	y-y z-z	d d	c c
Welded I-sections	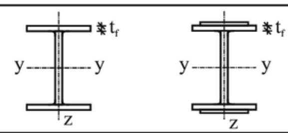	$t_f \leq 40$ mm		y-y z-z	b c	b c
		$t_f > 40$ mm		y-y z-z	c d	c d
Hollow sections	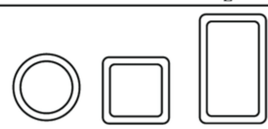	hot finished		any	a	a_0
		cold formed		any	c	c
Welded box sections	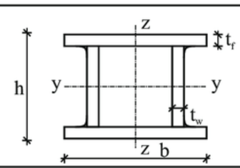	generally (except as bellow)		any	b	b
		thick welds: $a > 0.5\,t_f$ $b/t_f < 30$ $h/t_w > 30$		any	c	c

Table 27. Selection of buckling curve for a cross-section

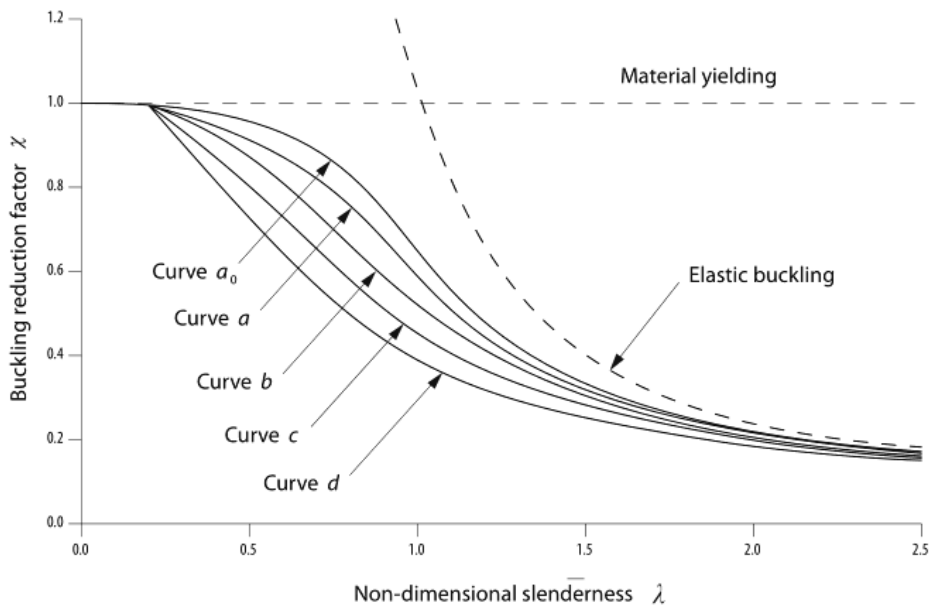

Table 28. Values of χ as a function of the buckling curves and non-dimensional slenderness

Non-dimensional slenderness:

$$\bar{\lambda} = \sqrt{\frac{f_y * A}{N_{cr}}}$$

In order to get the non-dimensional slenderness, we have to calculate N critical:

$$N_{cr} = \min\left(\frac{\pi^2 * E * I_y}{L_{0,y}^2}, \frac{\pi^2 * E * I_z}{L_{0,z}^2}\right) \quad , \qquad minimum\ between\ weak\ axis\ and\ strong\ axis$$

<u>Bending Verification :</u>

The bending elements may present the problem of flexural-torsional (lateral) buckling resulting from the presence of a compressive force.

$$M_{ed} < M_{b,Rd}$$

There are two approaches (A & B), which we are using approach A without lateral bracing and with direct load on the web, and is given by :

$$M_{b,Rd} = \chi_{LT} W_y (\frac{f_y}{\gamma_{M1}}) \text{ , } W_y\ depends\ on\ the\ Class$$

The lateral torsional buckling is defined by :

$$\chi_{LT} = \frac{1}{\phi_{LT} + \sqrt{\phi_{LT}^2 + \bar{\lambda}_{LT}^2}} \leq 1$$

$$\bar{\lambda}_{LT} = \sqrt{\frac{W_y * f_y}{M_{cr}}}$$

$$\phi_{LT} = \frac{1}{2}[1 + \alpha_{LT}(\bar{\lambda}_{LT} - 0.2) + \bar{\lambda}_{LT}^2]$$

To find M_{cr} :

$$M_{cr} = C_1 \frac{\pi^2 * E * I_z}{L^2}\left[\sqrt{\frac{I_w}{I_z} - \frac{L^2 * G * I_t}{\pi^2 * E * I_z}}\right]$$

Where,

L is the distance between points that have lateral constraint and I_z is the torsional constant.

For I or H profiles without end post stiffeners, the warping constant I_w is equal to :

$$I_w = \frac{I_z * (h - t_f)^2}{4}$$

Where,

I_z is the moment of inertia around the weak axis

h is the profile height

t_f is the thickness of the flange

And C_1 is obtained as a function of the moments at the end of the element from the following tables:

Loading conditions	Bending moment diagram	Factor k	Coefficients $C1$	$C2$	$C3$
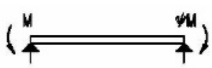	$\psi = +1$	1,0	1,000	—	1,000
		0,7	1,000		1,113
		0,5	1,000		1,144
	$\psi = +3/4$	1,0	1,141	—	0,998
		0,7	1,270		1,565
		0,5	1,305		2,283
	$\psi = +1/2$	1,0	1,323	—	0,992
		0,7	1,473		1,556
		0,5	1,514		2,271
	$\psi = +1/4$	1,0	1,563	—	0,977
		0,7	1,739		1,531
		0,5	1,788		2,235
	$\psi = 0$	1,0	1,879	—	0,939
		0,7	2,092		1,473
		0,5	2,150		2,150
	$\psi = -1/4$	1,0	2,281	—	0,855
		0,7	2,538		1,340
		0,5	2,609		1,957
	$\psi = -1/2$	1,0	2,704	—	0,676
		0,7	3,009		1,059
		0,5	3,093		1,546
	$\psi = -3/4$	1,0	2,927	—	0,366
		0,7	3,009		0,573
		0,5	3,093		0,837
	$\psi = -1$	1,0	2,752	—	0,000
		0,7	3,063		0,000
		0,5	3,149		0,000

Table 29. Values for C_1, C_2, and C_3

Loading conditions	Bending moment diagram	Factor k	Coefficients		
			$C1$	$C2$	$C3$
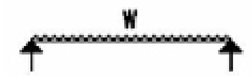	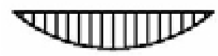	1,0 0,5	1,132 0,972	0,459 0,304	0,525 0,980
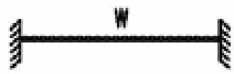		1,0 0,5	1,285 0,712	1,562 0,652	0,753 1,070
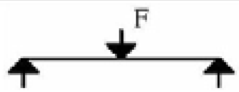		1,0 0,5	1,365 1,010	0,553 0,432	1,730 3,050
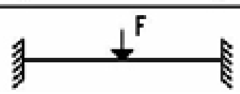		1,0 0,5	1,565 0,938	1,267 0,715	2,640 4,800
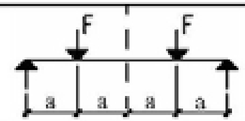	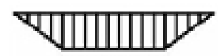	1,0 0,5	1,046 1,010	0,430 0,410	1,120 1,890

Table 30. Values for C_1, C_2,*and* C_3

<u>Shear Verification :</u>

For stiffened web :

$$\frac{h_w}{t_w} > 72 * \frac{\varepsilon}{\boldsymbol{\eta}}$$

Where,

h_w is the web height

t_w is the web thickness

For unstiffened web :

$$\frac{d}{t_w} > 31 * \frac{\varepsilon}{\boldsymbol{\eta}} * \sqrt{K_\tau}$$

Where,

K_τ is the shear buckling coefficient for tangential stresses as a function of stiffener spacing and section web height.

Compression + Bending :

$$\frac{N_{Ed}}{\frac{\chi_y * N_{Rk}}{\gamma_{M1}}} + k_{yy}\frac{M_{y,Ed} + \Delta M_{y,Ed}}{\chi_{LT} * \frac{M_{y,Rk}}{\gamma_{M1}}} + k_{yz}\frac{M_{z,Ed} + \Delta M_{z,Ed}}{\frac{M_{z,Rk}}{\gamma_{M1}}} \leq 1$$

$$\frac{N_{Ed}}{\frac{\chi_z * N_{Rk}}{\gamma_{M1}}} + k_{zy}\frac{M_{y,Ed} + \Delta M_{y,Ed}}{\chi_{LT} * \frac{M_{y,Rk}}{\gamma_{M1}}} + k_{zz}\frac{M_{z,Ed} + \Delta M_{z,Ed}}{\frac{M_{z,Rk}}{\gamma_{M1}}} \leq 1$$

Where,

The red box represents the compression part and the blue box represents the bending.

k represents the interaction coefficient, can be found from the table below :

Interaction factors	Type of sections	Design assumptions: elastic cross-sectional properties class 3, class 4	Design assumptions: plastic cross-sectional properties class 1, class 2
k_{yy}	I-sections RHS-sections	$C_{my}\left(1+0{,}6\bar{\lambda}_y\frac{N_{Ed}}{\chi_y N_{Rk}/\gamma_{M1}}\right)$ $\leq C_{my}\left(1+0{,}6\frac{N_{Ed}}{\chi_y N_{Rk}/\gamma_{M1}}\right)$	$C_{my}\left(1+\left(\bar{\lambda}_y-0{,}2\right)\frac{N_{Ed}}{\chi_y N_{Rk}/\gamma_{M1}}\right)$ $\leq C_{my}\left(1+0{,}8\frac{N_{Ed}}{\chi_y N_{Rk}/\gamma_{M1}}\right)$
k_{yz}	I-sections RHS-sections	k_{zz}	$0{,}6\ k_{zz}$
k_{zy}	I-sections RHS-sections	$0{,}8\ k_{yy}$	$0{,}6\ k_{yy}$
k_{zz}	I-sections	$C_{mz}\left(1+0{,}6\bar{\lambda}_z\frac{N_{Ed}}{\chi_z N_{Rk}/\gamma_{M1}}\right)$ $\leq C_{mz}\left(1+0{,}6\frac{N_{Ed}}{\chi_z N_{Rk}/\gamma_{M1}}\right)$	$C_{mz}\left(1+\left(2\bar{\lambda}_z-0{,}6\right)\frac{N_{Ed}}{\chi_z N_{Rk}/\gamma_{M1}}\right)$ $\leq C_{mz}\left(1+1{,}4\frac{N_{Ed}}{\chi_z N_{Rk}/\gamma_{M1}}\right)$
	RHS-sections		$C_{mz}\left(1+\left(\bar{\lambda}_z-0{,}2\right)\frac{N_{Ed}}{\chi_z N_{Rk}/\gamma_{M1}}\right)$ $\leq C_{mz}\left(1+0{,}8\frac{N_{Ed}}{\chi_z N_{Rk}/\gamma_{M1}}\right)$
For I- and H-sections and rectangular hollow sections under axial compression and uniaxial bending $M_{y,Ed}$ the coefficient k_{zy} may be $k_{zy} = 0$.			

Table 31. Interaction factors k for members not susceptible to torsional deformations

Interaction factors	Design assumptions	
	elastic cross-sectional properties class 3, class 4	plastic cross-sectional properties class 1, class 2
k_{yy}	k_{yy} from Table B.1	k_{yy} from Table B.1
k_{yz}	k_{yz} from Table B.1	k_{yz} from Table B.1
k_{zy}	$\left[1-\frac{0,05\bar{\lambda}_z}{(C_{mLT}-0,25)}\frac{N_{Ed}}{\chi_z N_{Rk}/\gamma_{M1}}\right] \geq \left[1-\frac{0,05}{(C_{mLT}-0,25)}\frac{N_{Ed}}{\chi_z N_{Rk}/\gamma_{M1}}\right]$	$\left[1-\frac{0,1\bar{\lambda}_z}{(C_{mLT}-0,25)}\frac{N_{Ed}}{\chi_z N_{Rk}/\gamma_{M1}}\right] \geq \left[1-\frac{0,1}{(C_{mLT}-0,25)}\frac{N_{Ed}}{\chi_z N_{Rk}/\gamma_{M1}}\right]$ for $\bar{\lambda}_z < 0,4$: $k_{zy} = 0,6+\bar{\lambda}_z \leq 1-\frac{0,1\bar{\lambda}_z}{(C_{mLT}-0,25)}\frac{N_{Ed}}{\chi_z N_{Rk}/\gamma_{M1}}$
k_{zz}	k_{zz} from Table B.1	k_{zz} from Table B.1

Table 32. Interaction factors k for members susceptible to torsional deformations

Moment diagram	range		C_{my}, C_{mz}, C_{mLT}	
			uniform loading	concentrated load
	$-1 \leq \psi \leq 1$		$0.6+0.4\psi \geq 0.4$	
	$0 \leq \alpha_s \leq 1$	$-1 \leq \psi \leq 1$	$0.2+0.8\alpha_s \geq 0.4$	$0.2+0.8\alpha_s \geq 0.4$
	$-1 \leq \alpha_s < 0$	$0 \leq \psi \leq 1$	$0.1-0.8\alpha_s \geq 0.4$	$-0.8\alpha_s \geq 0.4$
$\alpha_s = M_s/M_h$		$-1 \leq \psi < 0$	$0.1(1-\psi)-0.8\alpha_s \geq 0.4$	$0.2(1-\psi)-0.8\alpha_s \geq 0.4$
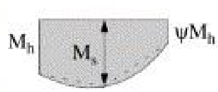	$0 \leq \alpha_h \leq 1$	$-1 \leq \psi \leq 1$	$0.9\ -0.0\ \ \alpha_h$	$0.90+0.10\alpha_h$
	$-1 \leq \alpha_h < 0$	$0 \leq \psi \leq 1$	$0.9\ +0.0\ \ \alpha_h$	$0.90+0.10\alpha_h$
$\alpha_h = M_h/M_s$		$-1 \leq \psi < 0$	$0.9\ +0.0\ \ \alpha_h\ (1+2\psi)$	$0.90+0.0\ \ \alpha_h\ (1+2\psi)$
For members with sway buckling mode the equivalent uniform moment factor should be taken $C_{my} = 0.9$ or C_{Mz} 0.9 respectively.				
C_{my}, C_{Mz} and C_{mLT} shall be obtained according to the bending moment diagram between the relevant braced points as follows:				

moment factor	bending axis	points braced in direction
C_{my}	y-y	z-z
C_{mz}	z-z	y-y
C_{mLT}	y-y	y-y

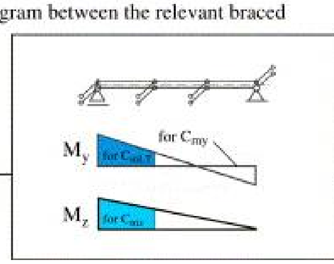

Table 33. equivalent uniform moment factors C_m

5.3.3. Deformability :

At the specific Serviceability Limit State (SLS), we need to ensure that the deformation at certain critical points in the structure remains below a specified threshold.

$$v \leq v_{Lim}$$

With v decrease in the elastic field obtained as a sum :

$$v = v_F + v_T$$

Where,

v_F is the flexural deformability

v_T is the Shear deformability

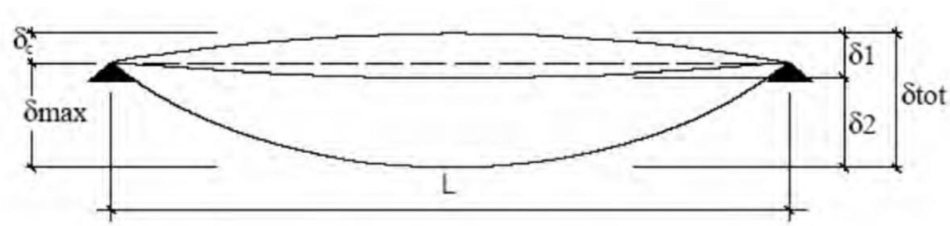

Figure 69. Deformability

Where,

δ_c is precamber in the unloaded structural member

δ_1 is the elastic displacement due to permanent loads

δ_2 is the elastic displacement due to variable loads

δ_{max} is the displacement in the final state, without the initial precamber = $\delta_{tot} - \delta_c$

5.4. Identification of Failed Structural Members :

Center (Fails):

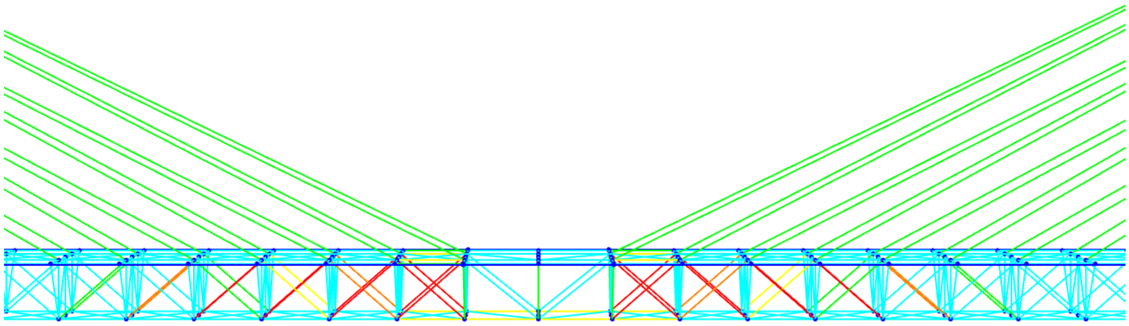

<u>Vertical longitudinal bracing:</u>

A)

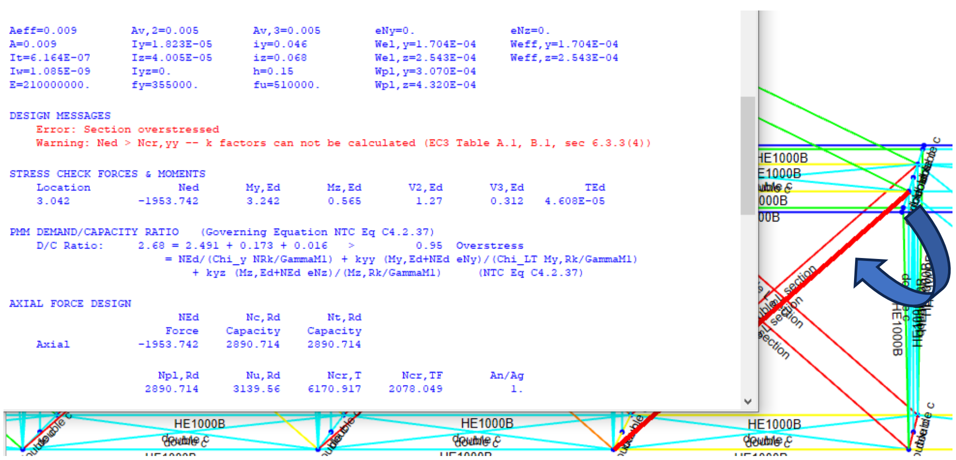

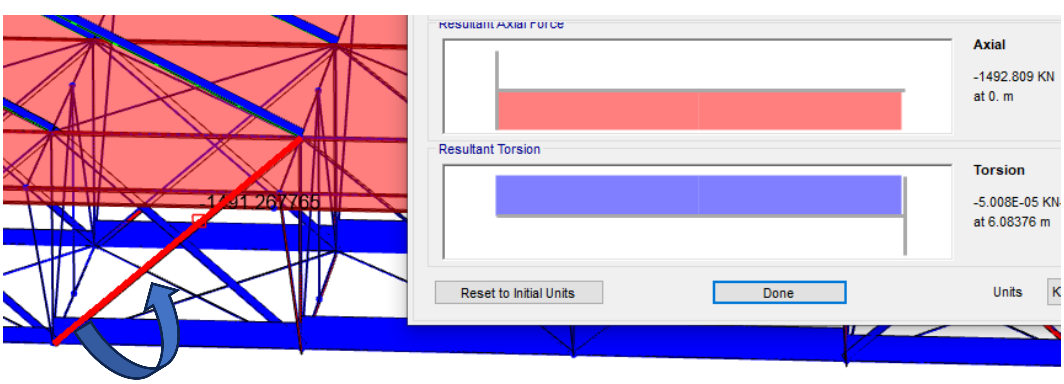

B)

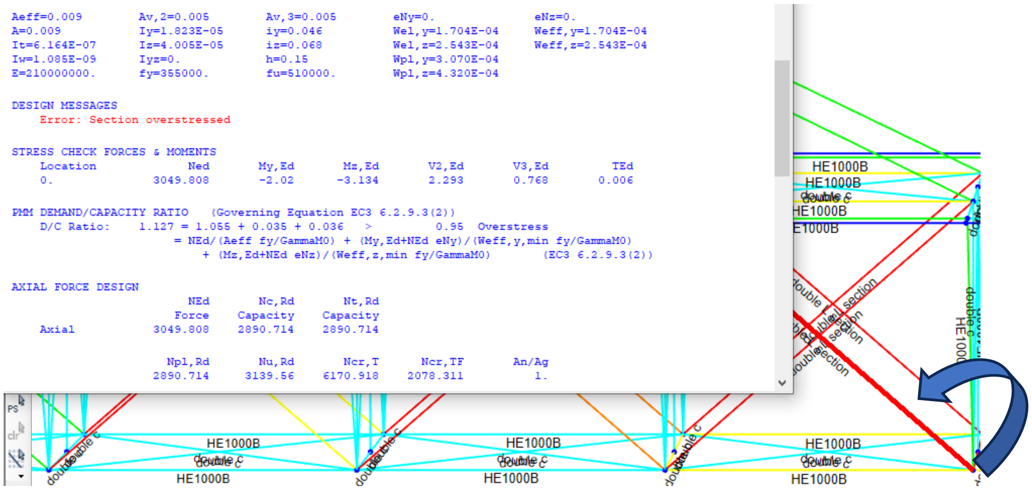
Aeff=0.009 Av,2=0.005 Av,3=0.005 eNy=0. eNz=0.
A=0.009 Iy=1.823E-05 iy=0.046 Wel,y=1.704E-04 Weff,y=1.704E-04
It=6.164E-07 Iz=4.005E-05 iz=0.068 Wel,z=2.543E-04 Weff,z=2.543E-04
Iw=1.085E-09 Iyz=0. h=0.15 Wpl,y=3.070E-04
E=210000000. fy=355000. fu=510000. Wpl,z=4.320E-04
DESIGN MESSAGES
Error: Section overstressed
STRESS CHECK FORCES & MOMENTS
Location Ned My,Ed Mz,Ed V2,Ed V3,Ed TEd
0. 3049.808 -2.02 -3.134 2.293 0.768 0.006
PMM DEMAND/CAPACITY RATIO (Governing Equation EC3 6.2.9.3(2))
D/C Ratio: 1.127 = 1.055 + 0.035 + 0.036 > 0.95 Overstress
= NEd/(Aeff fy/GammaM0) + (My,Ed+NEd eNy)/(Weff,y,min fy/GammaM0)
+ (Mz,Ed+NEd eNz)/(Weff,z,min fy/GammaM0) (EC3 6.2.9.3(2))
AXIAL FORCE DESIGN
NEd Nc,Rd Nt,Rd
Force Capacity Capacity
Axial 3049.808 2890.714 2890.714
Npl,Rd Nu,Rd Ncr,T Ncr,TF An/Ag
2890.714 3139.56 6170.918 2078.311 1.
HE1000B

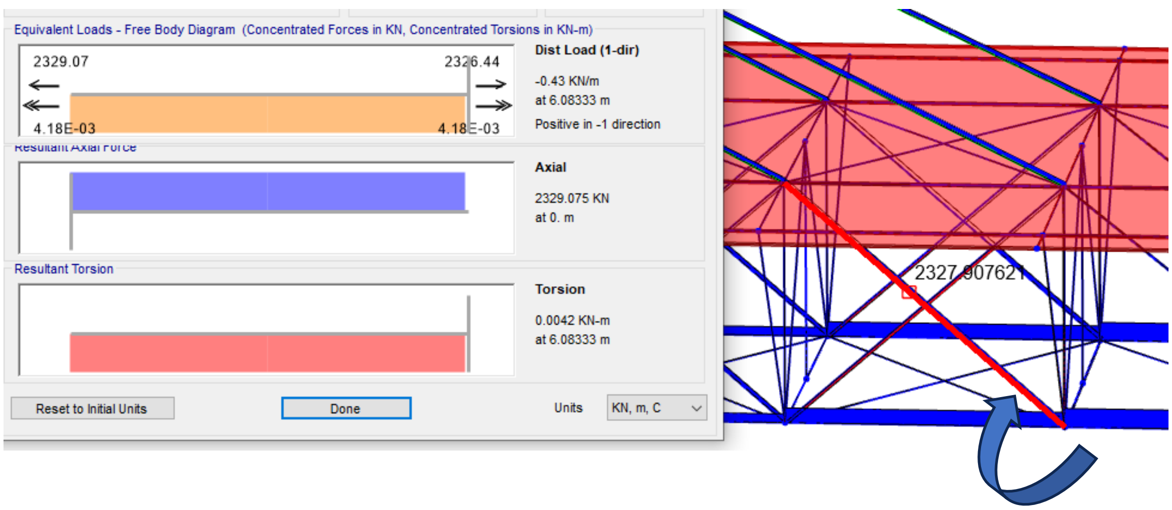
Equivalent Loads - Free Body Diagram (Concentrated Forces in KN, Concentrated Torsions in KN-m)
2329.07
2326.44
4.18E-03
4.18E-03
Dist Load (1-dir)
-0.43 KN/m
at 6.08333 m
Positive in -1 direction
Axial
2329.075 KN
at 0. m
Resultant Torsion
Torsion
0.0042 KN-m
at 6.08333 m
Reset to Initial Units
Done
Units
KN, m, C
2327.907621

<u>Bottom transversal double c section:</u>

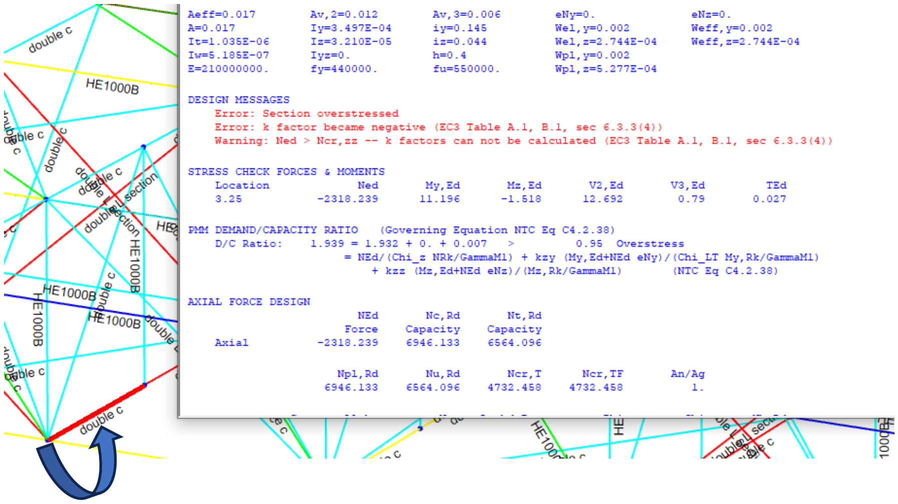

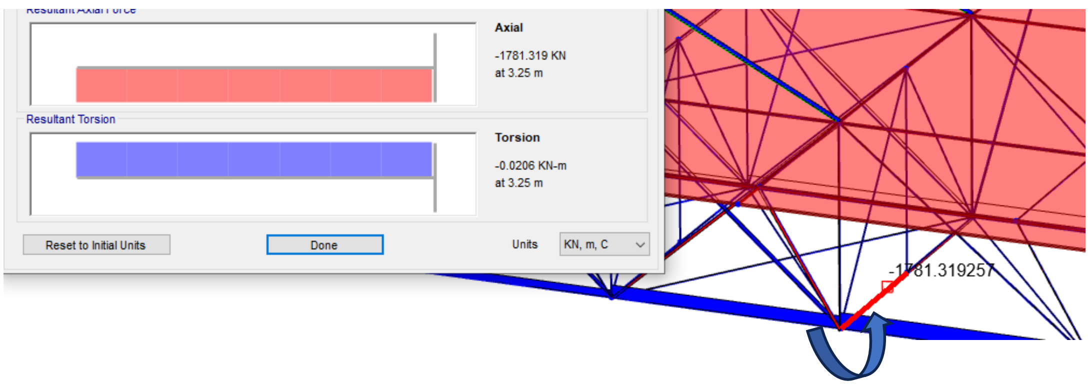

5.5. FORCES ACTING ON THE ABUTMENT:

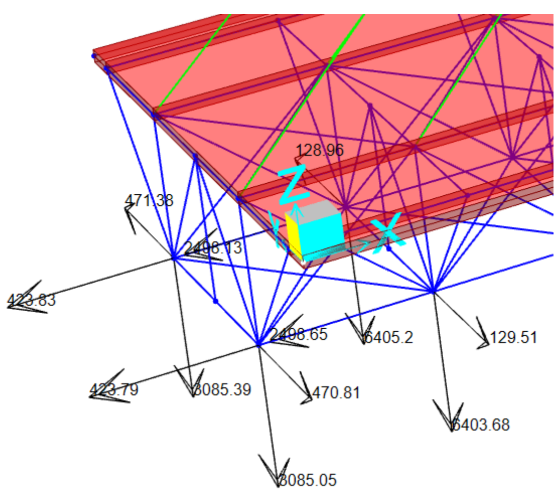

5.6. Bolt and Weld joints Verification :

5.6.1. Bolted Connections :

Bolted connections represent a widely adopted method for assembling different steel structural components. These connections play a vital role in streamlining on-site construction efforts, allowing steel structures to be prefabricated off-site. Consequently, the majority of assembly work occurs in controlled workshop environments, facilitating quicker and more efficient on-site installation processes.

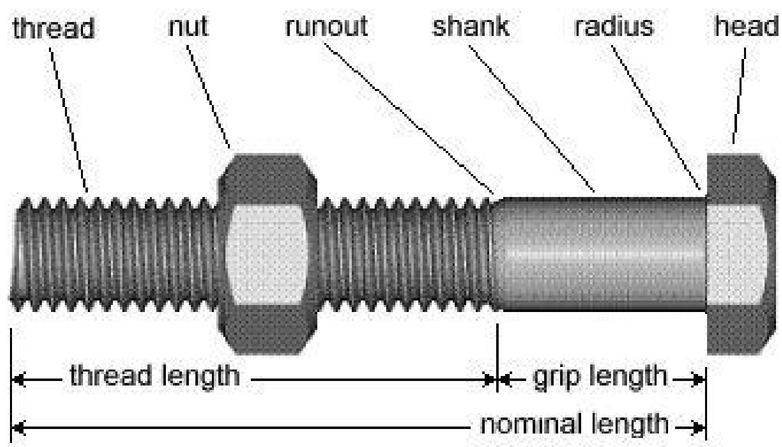

Figure 70. Components of a Bolt

Advantages :

1) Allow rapid preparation in the workshop and simplify assembly of members on site.
2) On-site workers require no specialized training and environmental condition.
3) Maintenance and inspection are straightforward
4) The design and verification are carried out with simplified models.

Bolt is considered under these load conditions :

- Forces parallel to the shank (tension)
- Forces perpendicular to the shank (shear)
- Combination of both (shear and tension)

Various factors can contribute to the failure of a shear bolted connection, including :

a) Bearing failure of plate : This occurs when the bearing stress between the bolt and the connected plate exceeds the materials capacity, resulting in deformation or crushing of the plate material around the bolt hole.

b) Tensile failure of plate : This happens when the plate material experiences excessive tensile stress, leading to its rupture or tearing apart under the applied load, typically due to inadequate material strength or excessive loading.

c) Shear failure of plate : In this case, the plate fails along a plane parallel to the direction of the applied shear force, usually resulting from shear stress exceeding the materials shear strength, causing it to split or tear off.

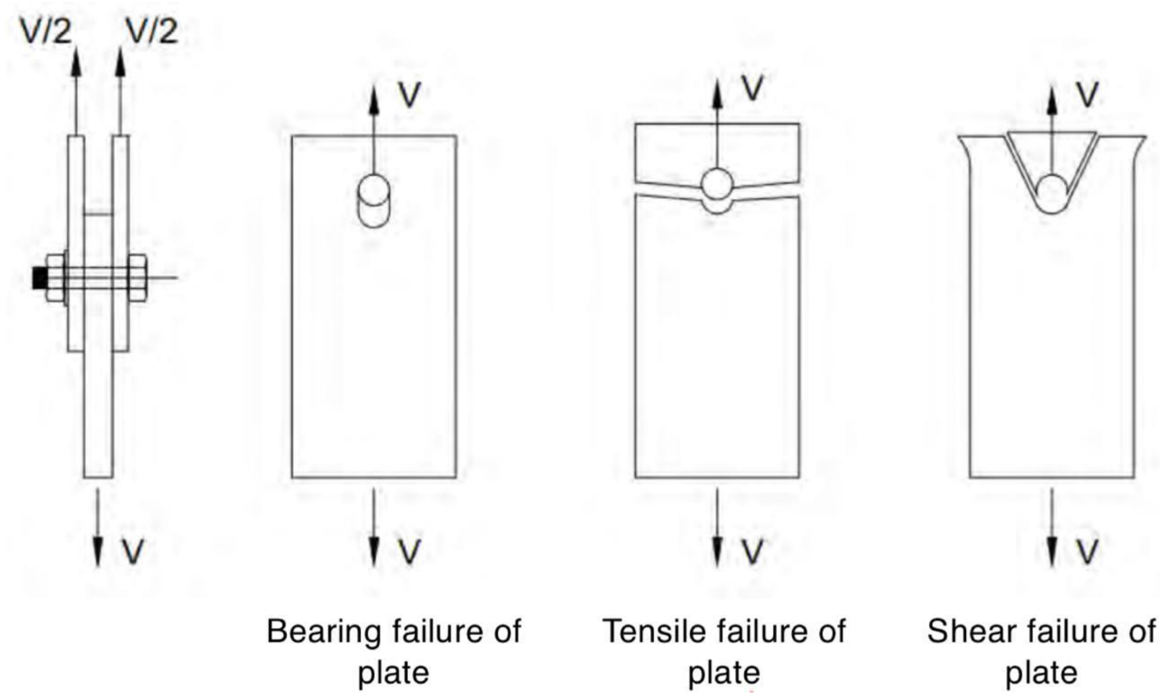

Figure 71. Different failures

Geometric requirements for bolted connections :

Bolt hole tolerance according to UNI EN 1090-2

$$d = 12 \div 14\ mm \qquad \phi - d = 1\ mm$$

$$d = 16 \div 24\ mm \qquad \phi - d = 2\ mm$$

$$d \geq 27\ mm \qquad \phi - d = 3\ mm$$

Bolt hole tolerance according to NTC 18

$$d \leq 20\ mm \qquad \phi - d = 1\ mm$$

$$d > 20\ mm \qquad \phi - d = 1.5\ mm$$

Bolt Spacing

A. Minimum Spacing :

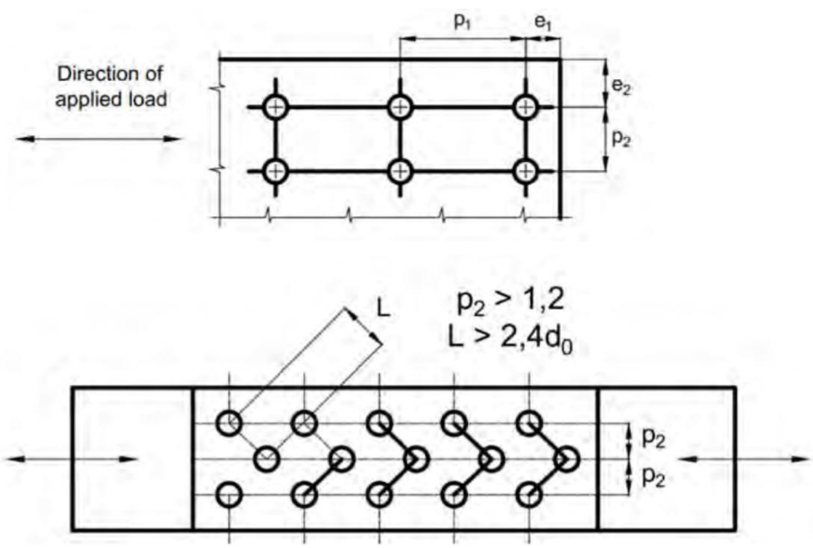

Figure 72. Minimum Spacing

$$P_1 \geq 2.2\ d_0$$

$$P_2 \geq 2.4\ d_0$$

B. Maximum Spacing :

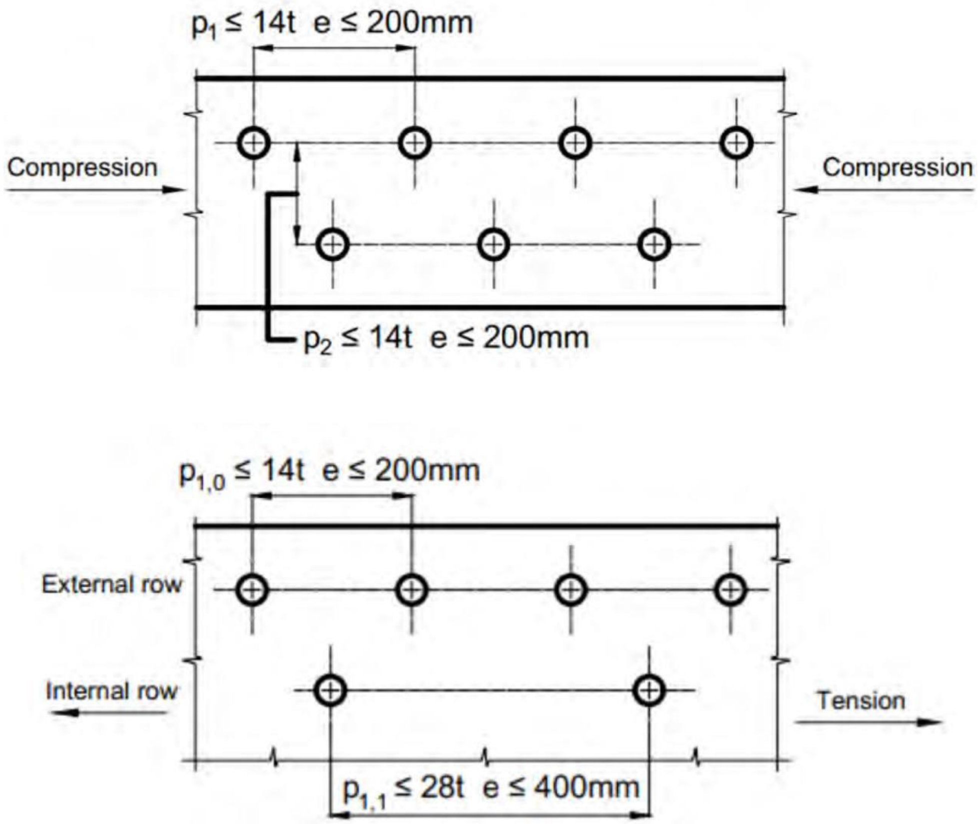

Figure 73. Maximum Spacing

Edge distance

C. Minimums and maximums

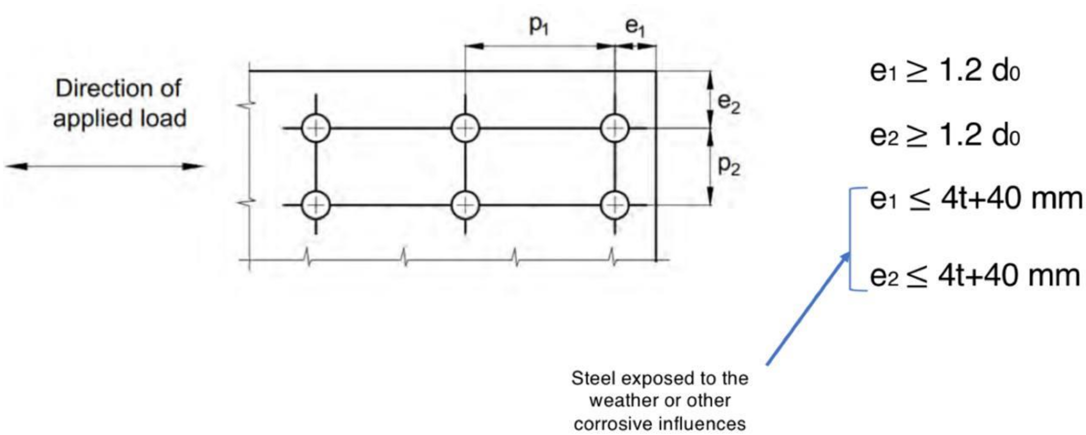

Figure 74. Edge distance

5.6.1.1. Design Resistance :

A. Tensile resistance

$$F_{t,Rd} = \frac{k_2 * f_{ub} * A_s}{\gamma_{M2}} \qquad (\,design\ tension\ resistance\ per\ bolt\,)$$

where,

f_{ub} is the ultimate tensile strength

$k_2 = 0.9$

A_s is the tensile stress area of the bolt

γ_{M2} is the partial safety coefficient for bolted connections $\gamma_{M2} = 1.25$

$$B_{p,Rd} = \frac{0.6 * \pi * d_m * t_p * f_u}{\gamma_{M2}} \quad (\,design\ punching\ shear\ resistance\ of\ bolt\ head\ and\ nut\,)$$

where,

f_u is the ultimate tensile strength of the plate below the bolt head

$k_2 = 0.9$

t_p is the thickness of plate below the bolt head

d_m is the minimum value between : 1) the mean value of the distance between the center points and between the plan surfaces of the bolt head 2) the average value of the distance measured between the center points and between the plan surfaces of the nut

B. Shear strength

Shear plane passes through the threaded portion of the bolt:

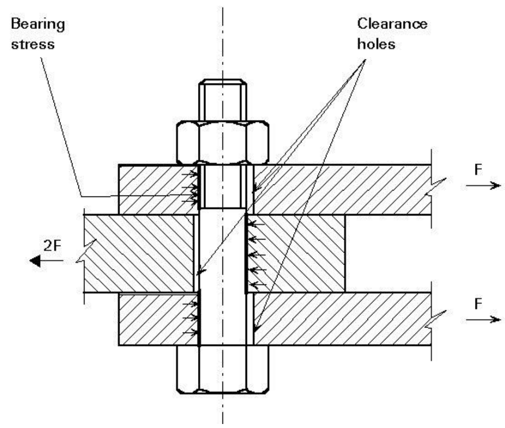

Figure 75. Shear Strength

$$F_{v,Rd} = n_s * \frac{0.6(0.5) * f_{ub} * A_s}{\gamma_{M2}}$$

Shear plane passes through the unthreaded portion of the bolt:

$$F_{v,Rd} = n_s * \frac{0.6 * f_{ub} * A}{\gamma_{M2}}$$

C. Tensile and shear strength

$$\frac{F_{v,Ed}}{F_{v,Rd}} + \frac{F_{t,Ed}}{1.4 * F_{t,Rd}} \leq 1$$

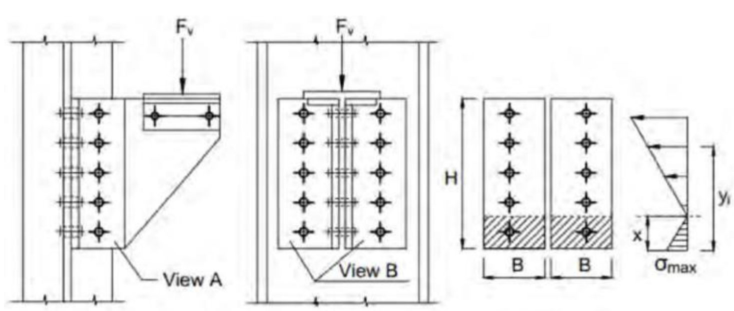

Figure 76. Tensile and shear strength

D. Bearing resistance

$$B_{p,Rd} = \frac{k_1 * \alpha_b * d * t * f_u}{\gamma_{M2}}$$

Where,

f_u is the ultimate tensile stress of the plate

D is the bolt diameter

T is the thickness of the plate

In the direction of load transfer:

For edge bolts $\alpha_b = \min\left\{\frac{e_1}{3*d_0}; \frac{f_{ub}}{f_u}; 1\right\}$

For inner bolts $\alpha_b = \min\left\{\frac{p_1}{3*d_0} - \frac{1}{4}; \frac{f_{ub}}{f_u}; 1\right\}$

Perpendicular to the direction of load transfer:

For edge bolts $k_1 = \min\left\{\frac{2.8*e_2}{d_0} - 1.7; 2.5\right\}$

For inner bolts $k_1 = \min\left\{\frac{1.4*p_2}{d_0} - 1.7; 2.5\right\}$

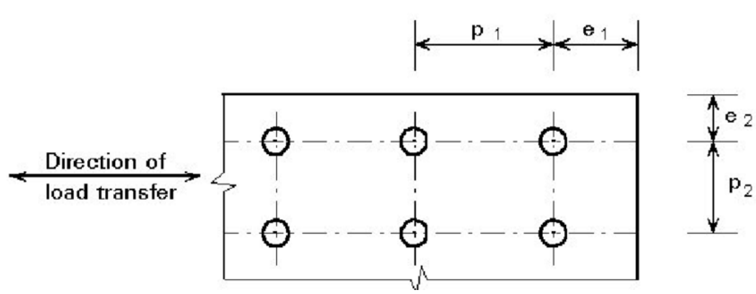

Figure 77. Spacing and edge distance

E. Slip resistance

$$F_{s,Rd} = \frac{k_s * n * \mu}{\gamma_{M3}} * F_{p,C}$$

Where,

k_s is the coefficient according to the type of hole

n is the number of friction surfaces

μ is the slip factor obtained either by specific tests for the friction surface

$F_{p,C}$ is the preload design force for high-strength bolts with controlled tightening

$F_{p,C} = 0.7 * f_{ub} * A_{res}$

Description	k_s
Bolts in normal holes.	1,0
Bolts in either oversized holes or short slotted holes with the axis of the slot perpendicular to the direction of load transfer.	0,85
Bolts in long slotted holes with the axis of the slot perpendicular to the direction of load transfer.	0,7
Bolts in short slotted holes with the axis of the slot parallel to the direction of load transfer.	0,76
Bolts in long slotted holes with the axis of the slot parallel to the direction of load transfer.	0,63

Figure 78. Values of k_s

5.6.2. Welded Connections :

Welding is a method to permanently join two metal pieces, with or without the use of filler material, by applying heat. The molten weld metal is distributed between properly prepared fusion lines. The weld face is formed by the solidification of all melted metal, including both the base metal and any filler material, as it cools.

Welding Procedure :

In an autogenous welding procedure, the joining is accomplished solely through the fusion of the base material without the addition of filler material. This process relies on the heat generated to melt and fuse.

In contrast, a heterogeneous welding procedure involves the use of filler material that is melted along with the base metals during the welding process. The filler material is added to the joint to provide additional strength, improve the weld's properties.

Welding can be classified according to the position of the workpiece or the position of the welded joint on the plates or sections being welded.

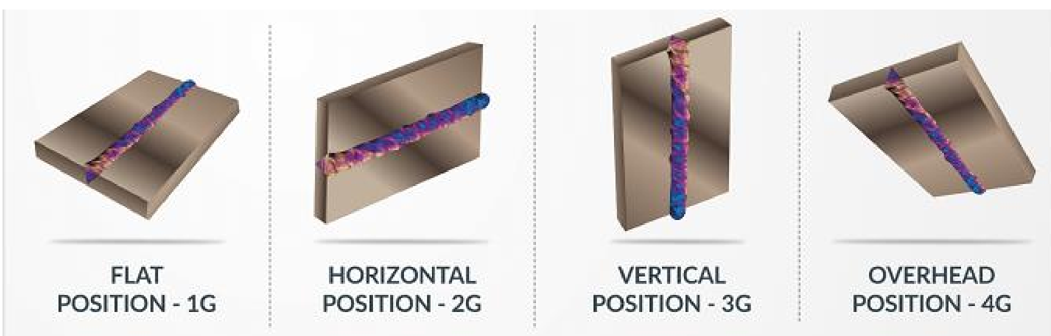

Figure 79. Weld Position

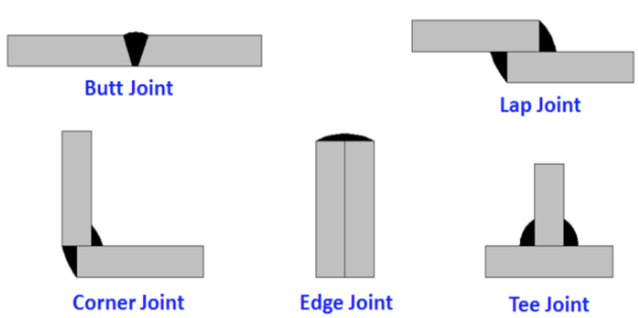

Figure 80. welding joints

Type of welds :

1) **Full penetration** : It involves the complete fusion of material through the thickness of the joint. This process ensures that molten material extends entirely from one side of the joint to the other, creating a seamless bond between the welded components. The straight side of the weld, facing the direction of welding, is intentionally kept small to facilitate melting and integration into the weld, ensuring structural integrity.

2) **Partial penetration** : It doesn't achieve complete fusion through the joint thickness. Instead, there is an absence of melted material extending entirely through the joint. This results in an incomplete bond between the welded surfaces, where only a portion of the material is fused together. Partial penetration welds are typically utilized in situation where full penetration is not necessary or desired, such as when joint thickness or welding conditions require a different approach to achieve the desired strength and integrity.

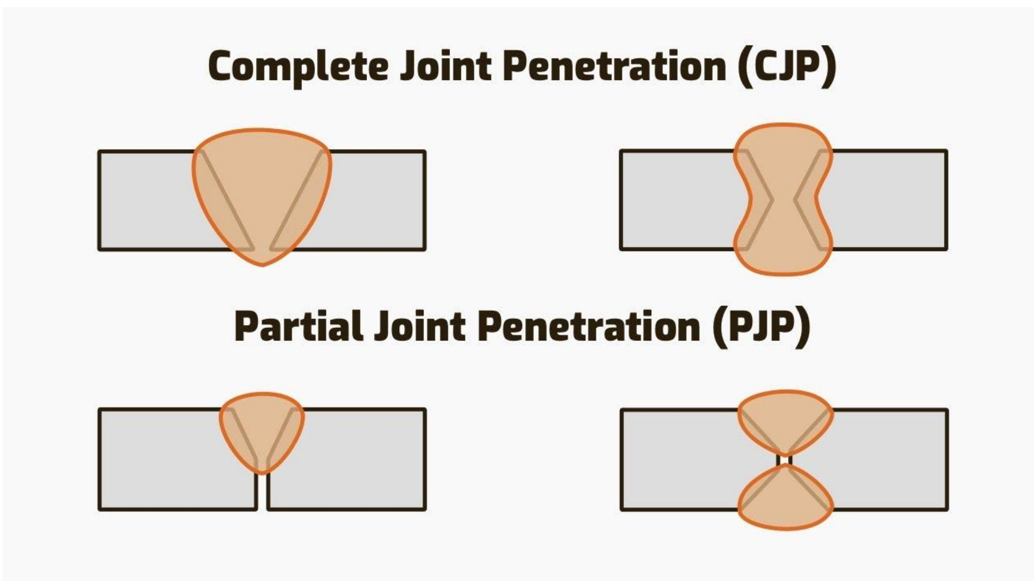

Figure 81. CJP-PJP

To prevent full penetration and achieve partial penetration, fillet welds can be employed. Fillet welds are designed to join two surfaces at an angle, typically perpendicular to or at a 45-degree angle, and they do not require full penetration through the joint. Instead, they create a strong bond by effectively reinforcing the joint with a triangular cross-section of weld material. This method ensures structural integrity while avoiding the need for complete fusion through the entire thickness of the joint.

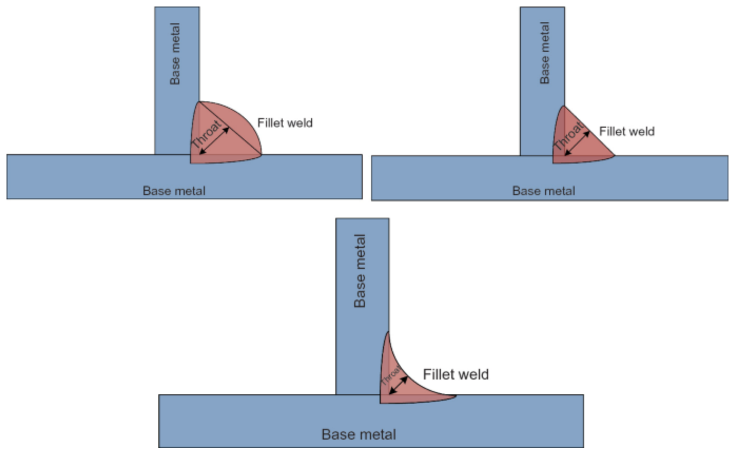

Figure 82. Fillet weld

Fillet welds are characterized by their dimensions, including the throat height and length of the weld. The throat height represents the distance from the root of the joint to the toe of the weld, while the length denotes the linear extent of the weld along the joint. In design practice, two main methods are commonly used ;

- **Directional method** : The stress state is determined by referring to the actual throat section, considering both normal and shear stresses. Verification involves assessing various boundary conditions, which are typically expressed using specific formulas :

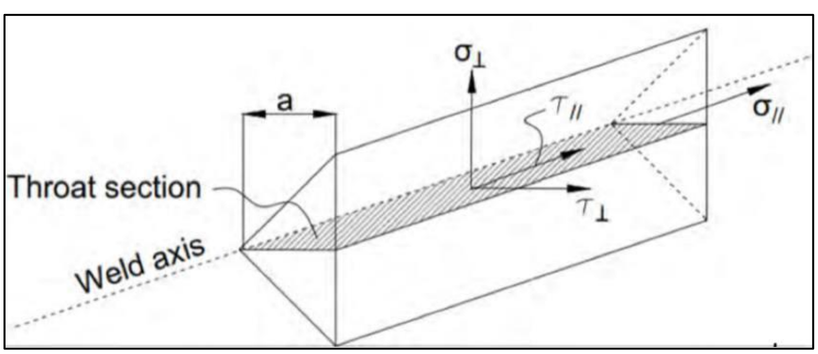

Figure 83. Weld cross section

$$\sqrt{\sigma_\perp^2 + (\tau_\perp^2 + \tau_\parallel^2)} \leq \frac{f_u}{\beta_w \gamma_{M2}}$$

$$\sigma_\perp \leq \frac{0.9 * f_u}{\gamma_{M2}}$$

Standard and steel grade			Correlation factor β_w
EN 10025	EN 10210	EN 10219	
S 235 S 235 W	S 235 H	S 235 H	0,8
S 275 S 275 N/NL S 275 M/ML	S 275 H S 275 NH/NLH	S 275 H S 275 NH/NLH S 275 MH/MLH	0,85
S 355 S 355 N/NL S 355 M/ML S 355 W	S 355 H S 355 NH/NLH	S 355 H S 355 NH/NLH S 355 MH/MLH	0,9
S 420 N/NL S 420 M/ML		S 420 MH/MLH	1,0
S 460 N/NL S 460 M/ML S 460 Q/QL/QL1	S 460 NH/NLH	S 460 NH/NLH S 460 MH/MLH	1,0

Figure 84. Correlation factor β_w for fillet welds

- **Simplified method :** It assumes a design resistance per unit length of weld, irrespective of the orientation of the weld throat plane. This method simplifies the analysis by disregarding the specific stress state and considering the weld's resistance as uniform along its length. Design calculations under the simplified method also involve applying specific formulas :

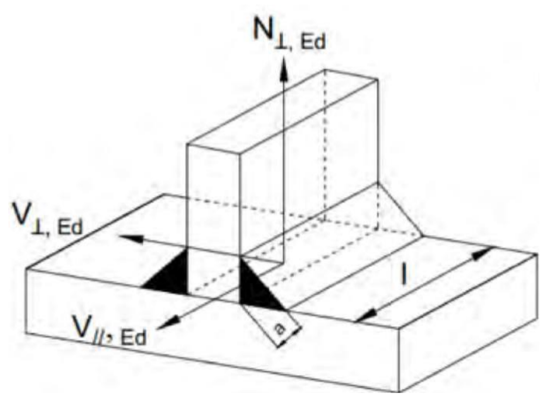

Figure 85. Simplified method

$$F_{W,Rd} \leq \frac{f_u}{\sqrt{3} * \beta_W * \gamma_{M2}} * a$$

Where, a is the throat height.

6. Issue Statement and Analytical Context :

In this methodology, reliance on optimization algorithms in finite element analysis was pivotal in determining the objective function, with a primary aim of reducing sections to achieve a more efficient structure, resulting in decreased weight and cost.

The optimization of the sections have been applied in two approaches, the initial approach 6.1, involved trial and error, where sections were manually adjusted in SAP2000 until the appropriate selection was determined, the second approach 6.2, involved leveraging Artificial Intelligence and machine learning through MATLAB, incorporating genetic algorithms for an automated process. This not only significantly reduces the time required but also enhance precision compared to manual method.

In the second approach the emphasis lies on optimization, beginning with the definition of genetic programming and design variables, the methodology proceeds with and overview of the utilized algorithm, depicted in a flowchart, with each step meticulously explained.

Conversely, the subsequent section, 6.3, delves into the Finite Element Analyses carried out with SAP2000, outlining the details of both the linear dynamic analyses and the non-linear static analyses conducted.

6.1. Trial and Error-Manual Approach:

The optimization process began with assigning random and oversized sections, such as HEB1000, to the entire bridge deck. While these sections ensured structural integrity, they also resulted in excessive weight. To reduce weight without compromising safety, a trial-and-error approach was employed. The process involved systematically decreasing the size of the sections, starting from HEB1000, and observing the resulting failure profiles in SAP2000. Each adjustment promoted a reevaluation of the model's performance, considering factors like structural stability and load-bearing capacity. Through iterative adjustments and analyses, a series of different optimization scenarios emerged, documenting the progression of changes and their effects on the overall structure. By refining the section sizes incrementally, the final model achieved optimal performance with minimized weight. This iterative optimization not only enhanced structural efficiency but also contributed significantly to cost reduction, manufacturing feasibility, and overall project viability. Detailed insights into the optimization journey and specific scenarios encountered can be found below :

- First try, by using HEB 300 for main beams and different double UPN sections for the bracings all over the structure to see the behavior of it :

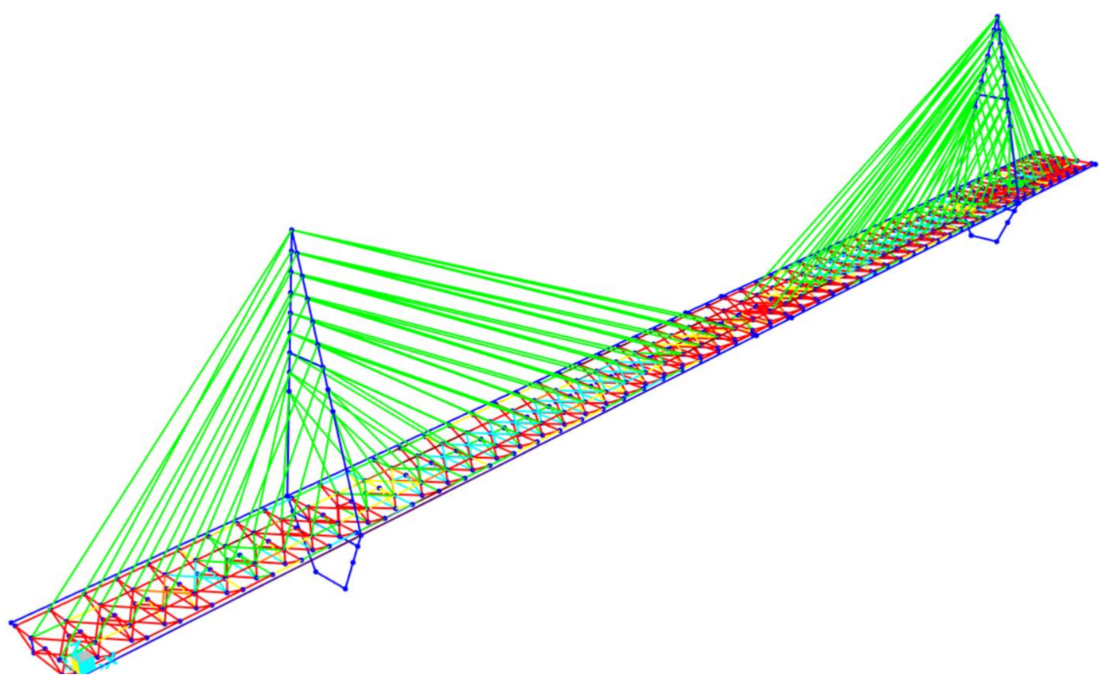

Figure 86. All Failure sections - at the beginning

- It's obvious that there are many sections that have to be changed in order to be verified.

6.1.1. Some failure examples:

The Edge (Failure):

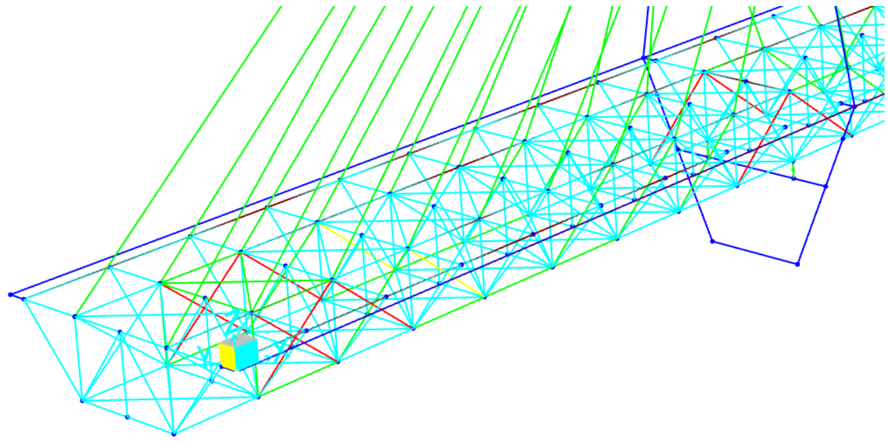

Figure 87. Edge Part

A) Vertical Longitudinal Bracings - double c section -1 :

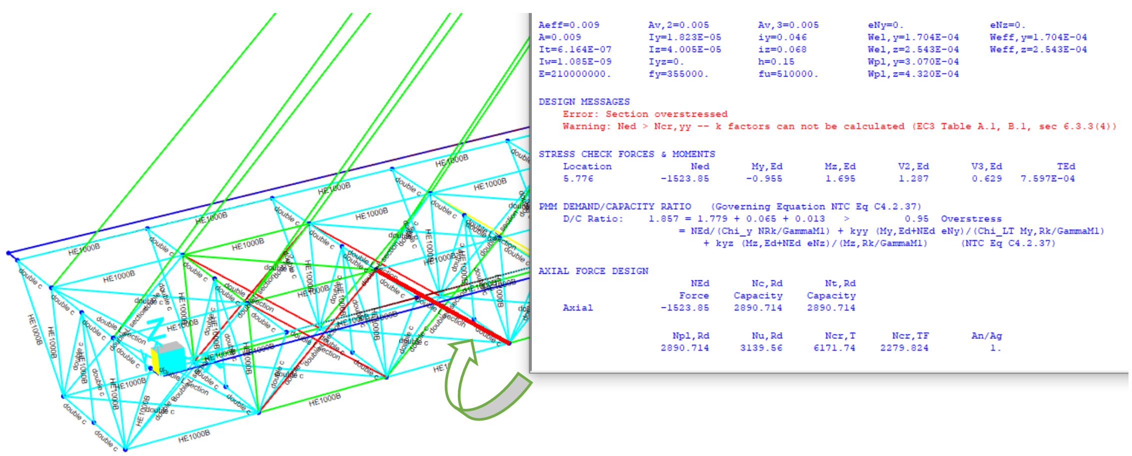

Figure 88. Vertical longitudinal bracing-fail-1

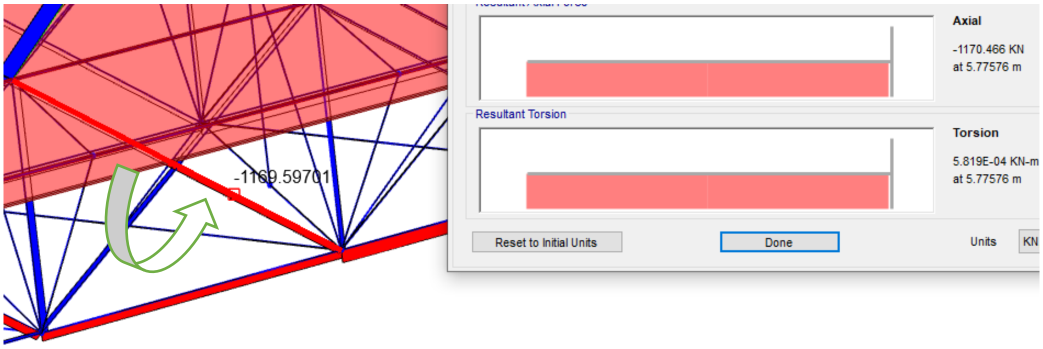

Figure 89.Vertical longitudinal bracing-axial load-1

B) <u>Vertical Longitudinal Bracings - double c section -2 :</u>

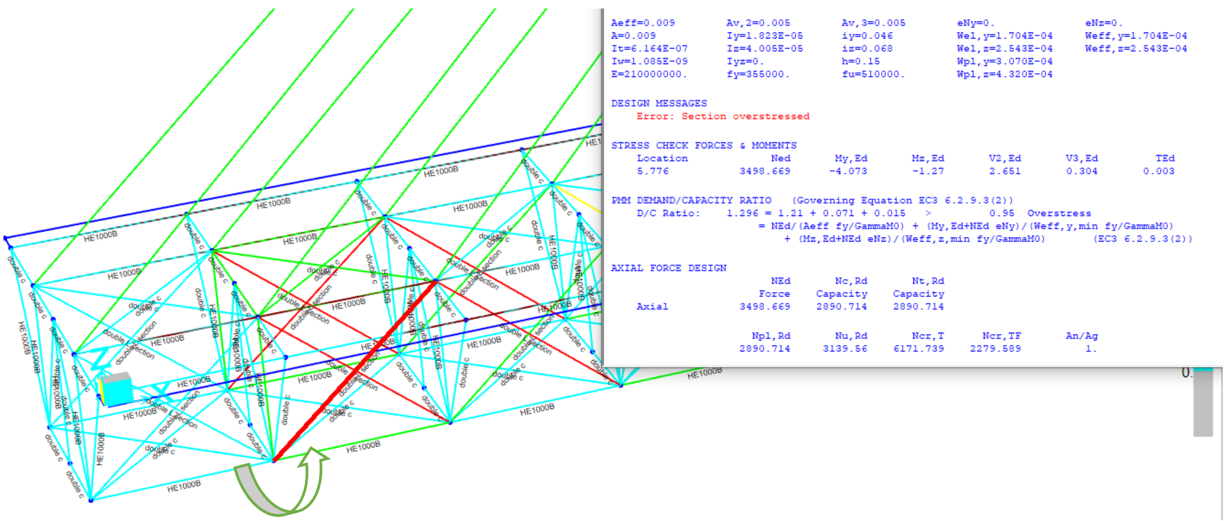

Figure 90. Vertical longitudinal bracing-fail-2

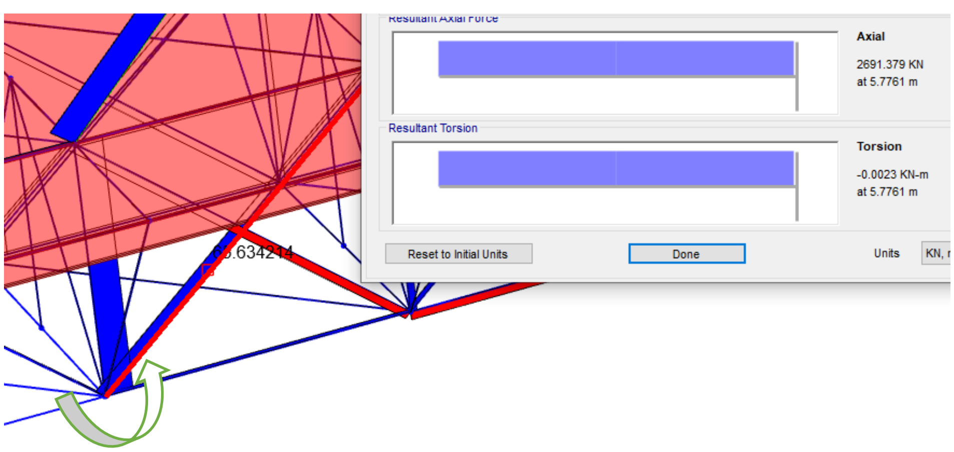

Figure 91.Vertical longitudinal bracing-axial load-2

C) Vertical Longitudinal Bracings at the pier :

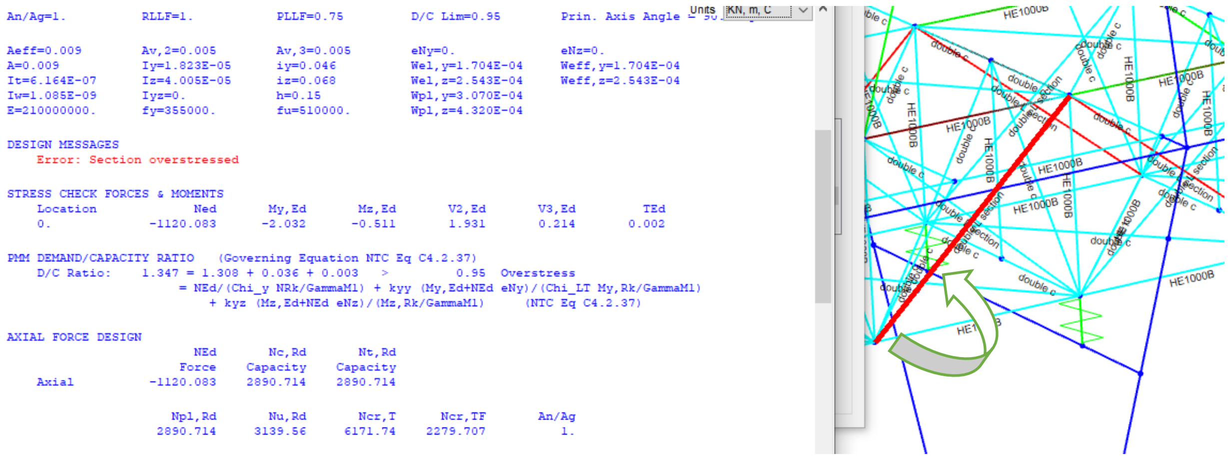

Figure 92. Vertical longitudinal bracing at the pier-fail

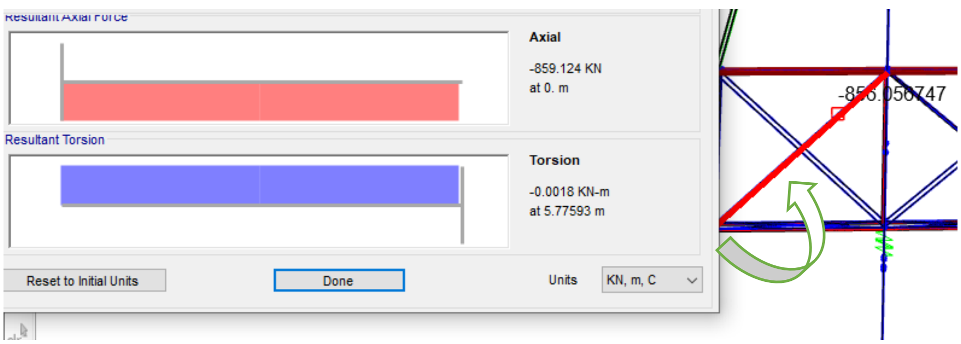

Figure 93. Vertical longitudinal bracing at the pier

D) Longitudinal Main Beams - Center :

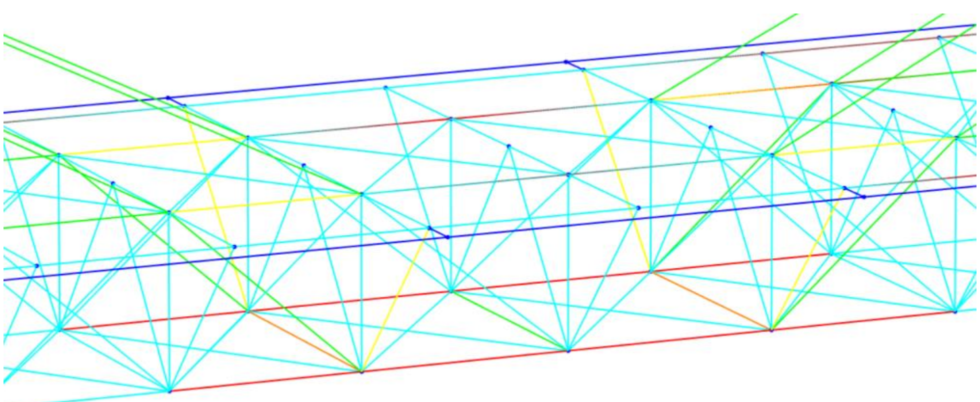

Figure 94. longitudinal main beams-center

6.1.2. Addressing Structural Failures :

Initially, failed sections were replaced with HEB 500 and HEB 1000 profiles. Subsequently, the optimization process focused on enhancing efficiency while reducing material usage and costs. Below, we will illustrate how the sections were optimized to achieve these objectives. This involved reducing the size of the sections to improve their efficiency and maximize the utilization of materials.

One of the primary challenges encountered the iterative process of optimizing sections. Each attempt to optimize a particular section would rectify issues in that specific area but inadvertently introduce failures elsewhere in the structure. This iterative trial-and-error approach required multiple adjustments and refinements to find a solution that addressed all critical areas effectively.

This transversal section was fixed by changing its profile from double UPN(100*6) to HEB 300:

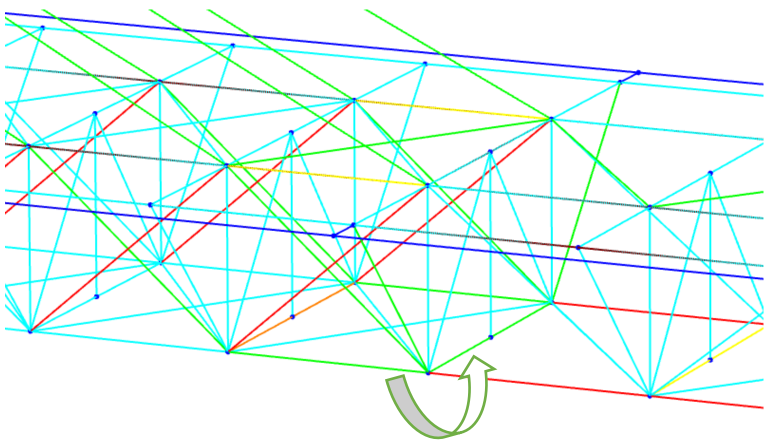

Figure 95. Transversal Profile

Changing all HEB 1000 to HEB 400 and the center as HEB 900:

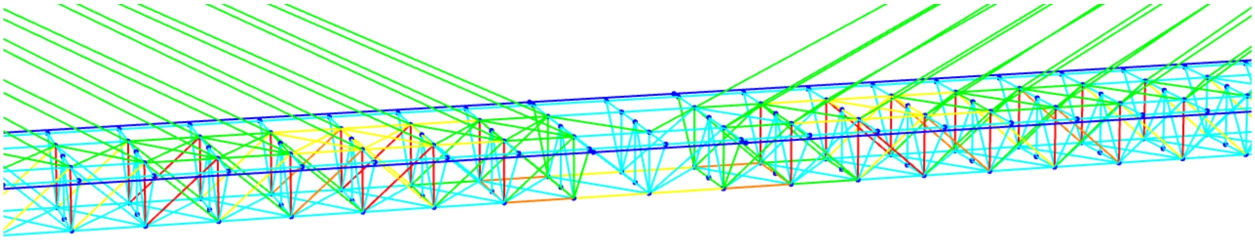

Figure 96. Center

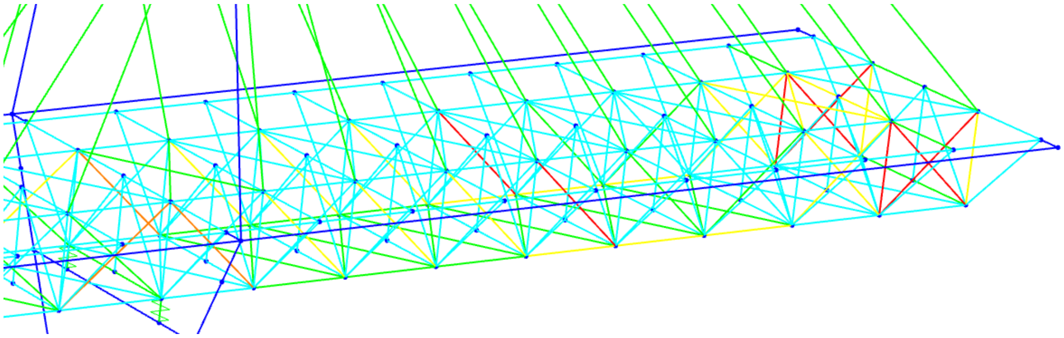

Figure 97. Edge-1

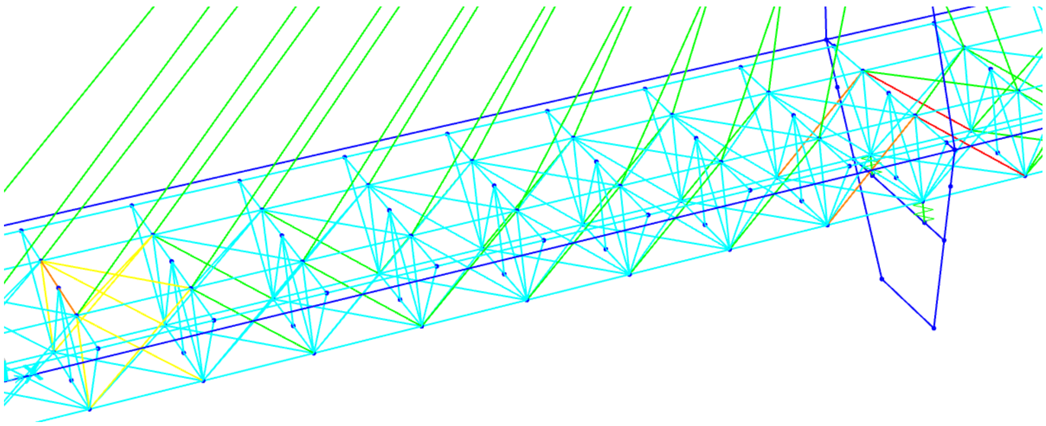

Figure 98. Edge -2

After changing the double UPN sections of the entire bridge from 100*6 to 300*100*10, all of them was verified except these sections:

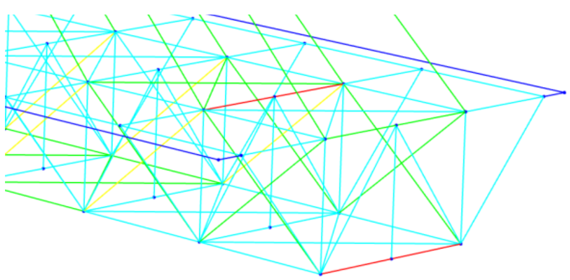

Figure 99. End transversal beams

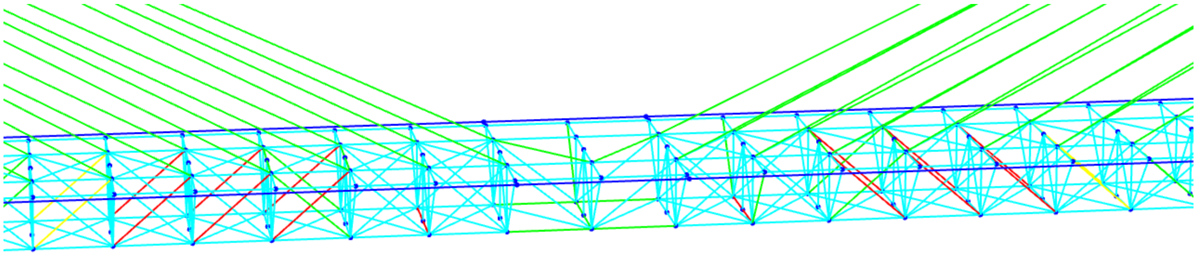

Figure 100. longitudinal bracings center-3d view

Changing the longitudinal bracings to 280*95*50 and transversal beams to 280*95*10

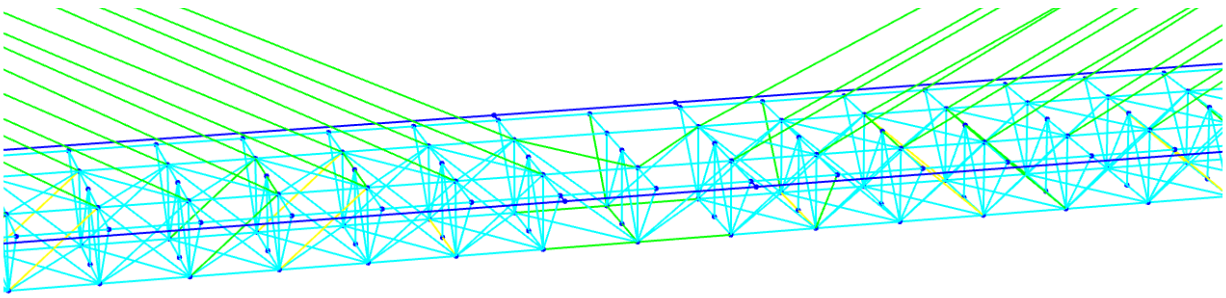

Figure 101. fixed longitudinal and transversal beams view

Increasing the section of the vertical ones to HEB600:

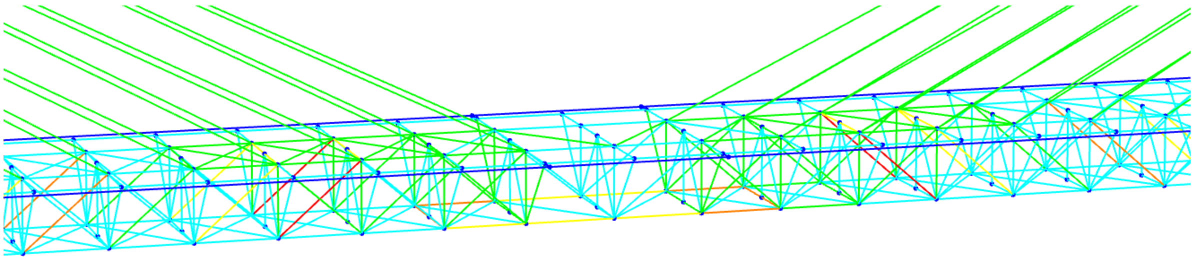

Figure 102. Vertical HEB 600

Changing the HEB400 and HEB900 in the bottom center to HEB500 and HEB800 respectively, and failure ones in longitudinal bracings to HEB 300 :

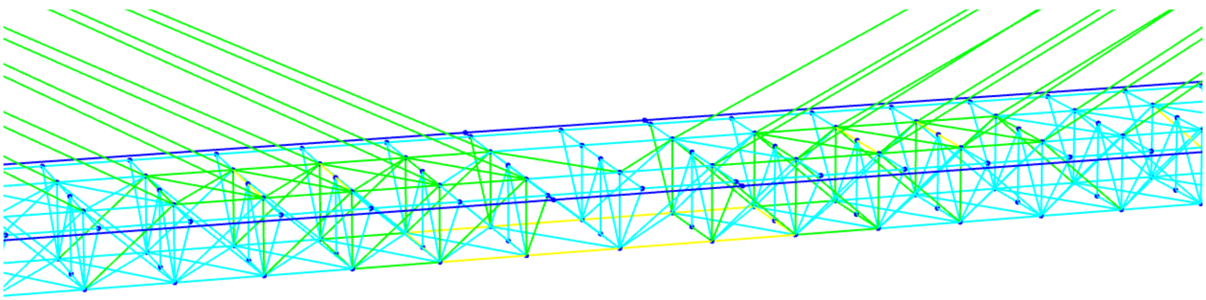

Figure 103. Center2

Changing bracings to 260*90*10 :

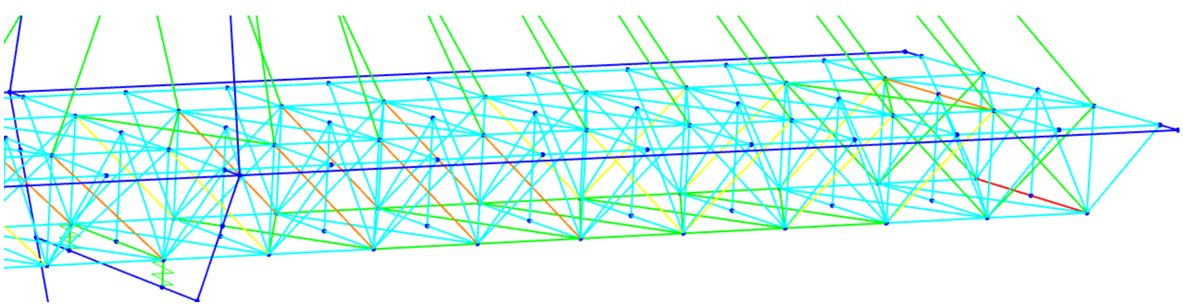

Figure 104. Edge 3 -fail

Changing longitudinal bracings to HEB300 and transversal ones to 280*95*50 :

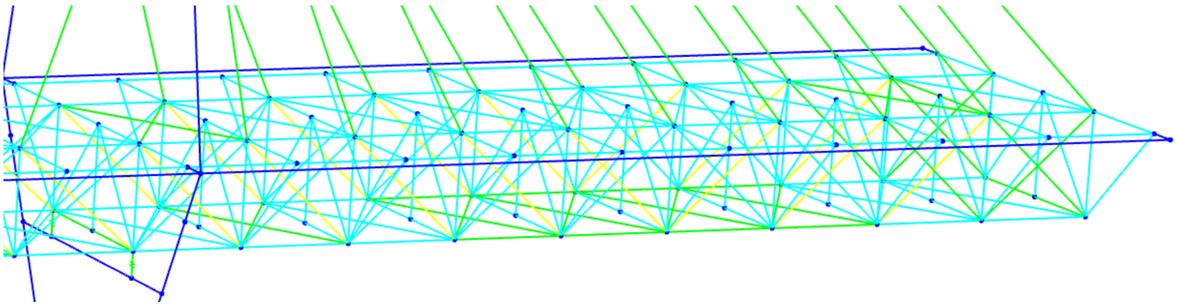

Figure 105. Edge 3 - Fixed

Left pier:

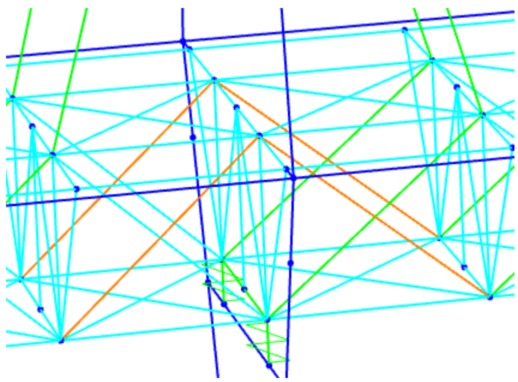

Figure 106. Pier - Fail

Changing to HEB300:

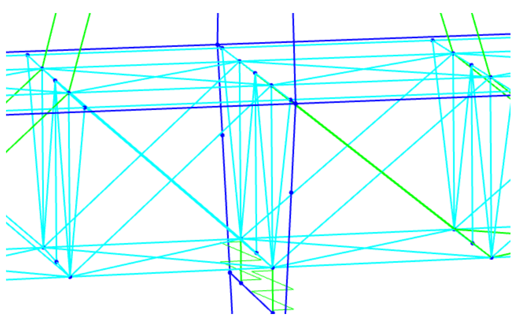

Figure 107. Pier - Fixed

Final Scheme :

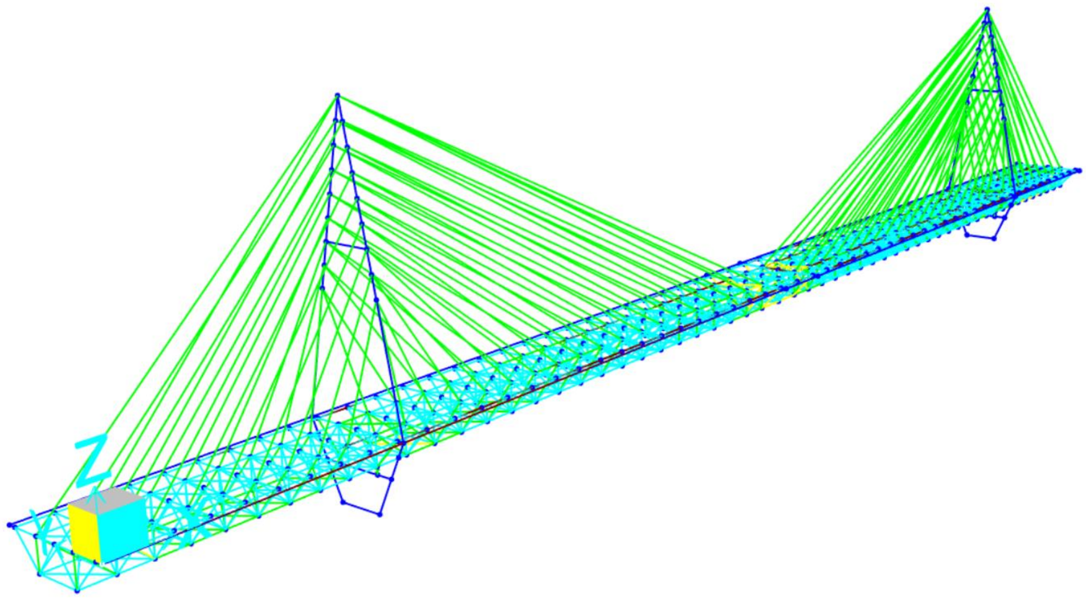

Figure 108. Whole fixed Structure – 1

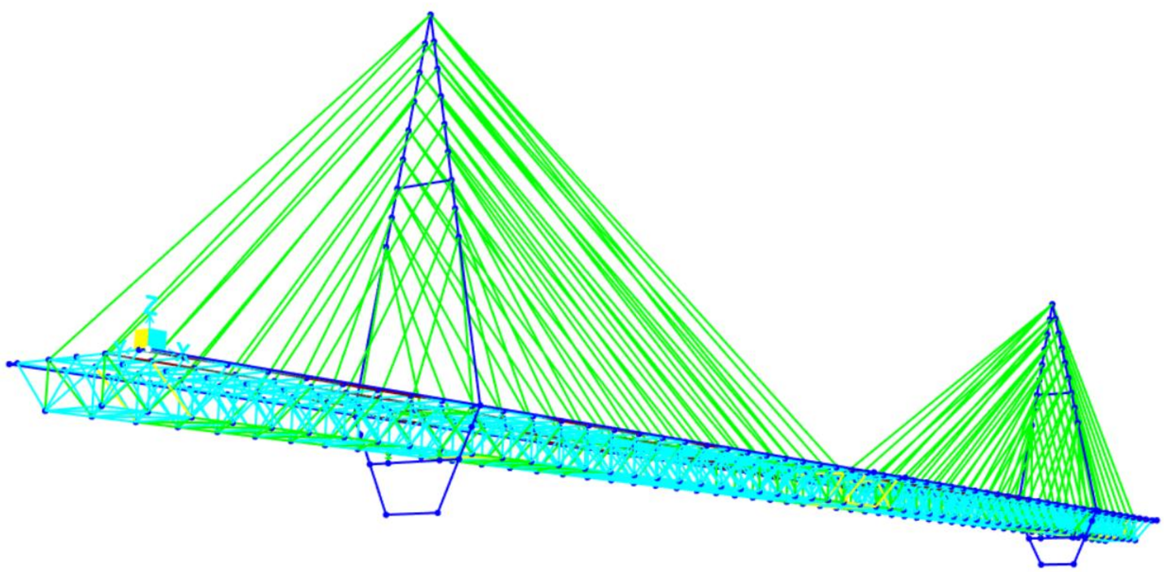

Figure 109. Whole fixed Structure - 2

❖ The most critical sections, such as those at the center and edges of the cantilever, underwent modifications aimed at ensuring structural integrity. These sections predominantly feature higher-profile elements to prevent overstressing. Below are examples of illustrating the process of consolidating sections to minimize variation.

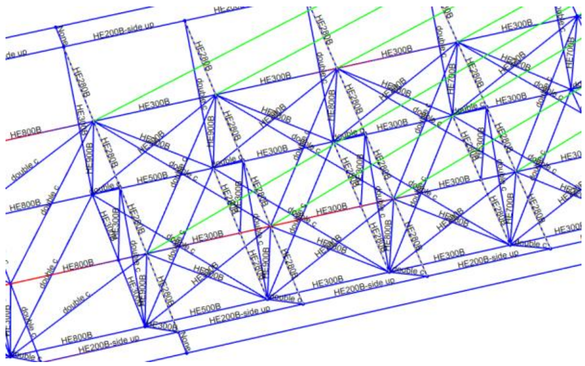

Figure 110. HEB 280 to HEB 300 in center transversal beams

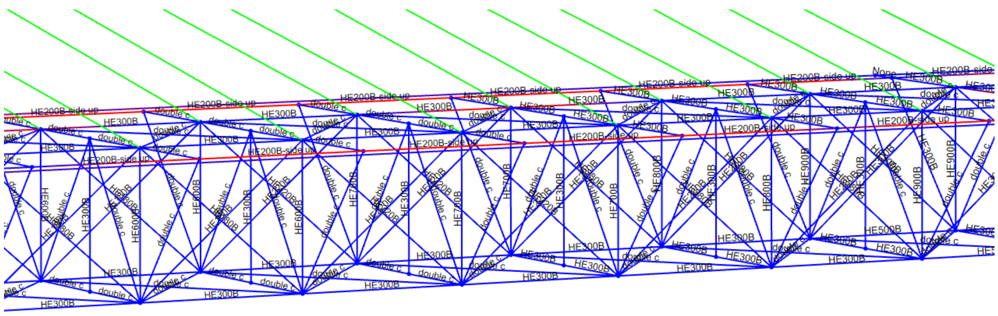

Figure 111. Rounding up the vertical side beams to 3 sections: HEB300-HEB600-HEB900

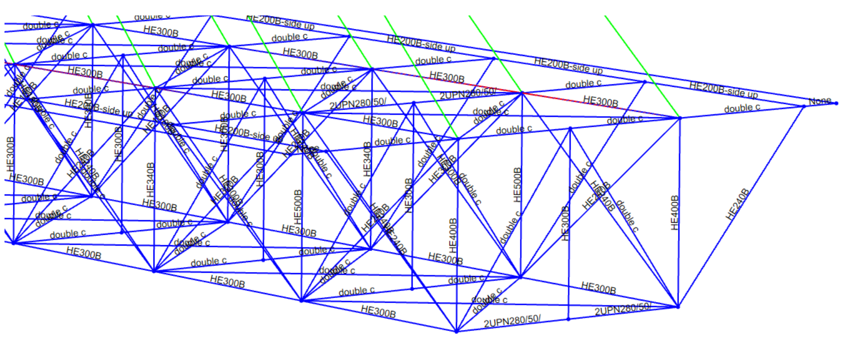

Figure 112. Rounding up the vertical side beams to HEB500

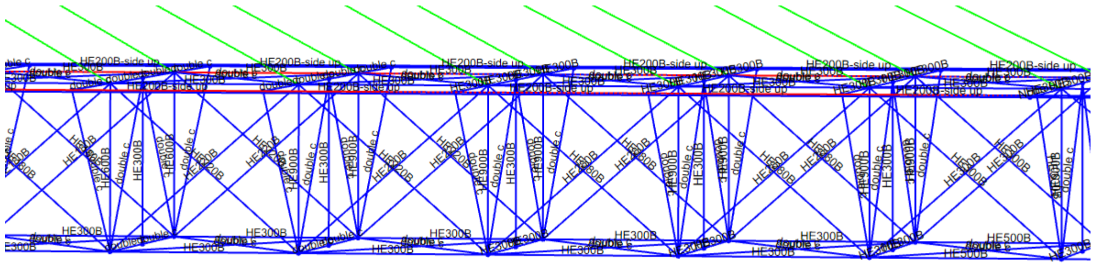

Figure 113. Rounding up the longitudinal bracings to HEB300:

After applying many changes to the sections and trying different probabilities manually all the sections have proper profiles except the center part, in order to solve this problem we have decided to change the profiles from HEB to HEM.

6.1.3. Correlation between the cables and deck profiles:

The correlation between cables and deck profiles is crucial in structural design, particularly in cable-stayed bridges. Altering the diameter of the strands (cables) directly impacts the stress distribution within the deck. Increasing or decreasing the diameter of the strands influence the load distribution across the deck, subsequently affecting the stress levels in different sections. This interdependences highlights the need for careful consideration and coordination between cable and deck design to ensure structural integrity and optimal performance of the bridge system.

By decreasing the cross section of the first two left cables from 250 mm of diameter to 150 to see the resistant behavior of the profile and the results were as below:

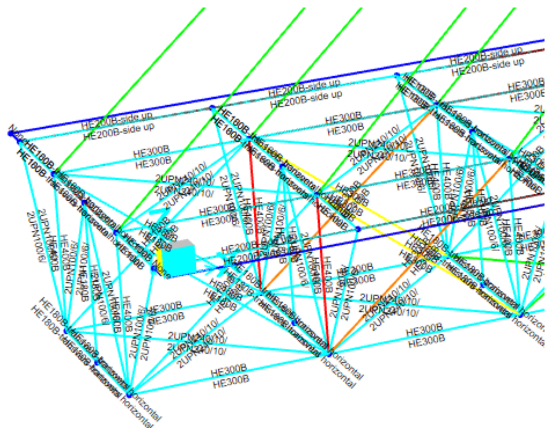

Figure 114. effect of cable on the edge vertical beams

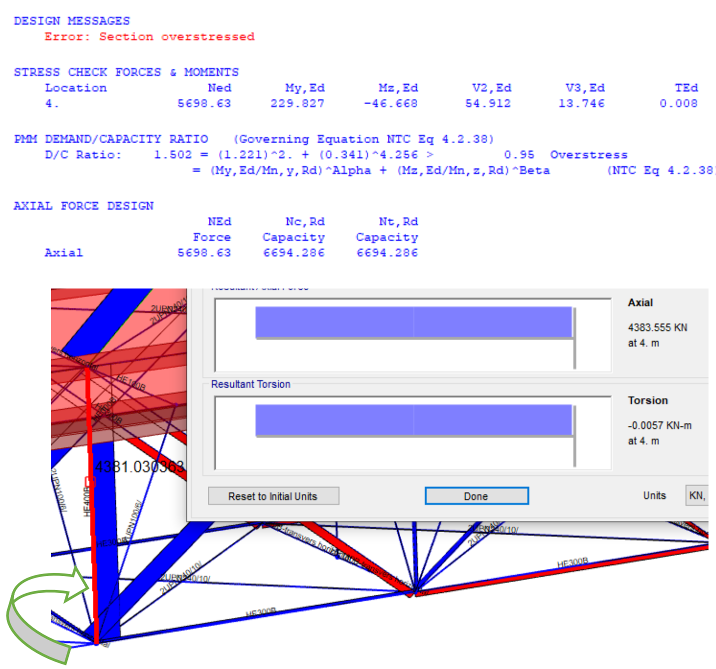

Figure 115. Overstressed vertical beams

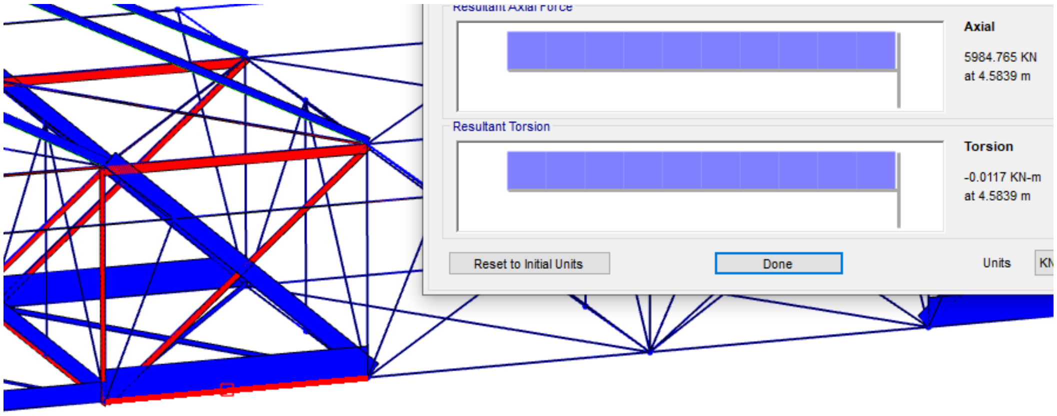

Figure 116. Axial load in the longitudinal beam

Axial load in the cables:

Upon reducing the cross-section of the cables, we observed a decrease in the axial load within these cables. However, this led to the vertical beam adjacent to them experiencing overstressing. To address this issue, we have two potential solutions. Firstly, we can maintain the diameter of the cables at approximately 200 mm. alternatively, we can increase the profile of the steel sections where overstressing occurred. Below, you'll find the impact of these changes on the sections at the edge of the bridge. Specifically, when the diameter of the first six left cables was reduced to 170 mm, most sections were adequately verified except for the longitudinal side bracings.

A) <u>At the Edge:</u>

Before the first change :

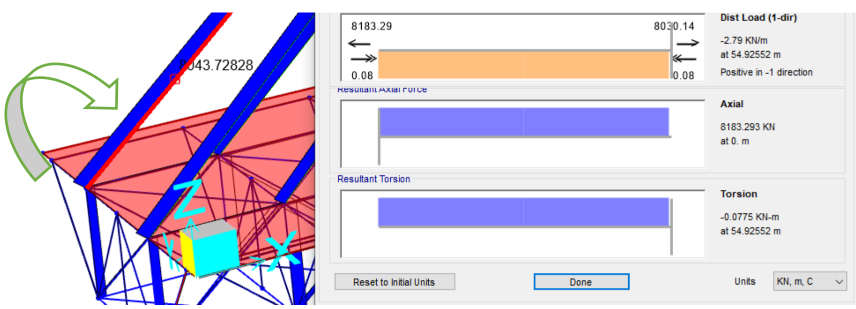

Figure 117. Cable axial load before changing the diameter - Edge

After the first change :

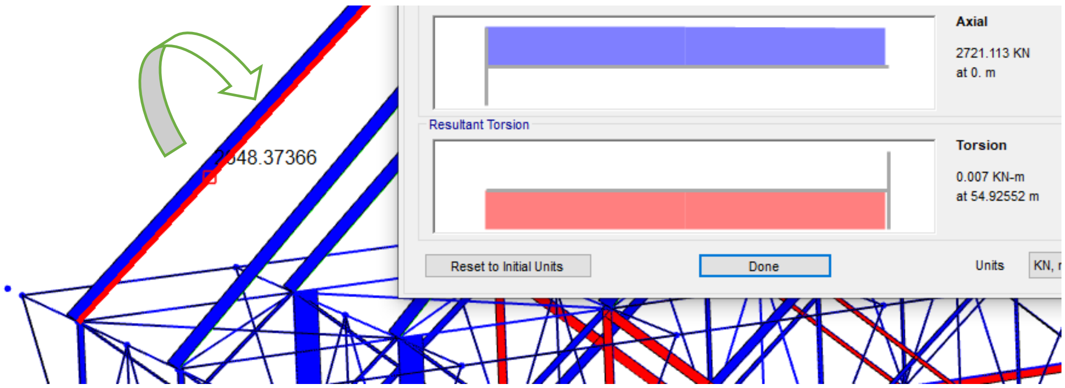

Figure 118. Cable axial load after changing the diameter - Edge

Slightly verified bracing due to changes in diameter of the cables :

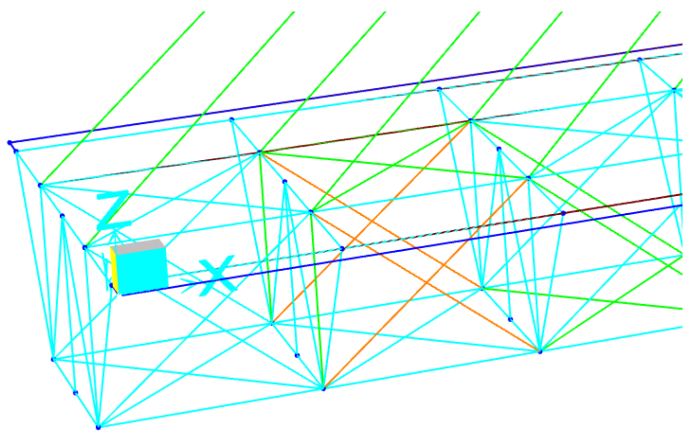

Figure 119. slightly verified bracing

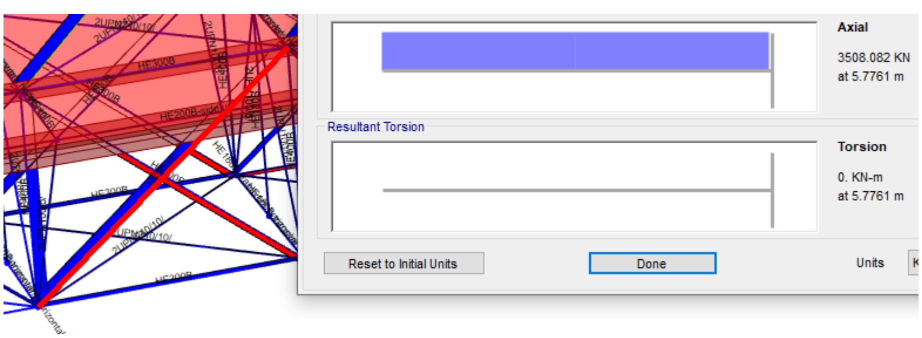

Figure 120. Axial load of the slightly verified bracing

B) <u>At the Center :</u>

Before :

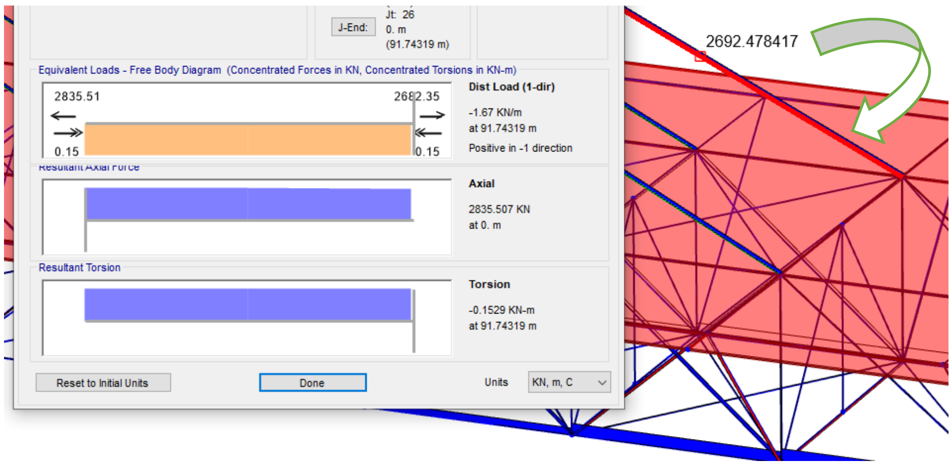

Figure 121. Cable axial load before changing the diameter - Center

After :

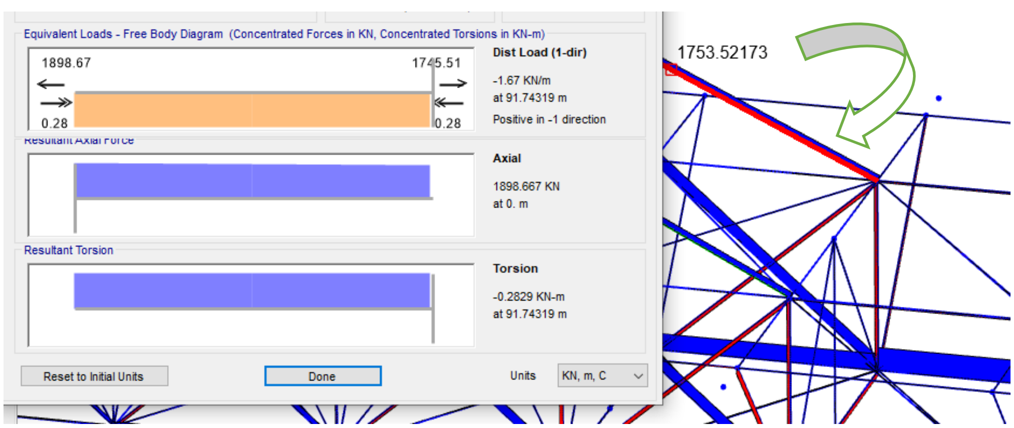

Figure 122. Cable axial load after changing the diameter - Center

6.2. Optimization via Genetic Programming:

6.2.1. Definition :

Genetic programming is a type of evolutionary algorithm, these algorithms provide a versatile framework that isn't limited to particular problems or math models. Instead, they offer general strategies for creating optimization methods.

These algorithms fall into categories such as evolutionary, physics-based, swarm-based, and nature-inspired. Here, the emphasis is on evolutionary algorithms, which draw inspiration from natural evolution and Darwinian Theory.

6.2.2. Methodology and Results Overview :

The optimization process using genetic algorithms followed a systematic sequence. It commenced with the initialization of the population, wherein potential solutions were generated. The subsequent step involved parent selection, where pairs of individual were chosen based on their fitness. Cross-over developed, facilitating the exchange of genetic information between selected parents. Mutation introduced random changes to maintain genetic diversity.

The fitness of each solution was evaluated using SAP2000, incorporating structural analysis. The outcomes were then sorted based on their performance. The primary goal of this optimization was to leverage genetic algorithms for efficient weight reduction in both the steel deck and cables. The iterative nature of the algorithm tried to identify the most optimal solution by considering lower weight, feasibility, and structural integrity. The chosen solutions were automatically assigned to the structure and subjected to verification. This iterative approach ensured the convergence toward a sustainable and optimized structural solution.

Additionally, the final results aimed for a weight ratio not exceeding 80 percent. Any steel deck section surpassing this limit was eliminated by the algorithms, selecting the most efficient solution within that threshold.

This entire procedure was conducted using a population size of 100 and 50 iterations in MATLAB.

6.2.3. Utilized Algorithm :

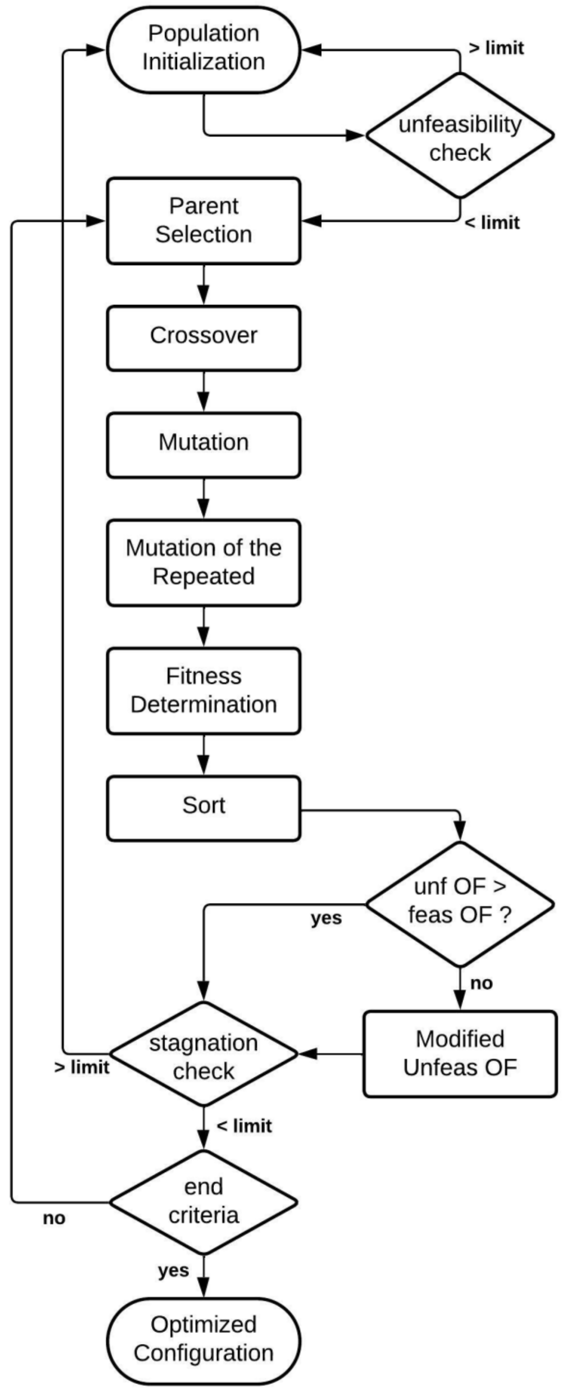

Figure 123. Flow diagram illustrating the adapted Genetic Algorithm utilized in the Optimization Procedure

Population Initialization:

The procedure initiates by forming a population consisting of a specified count of individuals (popsize), each serving as a prospective solution. Termed as "chromosomes," each individual's collection of design variables is allocated values delineate a solution. Initially, the population is created randomly, incorporating topology design variables (DVs) to guarantee a minimum of two exoskeletons in the retrofit configuration. Size DVs are chosen from a predefined range of profiles.

Once the initial population is defined, the objective function (OF) value is computed for each member. This involves creating a model in SAP2000 for each configuration and extracting the necessary results from the software analysis to determine the OF.

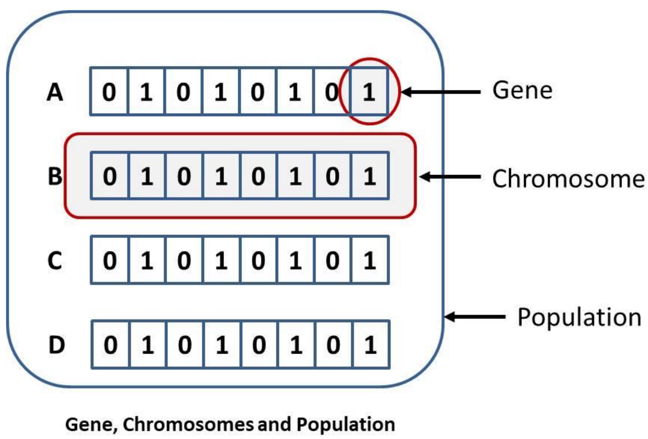

Figure 124. Population Initialization

Where, gene refers to a specific variable or parameter within an individual solution.

Feasibility Assessment:

When a potential solution fails to adhere to any of the constraints, such as the maximum allowable inter-drift of the original structure or the structural verifications of the exoskeleton's components, the corresponding population member is deemed *unfeasible*. The measure of unfeasibility is calculated as the ratio of unfeasible members to the total population size.

Ensuring the presence of at least one feasible member within a population serves a crucial guide for the algorithm towards solutions that meet the imposed constraints. Thus, once the fitness of each population member is determined, the level of unfeasibility is evaluated. In the absence of feasible elements, the initial population is regenerated to ensure progress in the optimization process.

Parent Selection:

The iterative process initiates by identifying the best promising solutions from the population, designated as *parents*. This selection is facilitated by a Roulette Wheel mechanism, where each member's probability of being chosen is determined by its fitness. Those with lower costs are more likely to be selected due to their higher probabilities.

Crossover:

Derived from the parents, new individuals emerge known as *children*. These children are formed through a combination of the parents chromosomes, shaping a fresh, evolved population. An internal iteration occurs, incorporating both parent selection and crossover steps. During each iteration, two parents are selected, from which a specified number of children is produced.

Various methods exist for conducting crossover operations, with the current implementation utilizing a Double-Point Crossover. In this approach, two points on the chromosome are randomly selected, excluding the beginning and end of the vector. These points determine where the chromosome. Conversely, the second child receives the opposite arrangement. This process continues iteratively until the desired number of children matches the population size.

Creating new children helps explore fresh potential solutions for the problem, resembling the best-performing ones obtained earlier. This involves retaining the values of variables that led to better outcomes but rearranging them differently.

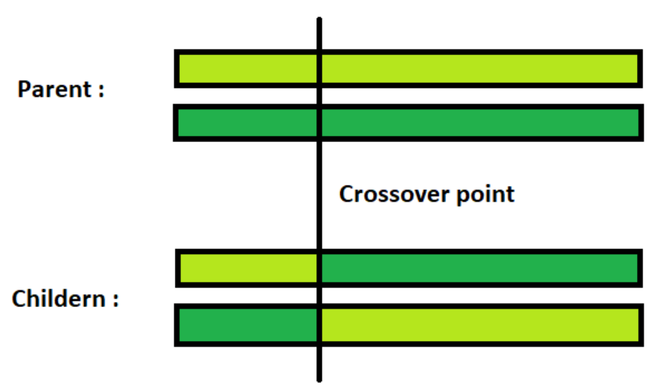

Figure 125. Crossover

Mutation:

After several iterations, potential solutions may start to resemble each other more closely. This occurs because new populations are formed by combining the best individuals from previous generations, guiding the algorithm toward convergence. This situation is termed *repetition*. However, the best solution may differ significantly in configuration from others, yet it is selected for standing out. Such a solution is termed *local optima*.

To counteract repetition, it is beneficial to explore solutions that deviate from the favored ones. An effective tactic is to randomly modify one or more variables on a chromosome of a population member. The decision to mutate a variable is made randomly, determined by a predefined probability. For binary variables, the value is switched, whereas for cross-section variables, a different section from the specified range is selected from a profile table.

In this algorithm, each variable in a chromosome has the chance of undergoing mutation, subject to a predefined probability. As a result, some population members may undergo multiple variable mutations, while others may retain all their original variables.

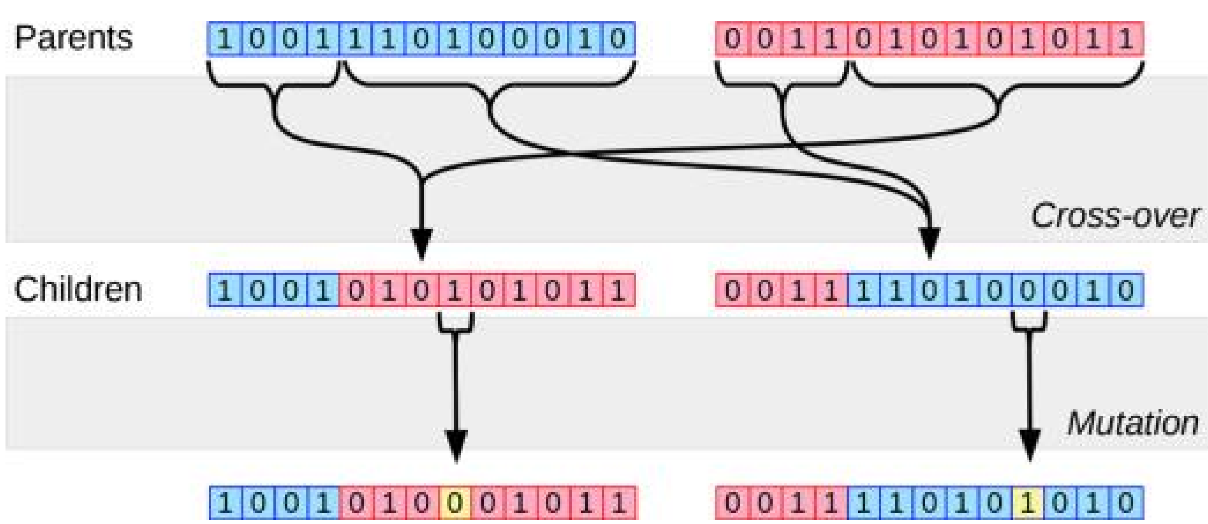

Figure 126. Selection procedure

Repetition Mutation:

As iterations progress, population members become increasingly similar, leading to repetition. In some cases, two or more individuals may share identical chromosomes, essentially representing the same solution. While repetition indicates the potential of a particular solution, having duplicated solutions reduces the diversity of options explored in each iteration, limiting algorithm exploration.

In contrast to the previous mutation strategy aimed at generating significantly different configurations, a new approach is introduced to refine existing solutions. This modified mutation targets population members sharing identical chromosomes. While one members remains uncharged, slight modifications are applied to other, allowing for exploration of solutions closely aligned with preferred ones.

Fitness Determination:

The fitness of each child is determined using Finite Element Analysis (FEA) conducted in SAP2000. Furthermore, the weight and stress ratio values are saved for each configuration.

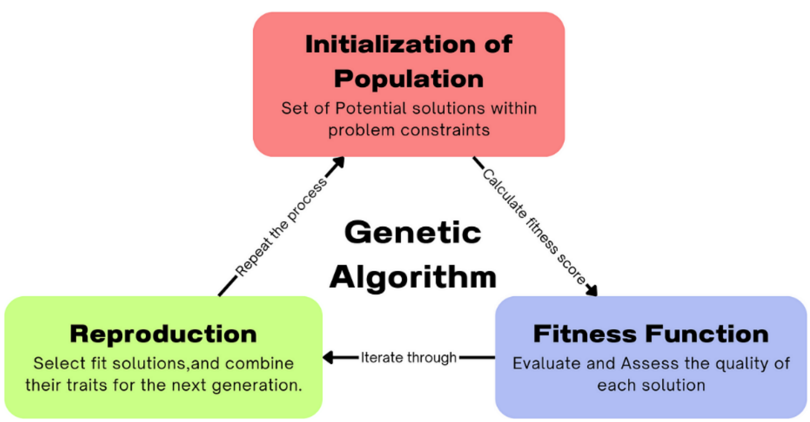

Figure 127. Loop function

Sort:

To organize the population, it is divided into two categories. Firstly, between feasible and unfeasible members, and secondly, between members with unique objective function (OF) values and those with repeated values.

Creation of Fresh population:

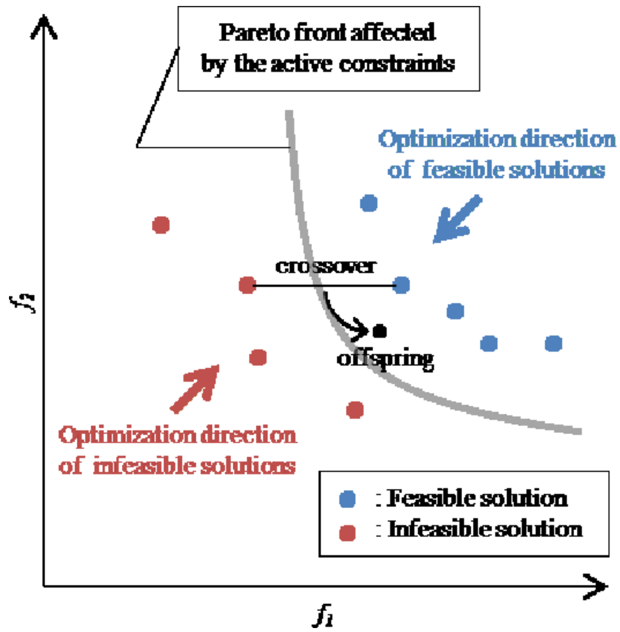

Figure 128. Feasible and infeasible solutions

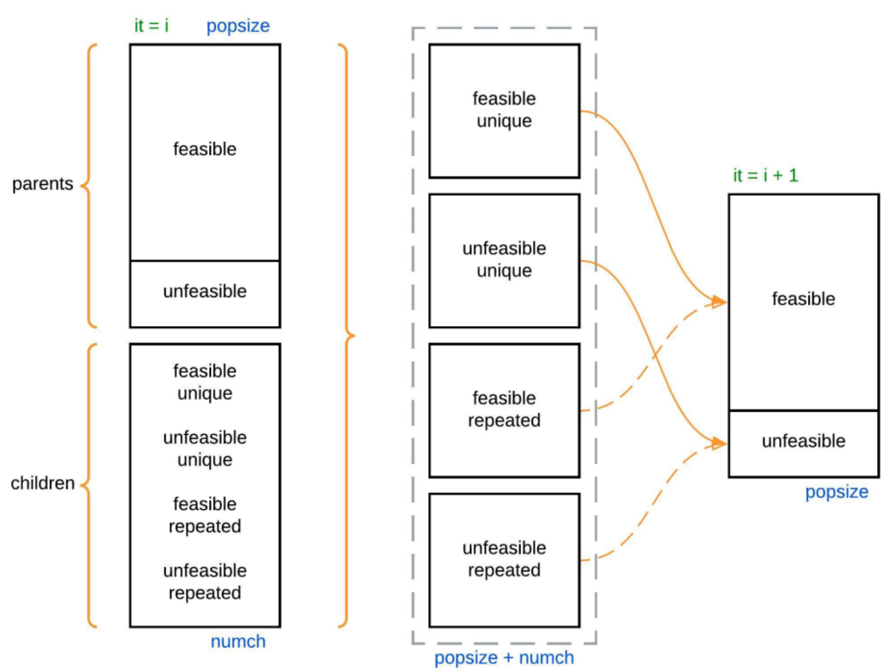

Figure 129. Approach for forming the population in the subsequent iteration

Stagnation:

A local optimal solution represents a configuration that offers superior performance compared to similar alternatives, although it may not be the globally optimal solution. As the algorithm progresses towards a local optimum, the population gradually converges towards this solution, leading to stagnation. Stagnation occurs when the algorithm struggles to explore diverse solutions, as indicated by the persistence of the preferred solution over multiple iterations. To address stagnation, the population can be re-initialized with a subset of the best-performing members, thereby enhancing the algorithm's exploration capabilities and increasing the likelihood of discovering the global optimum. However, if the preferred configuration remains uncharged despite re-initialization, it likely signifies the global optimum and remains unaffected by this adjustment.

Finalization:

Following the creation of the new population, the next iteration commences with the parent selection phase, wherein parents are chosen from the newly formed population. This iterative process continues until specific criteria for optimization conclusion are met. These criteria may involve achieving an individual with an objective function (OF) below a specified threshold or satisfying all constraints. In this scenario, optimization concludes when the number of iterations reaches a predetermined maximum limit.

FEM Analyses:

For conducting these analyses, SAP2000 OAPI was utilized. OAPI facilitates the control of the FEM software via automated routines programmed in MatLab. This entails the creation and modification of models directly by the algorithm at each iteration. Furthermore, the algorithm sets up the analysis, executes it, and extracts the results as variables for the optimization process.

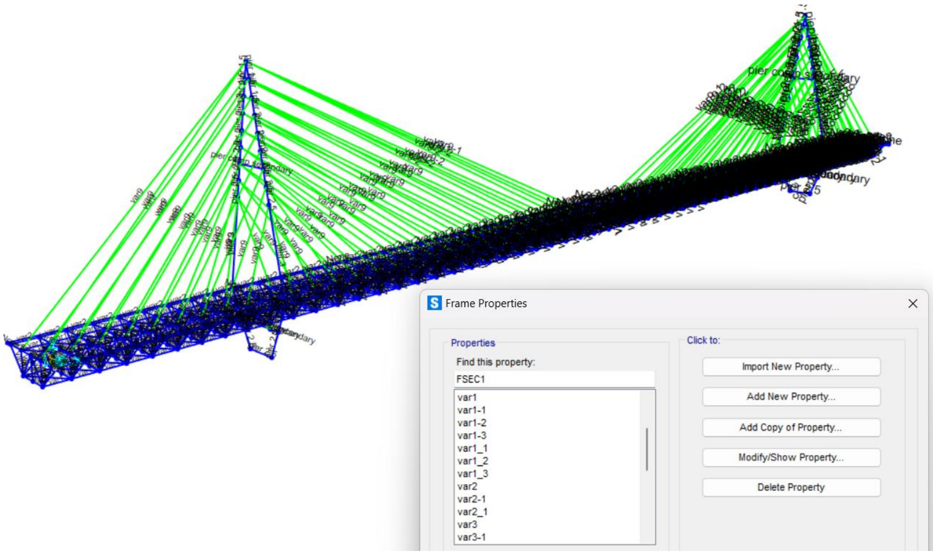

Figure 130. Variables defined in SAP2000

MATLAB:

As shown below, the groups are defined based on the selected sections, initially assessing the weight of each section, including both deck and cables.

Fields	name	sect	area	point1	point2	x1	y1	z1	x2	y2	z2	length	weight
1	"7"	'var5'	0.0212	'7'	'8'	250	1	0	250	4.7500	0	3.7500	6.1110
2	"9"	'var5'	0.0212	'9'	'10'	250	11.2500	0	250	15	0	3.7500	6.1110
3	"12"	'var5'	0.0212	'12'	'13'	0	1	0	0	4.7500	0	3.7500	6.1110
4	"14"	'var5'	0.0212	'14'	'15'	0	11.2500	0	0	15	0	3.7500	6.1110
5	"42"	'var5'	0.0212	'17'	'21'	37.5000	1	0	37.5000	4.7500	0	3.7500	6.1110
6	"44"	'var5'	0.0212	'25'	'29'	37.5000	11.2500	0	37.5000	15	0	3.7500	6.1110
7	"47"	'var5'	0.0212	'18'	'22'	120	1	0	120	4.7500	0	3.7500	6.1110
8	"49"	'var5'	0.0212	'26'	'30'	120	11.2500	0	120	15	0	3.7500	6.1110
9	"52"	'var5'	0.0212	'19'	'23'	130	1	0	130	4.7500	0	3.7500	6.1110
10	"54"	'var5'	0.0212	'27'	'31'	130	11.2500	0	130	15	0	3.7500	6.1110
11	"57"	'var5'	0.0212	'20'	'24'	212.5000	1	0	212.5000	4.7500	0	3.7500	6.1110
12	"59"	'var5'	0.0212	'28'	'32'	212.5000	11.2500	0	212.5000	15	0	3.7500	6.1110
13	"98"	'var1'	0.0192	'13'	'93'	0	4.7500	0	4.1667	4.7500	0	4.1667	6.1422
14	"100"	'var1'	0.0192	'94'	'94'	4.1667	4.7500	0	8.3333	4.7500	0	4.1667	6.1422
15	"101"	'var1'	0.0192	'94'	'95'	8.3333	4.7500	0	12.5000	4.7500	0	4.1667	6.1422

Table 34. Initial group assessing

In the initial attempt, the allocation of designated groups was conducted randomly, accompanied by steel verification using all approved sections and identified failure sections to validate the code's functionality. The numbers within brackets denote the row numbers in the Excel table containing the profile properties of HEB, primarily for the main beams, and UPN for secondary and bracing elements.

	A	B	C	D	E	F	G
1	HEB200	1	0.2	0.2	0.009	0.015	7.808
2	HEB220	2	0.22	0.22	0.0095	0.016	9.104
3	HEB240	3	0.24	0.24	0.01	0.017	10.599
4	HEB260	4	0.26	0.26	0.01	0.0175	11.844
5	HEB280	5	0.28	0.28	0.0105	0.018	13.136
6	HEB300	6	0.3	0.3	0.011	0.019	14.908
7	HEB320	7	0.32	0.3	0.0115	0.0205	16.134
8	HEB340	8	0.34	0.3	0.012	0.0215	17.09
9	HEB360	9	0.36	0.3	0.0125	0.0225	18.063
10	HEB400	10	0.4	0.3	0.0135	0.024	19.778
11	HEB450	11	0.45	0.3	0.014	0.026	21.798
12	HEB500	12	0.5	0.3	0.0145	0.028	23.864
13	HEB550	13	0.55	0.3	0.015	0.029	25.406
14	HEB600	14	0.6	0.3	0.0155	0.03	26.996
15	HEB650	15	0.65	0.3	0.016	0.031	28.634
16	HEB700	16	0.7	0.3	0.017	0.032	30.638
17	HEB800	17	0.8	0.3	0.0175	0.033	33.418
18	HEB900	18	0.9	0.3	0.0185	0.035	37.128

Figure 131. HEB profiles

	A	B	C	D	E	F	G
1	UPN200	1	0.2	0.075	0.0085	0.0115	0.00322
2	UPN220	2	0.22	0.08	0.009	0.0125	0.00374
3	UPN240	3	0.24	0.085	0.0095	0.013	0.00423
4	UPN260	4	0.26	0.09	0.01	0.014	0.00483
5	UPN280	5	0.28	0.095	0.01	0.015	0.00533
6	UPN300	6	0.3	0.1	0.01	0.016	0.00588
7	UPN320	7	0.32	0.1	0.014	0.0175	0.00758
8	UPN350	8	0.35	0.1	0.014	0.016	0.00773
9	UPN380	9	0.38	0.102	0.0135	0.016	0.00804
10	UPN400	10	0.4	0.11	0.014	0.016	0.00915

Figure 132. UPN profiles

RESULTS

1x1 struct with 4 fields

Field	Value
Best_Chrom	30x21 double
Best_OF	1x30 double
Best_Pen1	1x30 double
Best_Weight	1x30 double

Figure 133. Results

Best_Chrom :

Fields	chrom	weight	penalty_1	OF
1	[10,11,2,11,8,2,3,6,0.3900]	5.4808e+04	2.0046e+03	1.0987e+08
2	[12,2,12,12,6,10,2,5,0.3700]	5.1091e+04	150.1725	7.6725e+06
3	[10,12,8,1,11,12,7,8,0.3300]	4.4584e+04	[]	[]
4	[5,8,3,9,1,4,1,1,0.3500]	[]	[]	[]
5	[9,4,12,1,6,5,8,8,0.1900]	[]	[]	[]
6	[6,6,8,9,10,4,7,7,0.1900]	[]	[]	[]
7	[2,6,12,5,8,3,8,3,0.2700]	[]	[]	[]
8	[9,11,12,7,2,2,3,9,0.2100]	[]	[]	[]
9	[10,3,12,5,3,4,7,5,0.2300]	[]	[]	[]
10	[10,8,7,12,4,10,8,4,0.2900]	[]	[]	[]
11	[1,1,7,10,12,2,6,5,0.1500]	[]	[]	[]
12	[5,2,10,4,7,2,7,3,0.3100]	[]	[]	[]
13	[9,9,6,2,3,11,2,9,0.2700]	[]	[]	[]
14	[12,1,6,2,12,1,8,9,0.3700]	[]	[]	[]
15	[2,5,4,10,6,11,2,3,0.1700]	[]	[]	[]

Table 35. Initial Results of MatLab

RESULTS.Best_Chrom

	1	2	3	4	5	6	7	8	9	10	11	12	13	14
1	18	2	4	2	9	1	17	12	1	1	4	9	3	1
2	18	2	4	2	9	1	17	12	1	1	4	9	3	1
3	18	2	4	2	9	1	17	12	1	1	4	9	3	1
4	18	2	4	2	9	1	17	18	1	2	6	9	17	
5	18	2	4	2	9	1	17	18	1	2	6	9	17	
6	18	2	6	18	18	17	2	18	1	2	6	10	12	
7	18	5	9	12	13	8	13	5	1	1	4	9	3	
8	18	2	4	12	13	8	13	5	1	1	4	9	3	
9	18	2	4	2	16	1	17	18	1	2	6	17	4	
10	18	2	4	2	16	1	17	18	1	2	6	10	3	
11	18	2	4	2	16	1	13	5	1	1	6	9	3	
12	18	2	4	2	16	1	13	5	1	1	6	9	3	
13	18	2	1	8	16	12	15	1	1	1	16	9	5	
14	18	2	4	2	16	1	13	5	1	1	4	9	3	
15	18	2	4	2	16	1	13	5	1	1	4	9	3	
16	18	6	4	2	17	8	16	14	1	1	4	8	18	
17	18	6	4	2	17	8	16	14	1	1	4	8	18	
18	18	6	4	2	17	1	13	5	1	1	4	9	3	
19	18	6	4	2	17	1	13	5	1	1	4	9	3	
20	18	6	4	2	17	8	16	14	1	1	4	8	18	
21	18	6	4	2	17	8	16	14	1	1	4	8	18	
22	18	2	4	2	17	8	16	14	1	1	4	8	3	

Figure 134. Final Results of MatLab

Main Problem :

In the optimization of our bridge design, we encountered a significant challenge with the central section's longitudinal beams, which failed to meet verification standards through both manual optimization and genetic algorithms. This issue required the consideration of substantially larger profiles, like HEB 800 or 900, which was impractical due to the stark contrast with the existing HEB 300 beams. To resolve this, we ultimately chose to implement HEA 300 beams for these critical central sections, ensuring a coherent and structurally sound design.

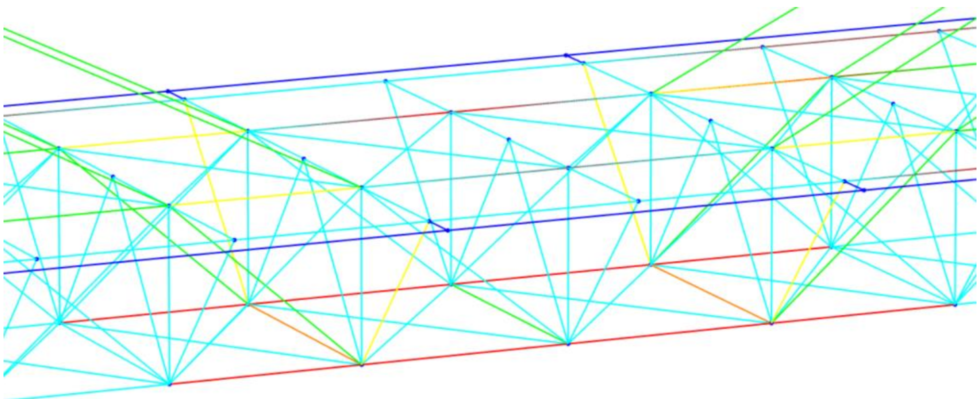

Figure 135. HEB 300 fail center section

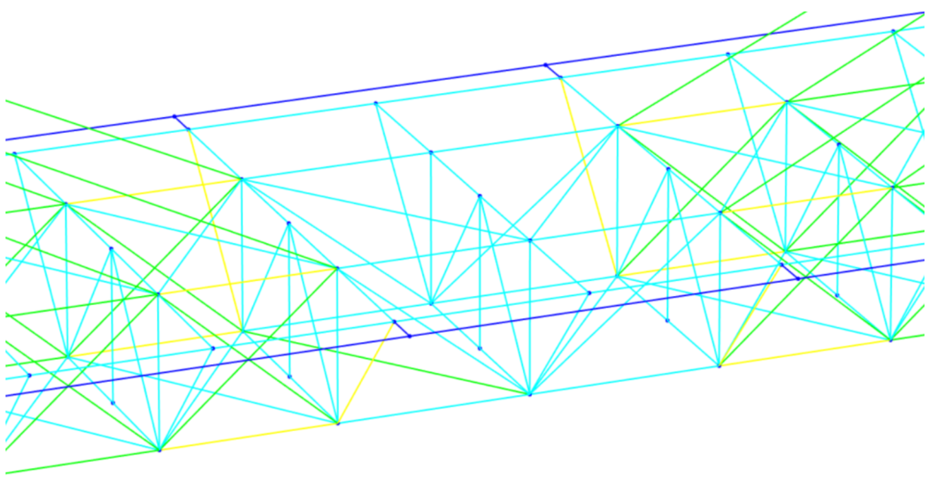

Figure 136. Fixed by HEA 300

7. B.I.M. Methodology :

7.1. General Information:

Building Information Modeling (BIM) methodology revolutionizes construction practices by offering a collaborative and digital approach to building design, construction, and management. BIM provides digital representations of physical spaces, enabling engineers to seamlessly navigate through conceptual design phases to operation and maintenance stages. Its adoption enables engineers to tackle complex challenges effectively while delivering high-quality, cost-effective, and sustainable bridge solutions.

Building Information Modeling (BIM) methodology not only revolutionizes construction practices but also enhances interoperability among various stakeholders involved in the lifecycle of a bridge project. Interoperability refers to the ability of different software systems to exchange and use information seamlessly. In the context of BIM, interoperability ensures that data can be shared efficiently among architects, engineers, leading to improved collaboration and coordination.

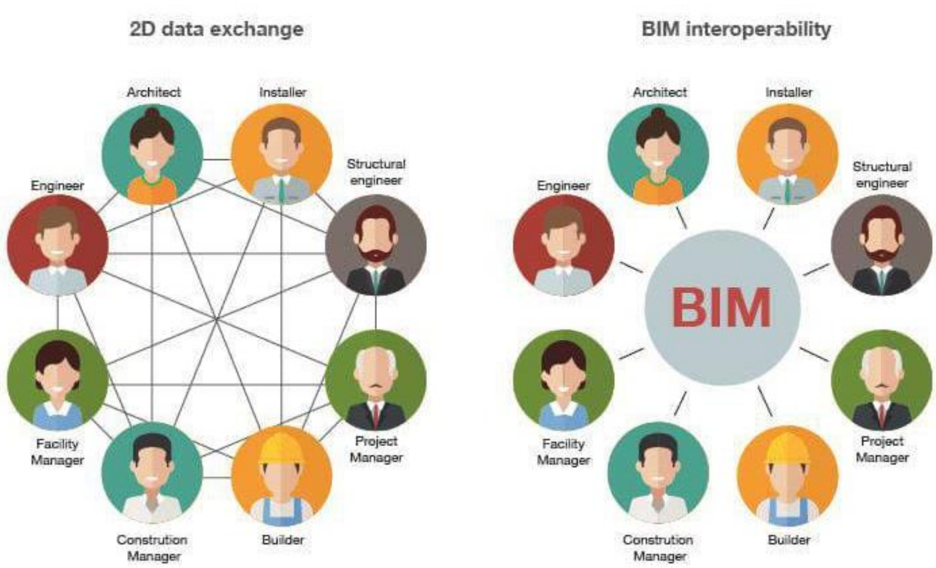

Figure 137. BIM Interoperability

Utilizing BIM in structural design streamlines the designer's workflow through seamless interaction between architectural and structural models. To remain competitive and efficient in both domestic and international markets, professionals and companies must address several key challenges. These include adhering to technical regulations for construction (NTC2018), integrating minimum environmental criteria (CAM). Adopting BIM methodologies for comprehensive building lifecycle management, and harnessing the capabilities of technologically advanced solutions offered by the digital industry, which are becoming increasingly accessible in terms of cost.

One essential aspect of interoperability in BIM is the use of Industry Foundation Classes (IFC), an open file format that facilitates the exchange of BIM data between different software platforms. IFC allows information to be transferred accurately across different software applications, ensuring consistency and accuracy throughout the project lifecycle.

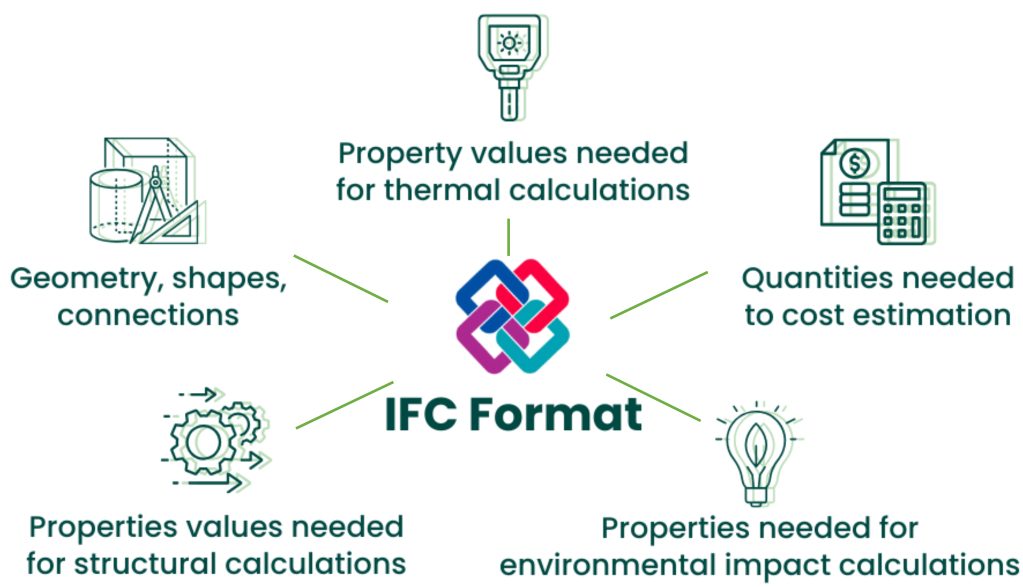

Figure 138. IFC Format

Different versions of IFC :

- IFC 4 : This protocol facilitates the transfer of IFC models for importation and modification within BIM-enabled software. It enables the transfer of parametric projects and intricate contexts, with the option for manual adjustments to accommodate software variations.

- IFC 2*3 : Also known as coordination view version 2, this format is tailored for the coordinated exchange of BIM models across various disciplines within the construction industry. It is presently the most prevalent model view definition endorsed by the BIM market. Coordination view supports basic parametric derivation of building components upon importation into planning tools, primarily utilized for exchanging architectural models, building technology, and engineering data.

- IFC 2*2 : Referred to as coordination view, this format is utilized in isolated instances, such as when exporting MVD definitions for software products incompatible with IFC 2*3. Each of these protocols can be manually adjusted to suit specific workflow requirements.

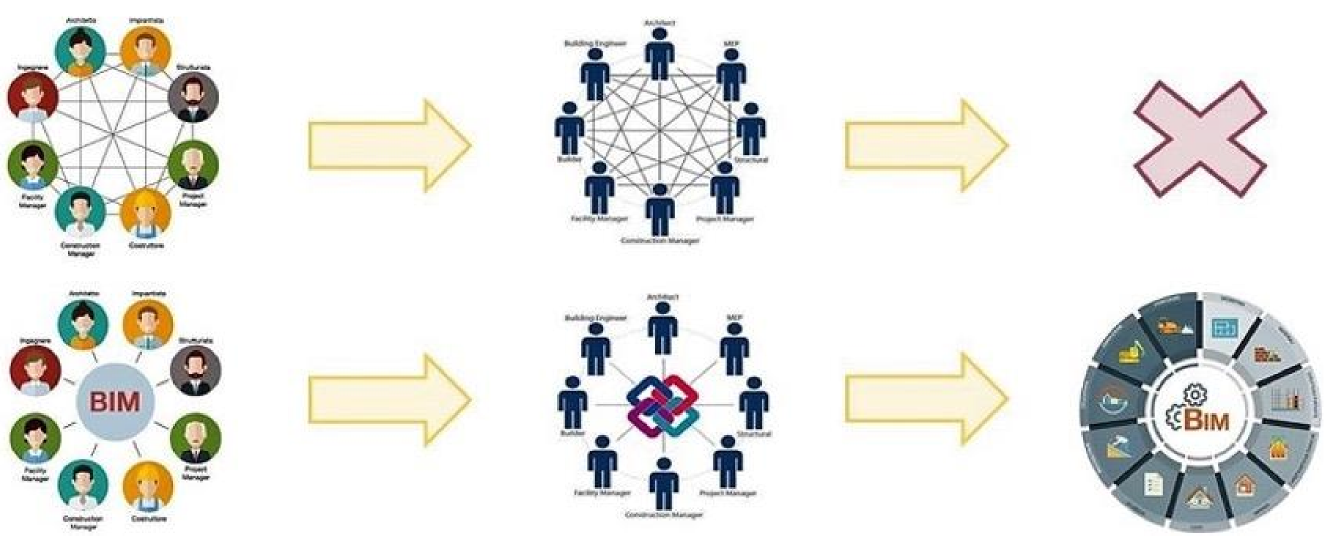

Figure 139. IFC & BIM

Additionally, BIM incorporates the concept of Level of Development (LOD), which defines the level of details and accuracy of the information contained within a BIM model at different stages of the project. LOD specifies the level of geometric details, as well as the level of information associated with each model element, such as material properties, dimensions, and performance data. By adhering to LOD standards, stakeholders can effectively communicate project requirements and expectations, leading to better decision-making and risk management.

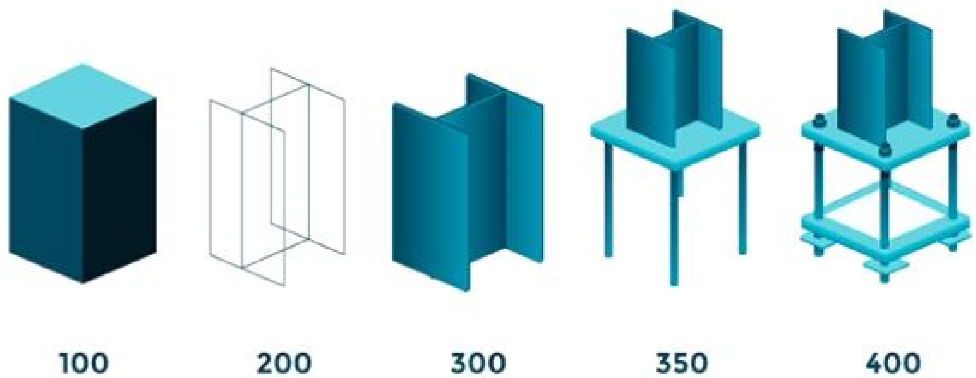

Figure 140. LOD

Essentially, the Level of Details (LOD) signifies the degree of information attributed to an element, aiming to enhance both the accuracy and comprehensiveness of the details provided.

LOD 100 : The model is represented symbolically or generically, offering a conceptual depiction and potential behavior.

LOD 200 : Model elements are depicted graphically as generic systems or assemblies, providing approximate quantities, sizes, orientation, etc.

LOD 300 : Model elements are detailed as specific systems, objects, or assemblies in terms of defined information, excluding graphical details attached to the model.

LOD 400 : The model is graphically detailed, depicting specific systems, objects, quantities, sizes, orientations, and other characteristics, along with fabrication and installation information.

LOD 500 : The model represents a field-verified depiction concerning size and component quantity.

7.2. Tekla Structures:

The integration of Building Information Modeling (BIM) methodology with Tekla software facilitated precise detailing of not only structural elements like beams, columns, and cables but also bolts and welding. Tekla's advanced tools allowed for accurate representation and placement of bolts and welding within the model, ensuring that every connection point was accurately captured. This level of detail was essential for structural analysis, optimization, and ensuring constructability. Additionally, the parametric modeling capabilities of Tekla enabled efficient management of bolted and welded connections, providing flexibility for design modifications and iterations. Overall, Tekla's capabilities for precise detailing of bolts and welding enhanced the accuracy and reliability of the bridge model, contributing to the overall success of the project.

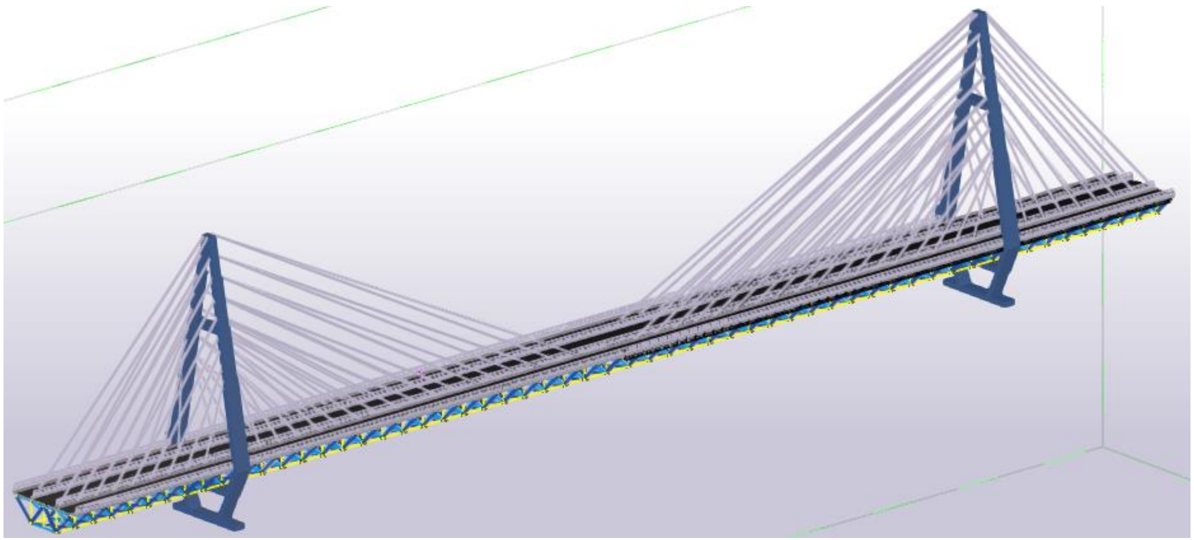

Figure 141. Bridge 3D

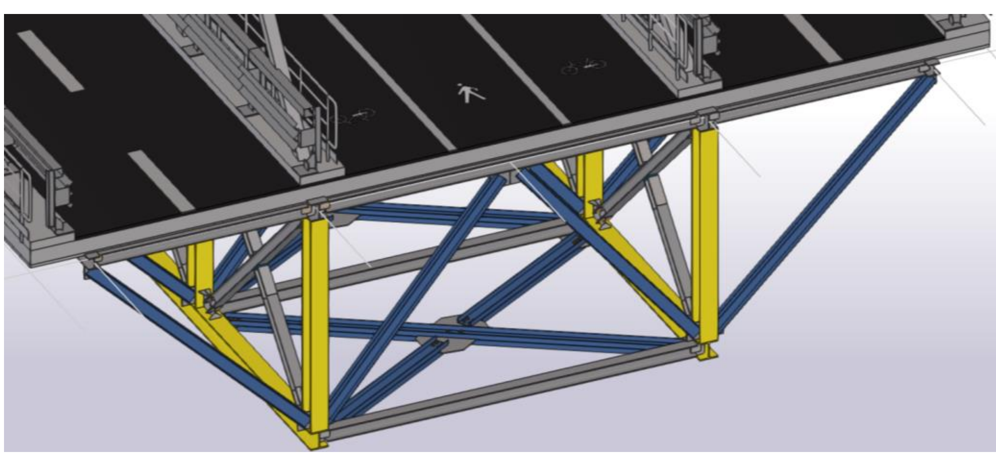

Figure 142. Transversal section

Figure 143. top view

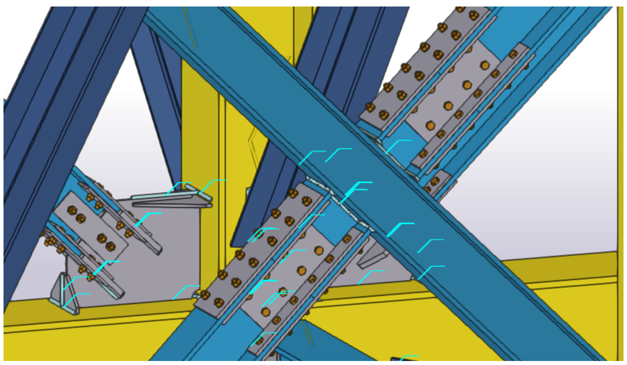

Figure 145. Vertical Bracing

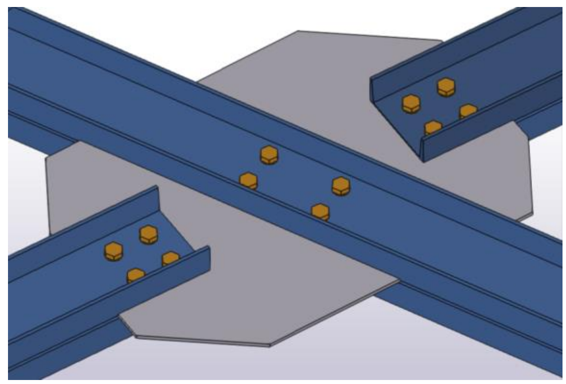

Figure 144. Horizontal Bracing

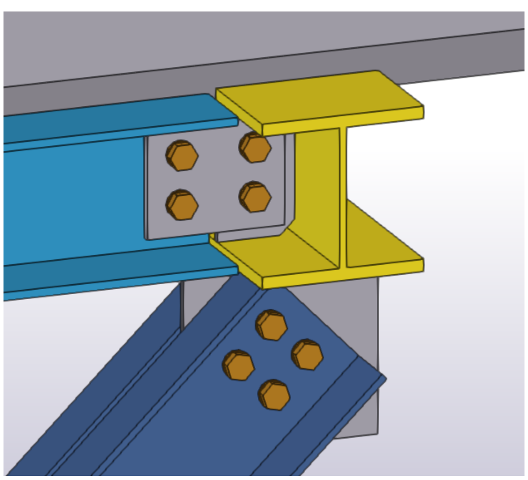

Figure 147. Top joint

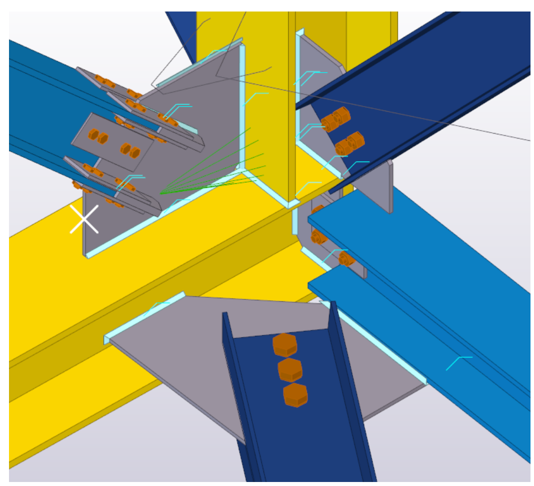

Figure 146. Bottom joint

7.3. Revit

Revit was employed due to the limitations of directly obtaining an FBX format from Tekla. Utilizing Revit allowed for the direct export of the FBX format, facilitating smooth integration with other software tools and ensuring compatibility within the workflow. Additionally, the process of transferring models from Tekla to Revit allowed for an exploration of interoperability between the two software platforms. This interoperability not only facilitated the export of models in the desired format but also provided insights into the compatibility between Tekla and Revit, enhancing the overall efficiency of the design and modeling process.

For the augmented reality (AR) integration, separate files of different parts of the bridge were required. Revit was used to export these different phases of the bridge, allowing for the creation of distinct AR experiences corresponding to each construction phase. This approach ensured a seamless transition between phases and enhanced the overall visualization and understanding of the project.

7.4. IDEA StatiCa

Idea Statica is a specialized tool for the design and analysis of steel connections in structural engineering. It simplifies the connection design process, enhances accuracy, optimizes material usage, and helps engineers meet code requirements for safe and efficient structural systems.

It enables engineers to calculate forces, including shear and tension, under varying loading conditions. Through checks on factors like bearing capacity ensure bolts meet safety and design standards. Checks on welds encompass assessments of throat and effective throat calculations under tension, compression, and shear, guaranteeing adherence to design codes.

The generated verification reports enhance transparency and documentation for regulatory approval and construction phases.

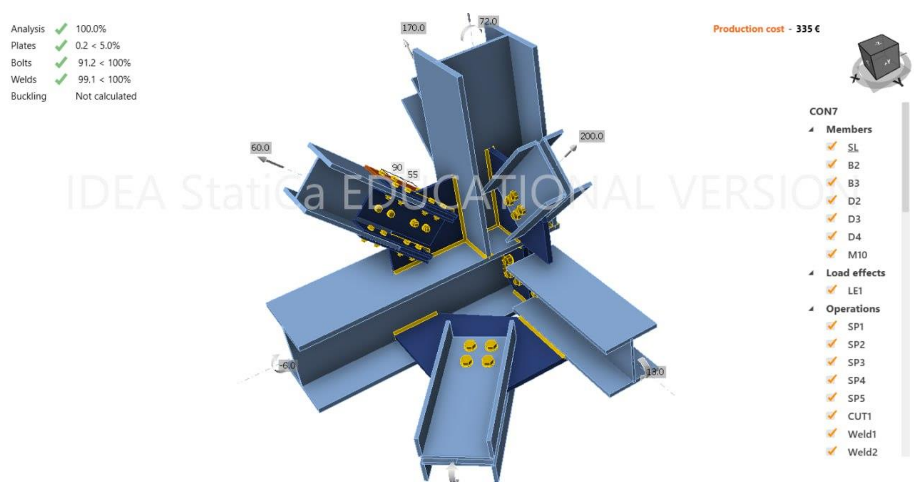

Figure 148. IdeaStatica - 1

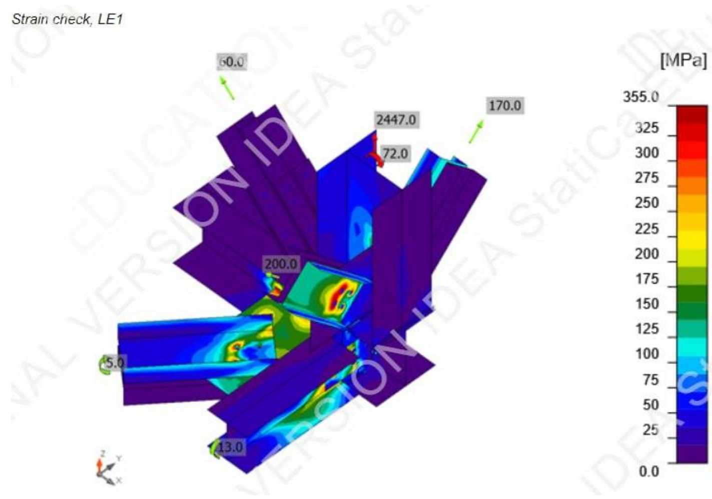

Figure 149. IdeaStatica - 2

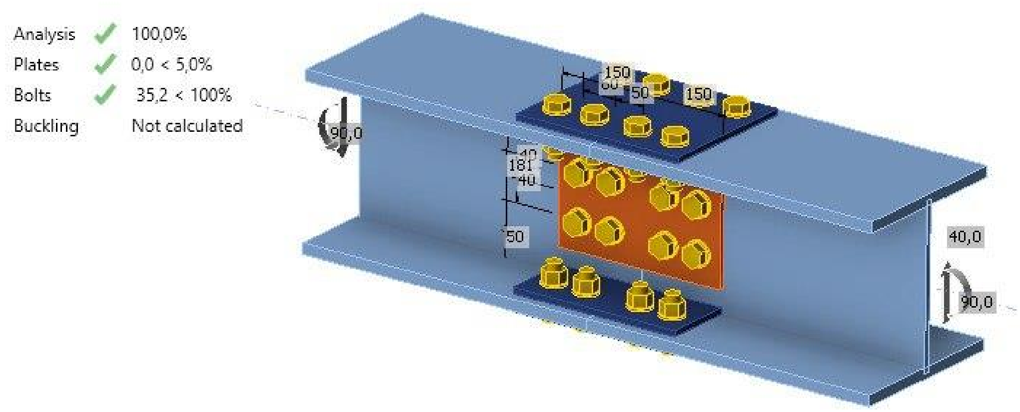

Figure 150. IdeaStatica - 3

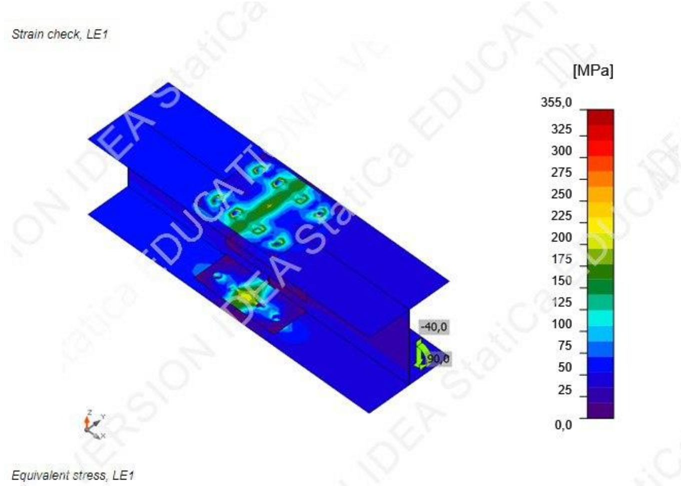

Figure 151. IdeaStatica - 4

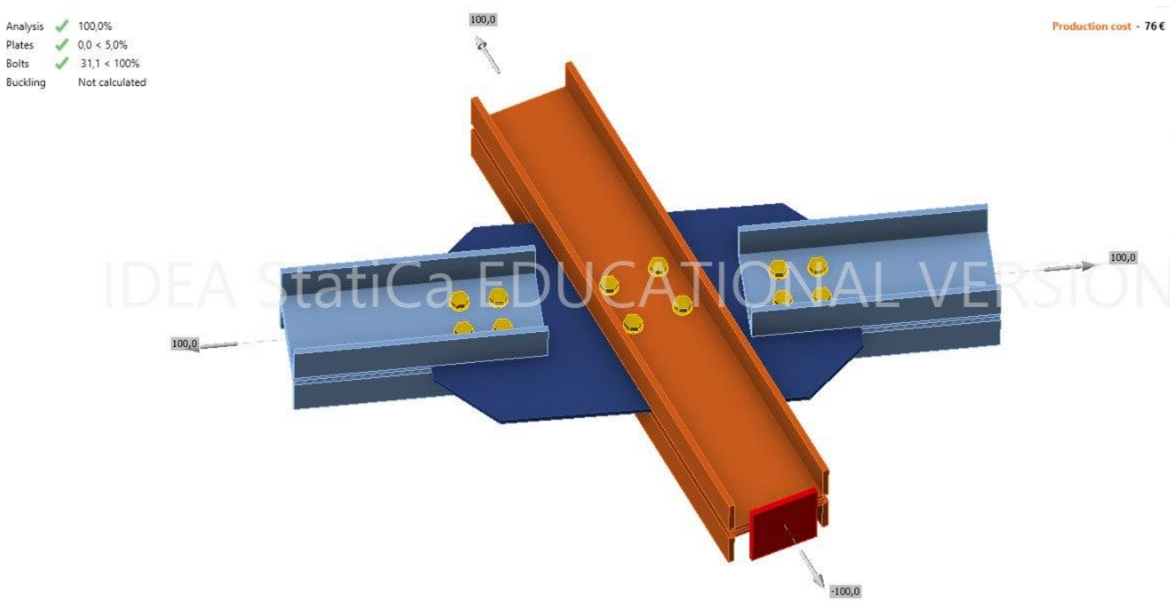

Figure 152. IdeaStatica - 5

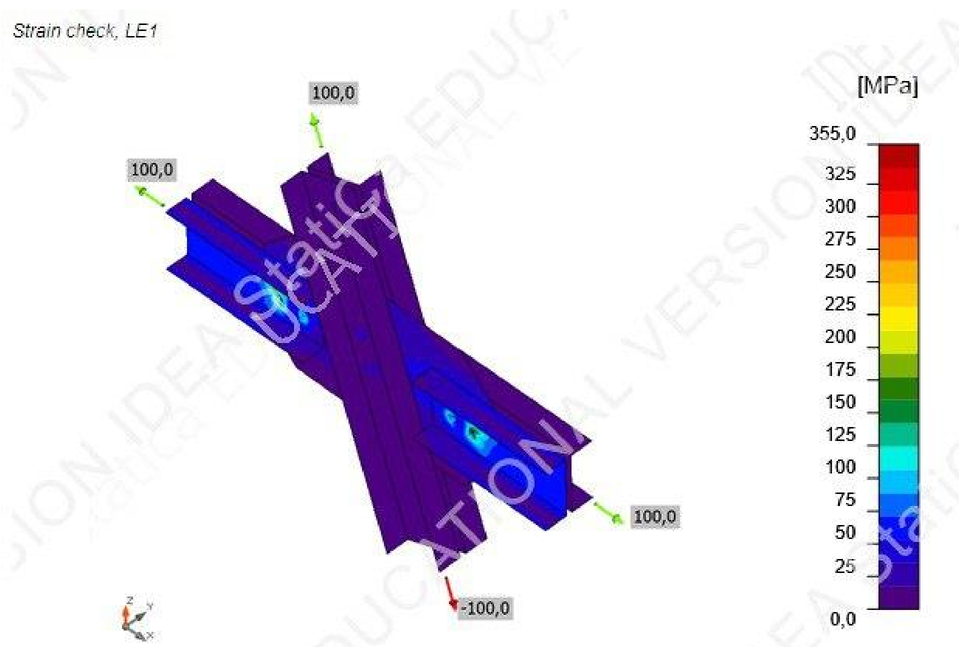

Figure 153. IdeaStatica - 6

Figure 154. IdeaStatica – 7

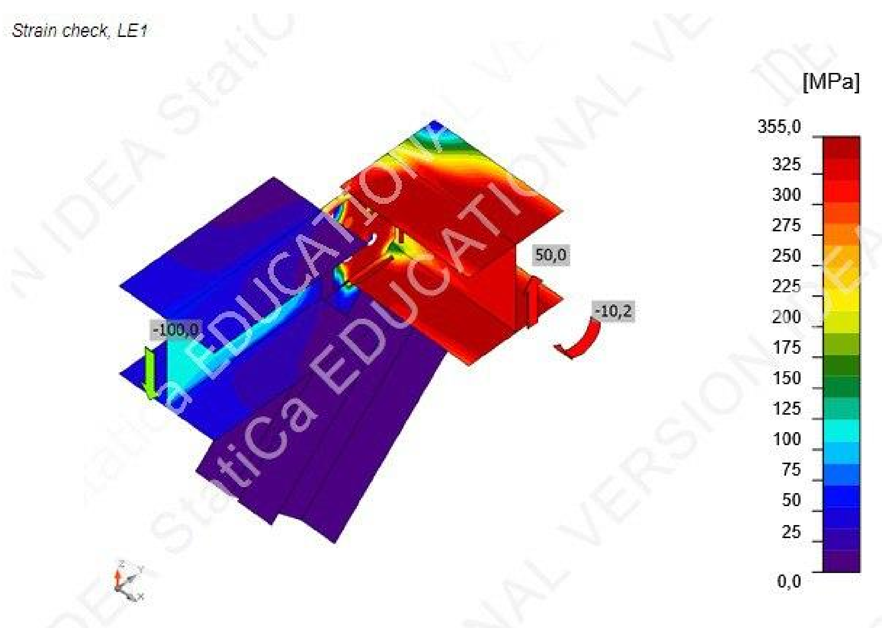

Figure 155. IdeaStatica - 8

8. Augmented Reality

8.1. Theory :

Augmented Reality (AR) integrates digital information with the user's real word environment in real time. AR serves as a link between digital design models and actual construction, enabling stakeholders to envision the project within its real world environment. Its utility in bridge construction extends to tasks such as conceptualizing design ideas, streamlining on-site assembly processes, assisting in quality assurance checks, and enhancing worker efficiency, safety protocols and accuracy.

Moreover, AR assists in identifying errors, ensuring quality control, and facilitating decision-making, resulting in reduced costs and time expenditures. Nonetheless, AR encounters its own set of constraints and obstacles. Challenges such as initial implementation expenses, technological constraints, and the necessity for specialized training pose significant hurdles. Additionally, the precision and dependability of AR tools depend on factors such as environmental conditions and the quality of digital models.

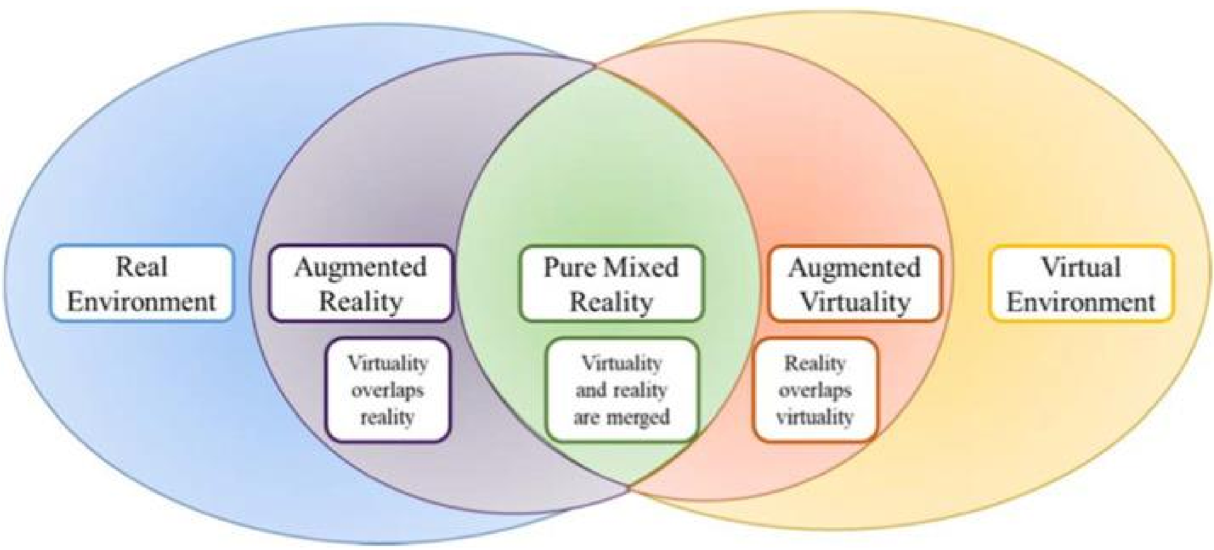

Figure 156. Augmented Reality

8.2. Procedure and Methodology :

In the augmented reality (AR) section of the project, Unity software served as the foundational tool for implementation. The primary objective was to visualize various phases of the construction process, achieved through toggles for sequential display. Furthermore, the integration of buttons facilitated the showcasing of critical bridge components and maintenance scenarios. To enhance the user experience, the implementation included sliders for rescaling the bridge, providing a dynamic perspective, and improving visualization. Rotation sliders were also introduced to encourage a comprehensive understanding of the bridge's design and construction phases. This approach contributed to a more immersive and user-friendly AR experience.

The process began by setting and image target obtained from Google Earth, ensuring accurate alignment with the actual construction site. Throughout the development, coding enhancements were applied to optimize features, ensuring a more efficient and smooth implementation.

An important milestone was the transformation of the Unity project into an Android build. This step enabled the presentation of the work on tablets, freeing it from computer dependencies. The central purpose of employing augmented reality was to demonstrate the feasibility of remote project management. By eliminating the need for physical presence on the construction site, the approach aimed to reduce costs, labor, and time. Moreover, the technology played a crucial role in identifying the potential issues, predicting future maintenance requirements, and safeguarding structures from hazards such as cracks. This not only contributes to environmental sustainability but also aligns with the wide-ranging goals of cost-effectiveness and efficiency in construction projects.

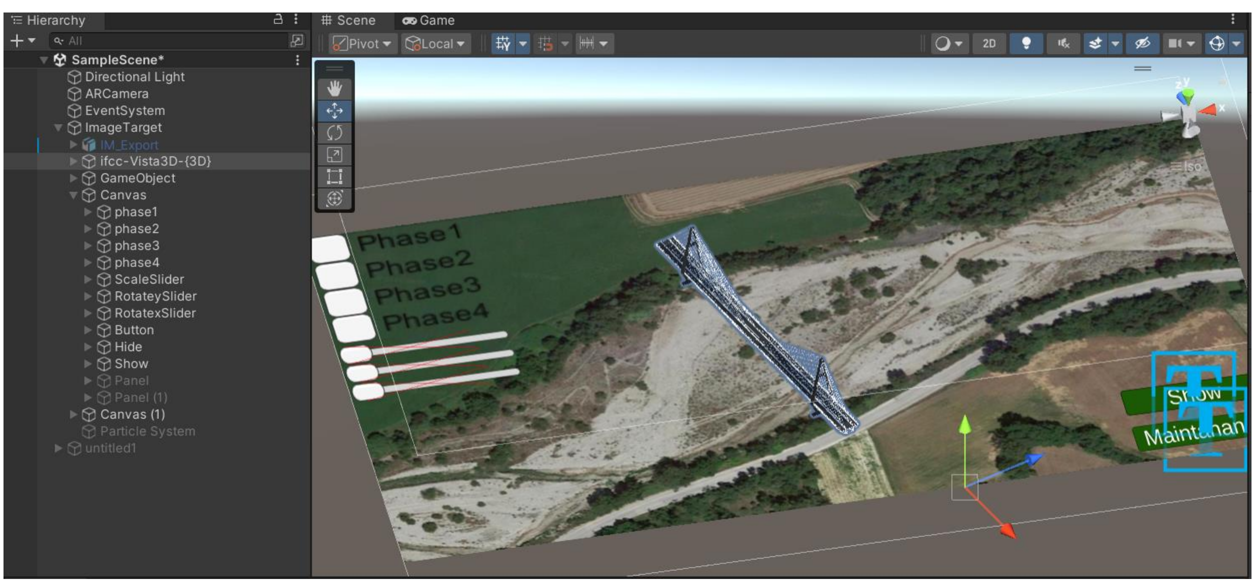

Figure 157. Unity

8.3. Results :

3D view:

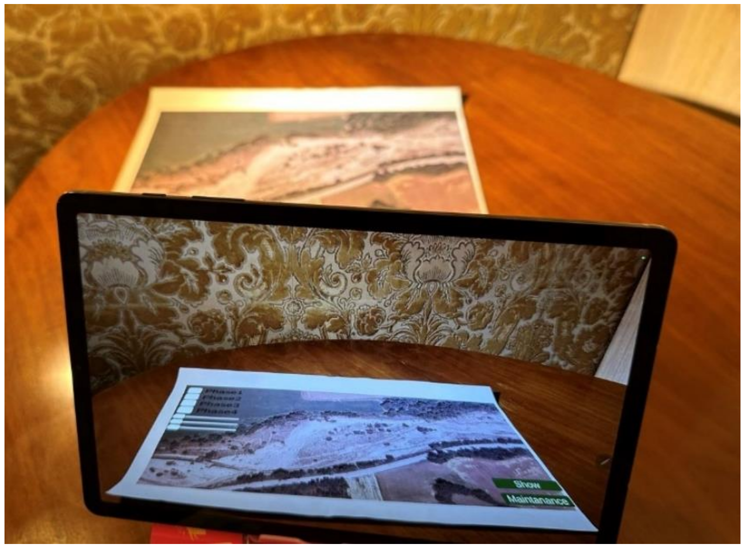

Figure 158. Entire Bridge-Invisible AR

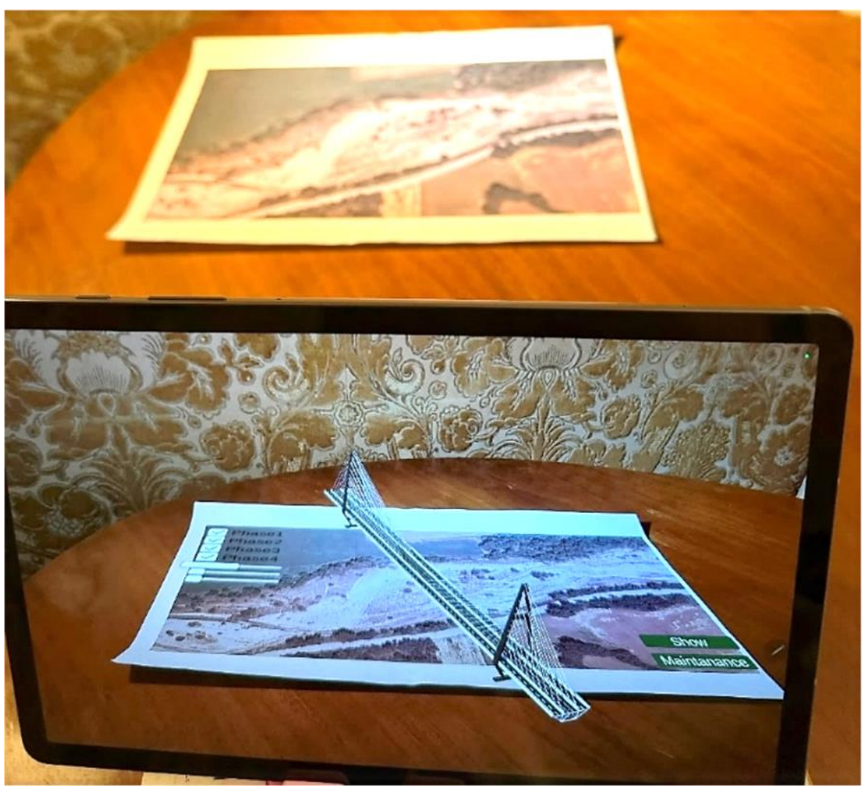

Figure 159. Entire Bridge-Visible AR

Cross section :

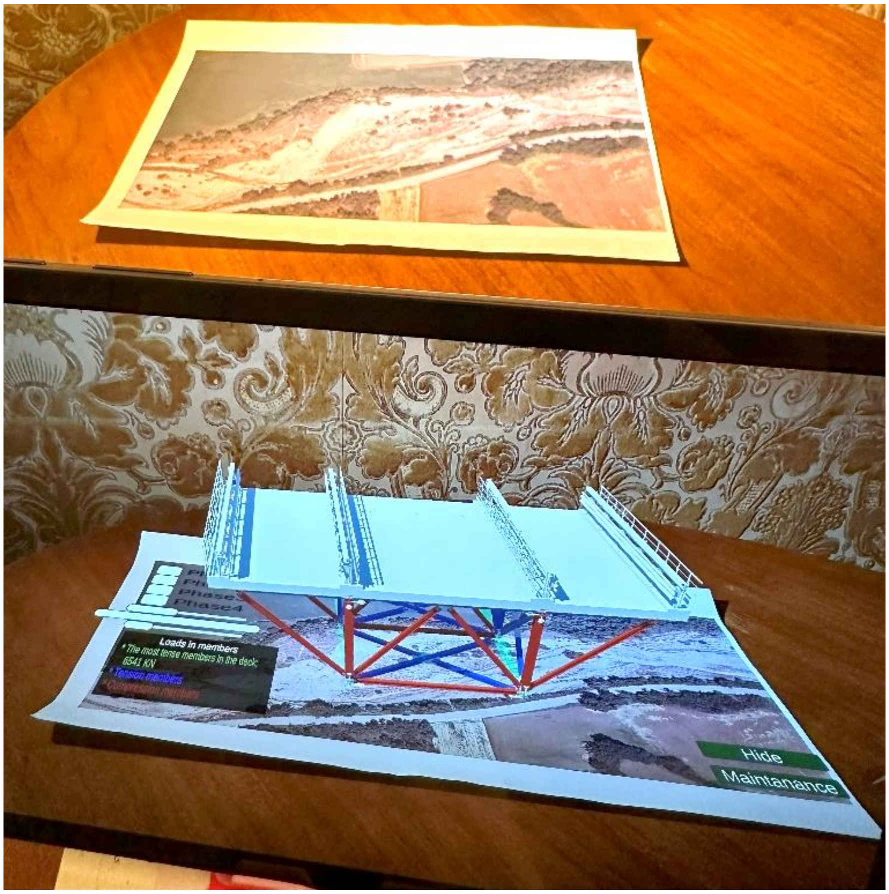

Figure 160. Center part of the bridge AR

8.4. Future Trends and Opportunities :

The future of Augmented Reality is promising, ongoing advancements in technology and increasing adoption across the industry. Emerging trends include the integration of Augmented Reality with Building Information Modelling (BIM), enabling seamless data exchange and collaboration among project stakeholders.

Furthermore, progressions in wearable AR gadgets and remote collaboration platforms present avenues for improved on-site visualization and communication. As AR technology continues to become more accessible and cost-effective, its integration into construction workflows is poised to expand. These developments offer the potential for streamlined project coordination, real time data sharing, and enhancing decision making processes.

The top Augmented Reality (AR) trends are diverse and innovative, signalling significant technological advancements and applications across the industries. Connecting the physical and digital worlds gives users a new quality, which is why they are used in many industries. Some of the key trends are as follows :

- Advancements in AR Hardware
- WebAR and Cross-Platform AR
- AR in Retail and Live Shopping
- AR in Diverse Industries
- AR-Based Gaming
- Mobile AR Tools
- Wearables and AR Controllers
- Harmonious Fusion of Virtual Reality and AR
- AR Super Apps

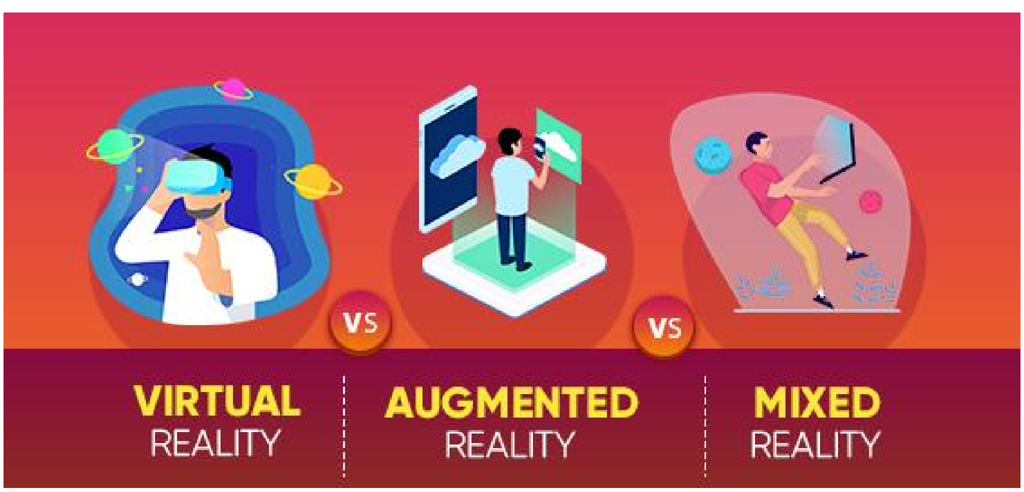

Figure 161. Types of Reality

Conclusion :

This thesis undertook the challenge of applying a B.I.M methodology approach to design a cable-stayed bridge, with a clear focus on structural efficiency, optimal design selections, and technological innovation. The decision to employ HEB profiles for the adopted reticular section of the steel deck not only reflected sustainability but also introduced commercial advantages. This preference for HEB was driven by several factors, including the ease of acquisition due to its commercial availability, requiring less effort in manufacturing. Additionally, the reduced height of HEB contributed to enhanced resistance in terms of inertia and torsion, offering more welding space and facilitating a smoother assembly process.

Utilizing genetic algorithms in the optimization process, with a primary goal of reducing the overall weight of the bridge, not only showcases a sustainable perspective in structural design but also enhances efficiency, resulting in time savings and faster outcomes.

The project's innovation extends to the incorporation of augmented reality (AR) for construction visualization and maintenance, providing a dynamic and accessible understanding of the project phases. Additionally, significant point of integrating the maintenance for long-term infrastructure management. Looking ahead, the evolution of AR could introduce 'smart' bridges equipped with sensors and AR capabilities, enabling real-time monitoring and maintenance.

In essence, the cable-stayed bridge design presented in this thesis signifies a harmonious fusion of B.I.M methodology, structural efficiency, sustainability, and groundbreaking innovation. By creating this model, it can impact and define the path of future bridge engineering.

The bridge designed in this thesis, therefore, is not just and endpoint but a beginning. It sets the stage for a new generation of smart bridges, integrated with sensors and AR, that can communicate their status and needs. This could lead to an era of sustainable infrastructure, where longevity and adaptability are built into the very fabric of bridges, ensuring they are better suited to the changing demands of the environment and society. Such forward-looking approaches exemplify the potential for this thesis to influence the trajectory of bridge engineering, steering it towards a future where the synergy of design, technology, and sustainability defines the skylines of our world.

Acknowledgements :

I would like to express my sincere gratitude to all those who supported me throughout this journey. First and foremost, I am deeply grateful to my family, whose unwavering love and encouragement sustained me during the entirety of this endeavor.

Special thanks are owed to Professor Giuseppe Carlo Marano for his invaluable guidance and mentorship throughout the course of my thesis. His expertise and support were instrumental in shaping my research and academic development.

I am also indebted to Professor Andrea Alberto and the team at L.G.A Engineering in Savigliano, as well as the province of Cuneo, for providing me with opportunity to gain practical experience in the field of Civil Engineering. Working alongside such dedicated professionals was truly inspiring, and I am grateful for the knowledge and insights they imparted to me. Additionally, I extend my special thanks to Eng. PierPaolo Cairo for his unwavering assistance and support throughout my tenure at L.G.A Engineering.

Furthermore, I extend my appreciation to Eng. Raffaele Cucuzza and Eng. Jana Olivo for their invaluable support and significant contributions to the optimization phase. Their assistance and encouragement were deeply appreciated and contributed significantly to the accomplishment of my goals.

Lastly, I would like to thank Professor Anna Osello for being supportive. Special appreciation is also due to Eng. Nicola Rimella for his amazing support and remarkable advancement were achieved in integrating augmented reality technology. His assistance played a crucial role in the successful completion of this project.

Website Citations :

- https://www.buildingsmart.org/about/openbim/
- National BIM Guide for Owners (NIBS):
- www.nibs.org
- https://bimerr.eu/bimerr-tools/interoperability-framework-bif/
- https://www.buildingsmart.org/users/services/buildingsmart-data-dictionary/
- https://www.ideastatica.com/it/idea-statica-and-graitec/
- https://www.ideastatica.com/idea-statica-and-trimble/
- https://webthesis.biblio.polito.it/28972/
- https://nsflow.com/blog/the-future-of-augmented-reality-ar-trends-devices-and-applications
- https://www.researchgate.net/
- https://webthesis.biblio.polito.it/

Bibliography :

1. Marano, G. C., & Smith, J. (Year). "Advanced Techniques in Bridge Engineering.
2. Alberto, A. Innovations in Civil Engineering: A Comprehensive Guide.
3. Jones, R. W. Structural Analysis and Design of Bridges.
4. Engineering News-Record. Latest Developments in Bridge Construction Technologies.
5. Construction Industry Institute. Best Practices in Bridge Design and Construction.
6. American Society of Civil Engineers. Guidelines for Bridge Load Testing. Journal of Bridge Engineering.
7. Federal Highway Administration. Design and Construction Guidelines for Highway Bridges.
8. International Journal of Bridge Engineering. Recent Advances in Bridge Design and Construction.
9. Li, Z., & Wang, Y. Optimization Methods for Bridge Design: A Comprehensive Review. Journal of Structural Engineering.
10. Smith, A. B., & Johnson, C. D. Augmented Reality in Construction: Applications, Challenges, and Future Directions. Construction Research Institute.

Technical regulations:

- - UNI EN 1991, Actions on structures.
- - UNI EN 1992, Design of concrete structures.
- - UNI EN 1993, Design of steel structures.
- - UNI EN 1994, Design of composite steel and concrete structures.
- - NTC 18

User guide:

- SAP 2000
- Tekla
- IDEA Statica
- Revit
- Matlab
- Unity